Flow split phenomena of two-phase flow in a large-scale horizontal upward *T*-junction

J.S. Groen

Graduation Thesis

October/November 1991

Kramers Laboratorium voor Fysische Technologie
Delft University of Technology
Prins Bernhardlaan 6
2628 BW Delft

supervisors:
Prof.Dr.Ir. H.E.A. van den Akker
Dr. R.F. Mudde

"Thesis - A postgraduate work which could earn you a doctorate, generally as long as the London Telephone Directory, and almost as exciting to read"

Robert Ainsley, Bluff your way at University (1988)

"Motionless they hung, huge, heavy, steady in the sky, a blasphemy against nature. Many people went straight into shock as their minds tried to encompass what they were looking at. The ships hung in the sky much in the same way that bricks don't.
And still nothing happened"

Douglas Adams, The Hitch Hiker's Guide to the Galaxy (1979)

"Tell me why
is it hard to make arrangements with yourself
when you're old enough to repay
but young enough to sell"

Neil Young, After the Goldrush (1970)

SUMMARY

Phase separation and pressure drop phenomena of two-phase flow splitting in a horizontal upward reduced T-junction were measured in a rig of industrial scale (inlet and run diameter 23 cm, branch diameter 10 cm). Measurements were performed in the stratified smooth, stratified wavy, and bubbly flow regimes, at low inlet qualities (less than 0.3 %). The inlet liquid mass flow was varied between 90 and 220 m^3/h.

In general, the phenomena are qualitatively the same as in smaller-scale equipment.

It appeared that the fraction plot started deviating considerably from the total separation line at the moment the transition from churn to slug flow occurred in the branch pipeline. It could be concluded that not only the flow regime in the inlet, but also that in the branch, does influence the phase redistribution.

The Seeger 'engineering model' could be used to describe these large-scale experiments. For the inlet-to-branch pressure drop, the homogeneous model and the Chisholm model gave better predictions than the Reimann and Seeger model. The inlet-to-run pressure model was found not to apply for large-scale equipment.

CONTENTS

SYMBOLS USED

symbol	description	unit
A	tube cross-sectional area	m^2
A_G	constant in model of Reimann et al.	-
a,b	parameters in Zetzmann's model	-
C_{13}^*, C_3	parameters in Chisholm's model	-
Cp	specific heat per unit mass	kJ/kg K
D	diameter	m
d	inaccuracy in	-
f	friction factor	-
G	gas mass flow	kg/s
g	mass flux	kg/m^2s
g	acceleration of gravity	9.81 m/s^2
H_{abs}	absolute humidity	-
K	correction factor	-
K_{li}	loss coefficient	-
L	liquid mass flow	kg/s
L	length of the T-junction	m
Δp	pressure drop	Pa
R	radius of curvature	m
S	slip	-
u	velocity	m/s
w	mass flow	kg/s
X_{tt}	Lockhart-Martinelli parameter	-
x	quality	-

Greek symbols

symbol	description	unit
α	volume fraction of gas	-
θ	angle	°
μ	kinematic viscosity	Pa s
ρ	density	kg/m^3
σ	surface tension	N/m
φ	loss two phase multiplier	-
ϕ	angle	°
ψ	angle	°

Subscripts

symbol	description
G	of the gas
HYD	hydrostatic
IRREV	irreversible
i	of leg i
J	due to junction
L	of the liquid
R	'reduced', i.e. predicted/measured
REV	reversible
RV	reduced, yet involving the correction factor K
S	superficial
s	specific (diameter)
TOT	total
v	vapour
1	of the inlet
2	of the run
3	of the branch

Dimensionless numbers

symbol	name and description
Fr	Froude number, centrifugal forces/gravity forces
Re	Reynolds number, inertia forces/viscous forces

Graphical symbol

symbol	description
$\bar{}$	(overline): average

1. INTRODUCTION

Someone who visits a chemical plant for the first time is mostly struck by the very large number of pipelines in between and surrounding the equipment. Not only the various apparatus have to be interconnected in the correct way, but also the right amounts of process water, steam, natural gas or pressured air have to be directed to the right position, or removed from an apparatus (condensate, waste gases, etc.). This results in an enormous amount of pipelines, junctions, valves, pumps, and so on.

For optimal operation of the plant, it is of great use to be able to predict the flows in the pipes. Especially for dividing equipment like T- and Y-junctions, it is valuable to know which part is going which way. For one-phase flow, these things are quite well known nowadays. For two-phase flow, however, things are a lot more complicated, a reason why two-phase pipelines are avoided where possible. Two-phase flow behaviour in a complicated pipeline system is still far from being fully understood, let alone being predictable.

Two-phase flows appear in many different areas of interest, sometimes even on purpose. Examples are: injection of steam into oil wells for enhanced oil recovery, vapour-condensate flow in pipelines of industrial heat exchangers (coolers, evaporators, etc.), condensation of higher hydrocarbons in natural gas pipelines due to low temperatures of surrounding air or soil, and, where safety comes in, two-phase flow caused by a so-called Loss Of Coolant Accident (LOCA) in a light water nuclear reactor (not on purpose).

Two-phase flow passing a dividing junction is one of the most complicated aspects of the area. When a two-phase flow is split in for instance a T-junction, the phases usually do not split evenly over the two branches of the junction. In fact, this is hardly ever the case. It has been found quite difficult to predict the flow split of the two phases in a T-junction over a large area of parameters. Up till now only a few models exist, all applicable within a very small region.

Experiments that have been performed were done in small diameter (1 or 2, sometimes 4 inch) pipes. Industrial pipelines can be a lot bigger, diameters of about 10 inch are quite usual. Values

calculated in small-scale experiments may, however, not be translated directly to larger scales. So, for upscaling purposes it is of interest to compare large-scale results with known smaller-scale values. This project deals with an industrial scale T-junction.

The objectives of this project were the following: first, to extend the existing data on phase separation and pressure drop with these large-scale data. Second, to determine if, within the region of these measurements, a velocity effect on the phase separation or pressure drop could be observed. Third, existing -smaller scale- models should be compared to the measurements, to see if the large scale experiments differ fundamentally from the small scale measurements.

The project was carried out for Exxon Chemical International, in this represented by R.D. Garton and Ir. J.M. de Rijke. The measurements were performed at the Kramers Laboratorium voor Fysische Technologie, at the faculty of Applied Physics of the Delft University of Technology, under the direction of Prof.Dr.Ir. H.E.A. van den Akker. The superviser of the project was Dr. R.F. Mudde.

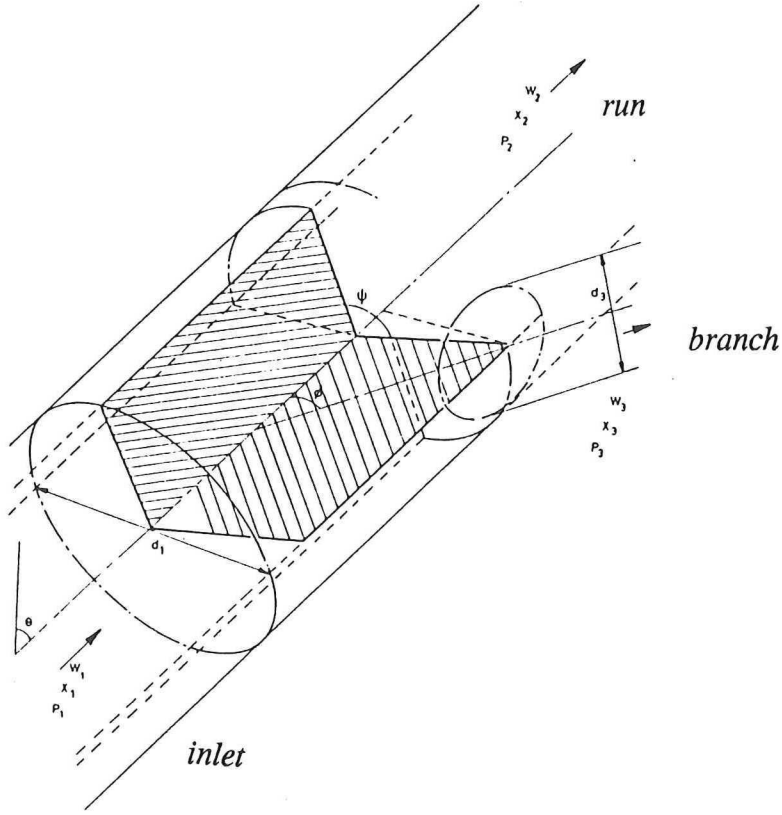

Figure 2.1. Geometric definition of a T-junction

2. THEORY AND BACKGROUNDS

This chapter can be divided into roughly two parts. First, a general introduction in two-phase flow and the definitions of a T-junction is given. The second part comprises theoretical backgrounds on phase separation and pressure drop phenomena due to a two-phase flow splitting in an upward T-junction.
In the second part of this chapter a short review on modeling phenomena is given. It contains by far not all the models published so far, only the models that are compared with the measured values are treated. For a more extensive review on models and qualitative considerations published the reader is referred to my literature review essay written for this project, in which most of the information in this chapter is mentioned as well [1].

2.1. General definitions and terminology

The definitions and terms used in this project are the ones that are more ar less standardized world-wide. However, some publications, mainly older ones, do differ in this, and can cause trouble. To avoid ambiguities a short reference on the terms and definitions used in this report is given in this section. For most quantities see figure 2.1.

2.1.1. Description of a T-junction

A junction consists of a main pipe with another pipe attached to it, so three 'legs' can be distinguished. The leg through which the flow enters the junction, is termed the *inlet*. The leg which can be considered as the prolongation of the inlet, is named the *run*. The side arm is usually referred to as the *takeoff* or *branch*. A quantity specified for one of these (for instance pressure, flows, etc.) is indexed 1, 2 or 3 (or i, meaning either of these) respectively.

The orientation of an arbitrary junction can be specified using three angles, named θ, ϕ and ψ. θ denotes the deviation of the axis of the main pipe from the vertical, ϕ is the angle between the

axes of the main pipe and the takeoff, and ψ refers to the orientation of the takeoff with respect to the vertical.
A junction can be said to be either horizontal or vertical. This term refers to the orientation of the main pipe. A horizontal T-junction can be either upward, downward or horizontal dividing, this term refers to the orientation of the branch.

This project deals with a horizontal upward T-junction, so θ and ϕ are 90° and ψ equals 0°.

Each of the 'legs' of the T-junction has a diameter D_i, and thus a cross-sectional area A_i. When all diameters are equal the T-junction is called straight. When the takeoff diameter is smaller than that of the inlet-and-run the term reduced T-junction is used.

2.1.2. Definition of two-phase flow quantities

The liquid or gas mass flow in one of the pipes is referred to as L_i or G_i, respectively. The total amount of mass flowing through one of the pipes is denoted by w_i, sometimes the mass flux, g_i is used. So:

$$g_i = \frac{w_i}{A_i} \tag{2.1}$$

Quantities referring to the liquid or gas are indexed L or G, respectively. Velocities u_i can be additionally indexed S, denoting that the superficial velocity is meant. The gas and liquid phases have densities ρ_G and ρ_L, of which, of course, the gas density is depending on the local pressure.

The quality of a flow in one of the pipes, called x_i, is defined as the gas mass flow divided by the total mass flow:

$$x_i = \frac{G_i}{L_i + G_i} \tag{2.2}$$

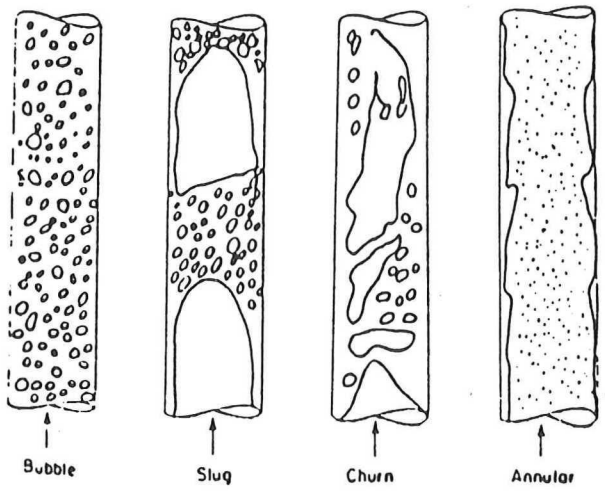

Figure 2.2. Flow regimes in vertical flow

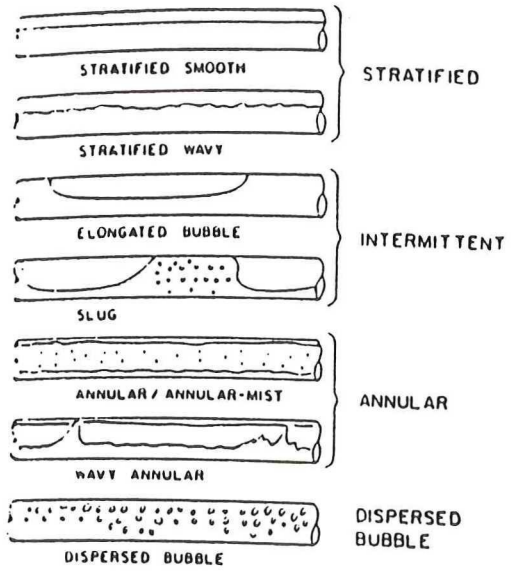

Figure 2.3. Flow regimes in horizontal flow

The density of the two-phase flow, $\overline{\rho_i}$, is defined as the harmonic mean of the phase densities:

$$\overline{\rho_i} = \left[\frac{x_i}{\rho_{Gi}} + \frac{(1-x_i)}{\rho_{Li}} \right]^{-1} \tag{2.3}$$

The mean velocity of the two-phase flow, $\overline{u_i}$, is defined using a mass balance:

$$\overline{\rho_i}\,\overline{u_i} = (\rho_G u_{GS})_i + (\rho_L u_{LS})_i \tag{2.4}$$

The gas volume fraction (gas volume divided by total volume) is referred to as α_i. This volume fraction is related to the quality as follows:

$$x_i = \left(\frac{\alpha \rho_G u_G}{\alpha \rho_G u_G + (1-\alpha)\rho_L u_L} \right)_i \tag{2.5}$$

Pressure drops the flow experiences passing the T-junction, are named Δp_{12} and Δp_{13}, for inlet-to-run and inlet-to-branch pressure drop, respectively. The pressure drop Δp_{1i} is defined as $p_1 - p_i$. *Note* that this way of definition implies that a pressure *drop* is *positive* and vice versa. This should be kept in mind using the other pressure drop definitions and the models.
When a pressure drop is caused by the junction itself, the index J is added: $(\Delta p_{1i})_J$.

A fluid entering the branch ('turning the corner'), is said to be *extracted* from the two-phase flow. The fraction of the mass flow that enters the branch (i.e. w_3/w_1) is called the *mass extraction ratio*, or *mass extraction fraction*.

2.2. *Flow regimes in two-phase flow*

The distribution of a two-phase flow over the area of the pipe it is flowing through can take place in various ways. The way in which the two-phase flow flows through the pipe depends on the superficial velocities of both phases, the geometry and orientation of the pipe and of course the physical properties of the two phases involved.

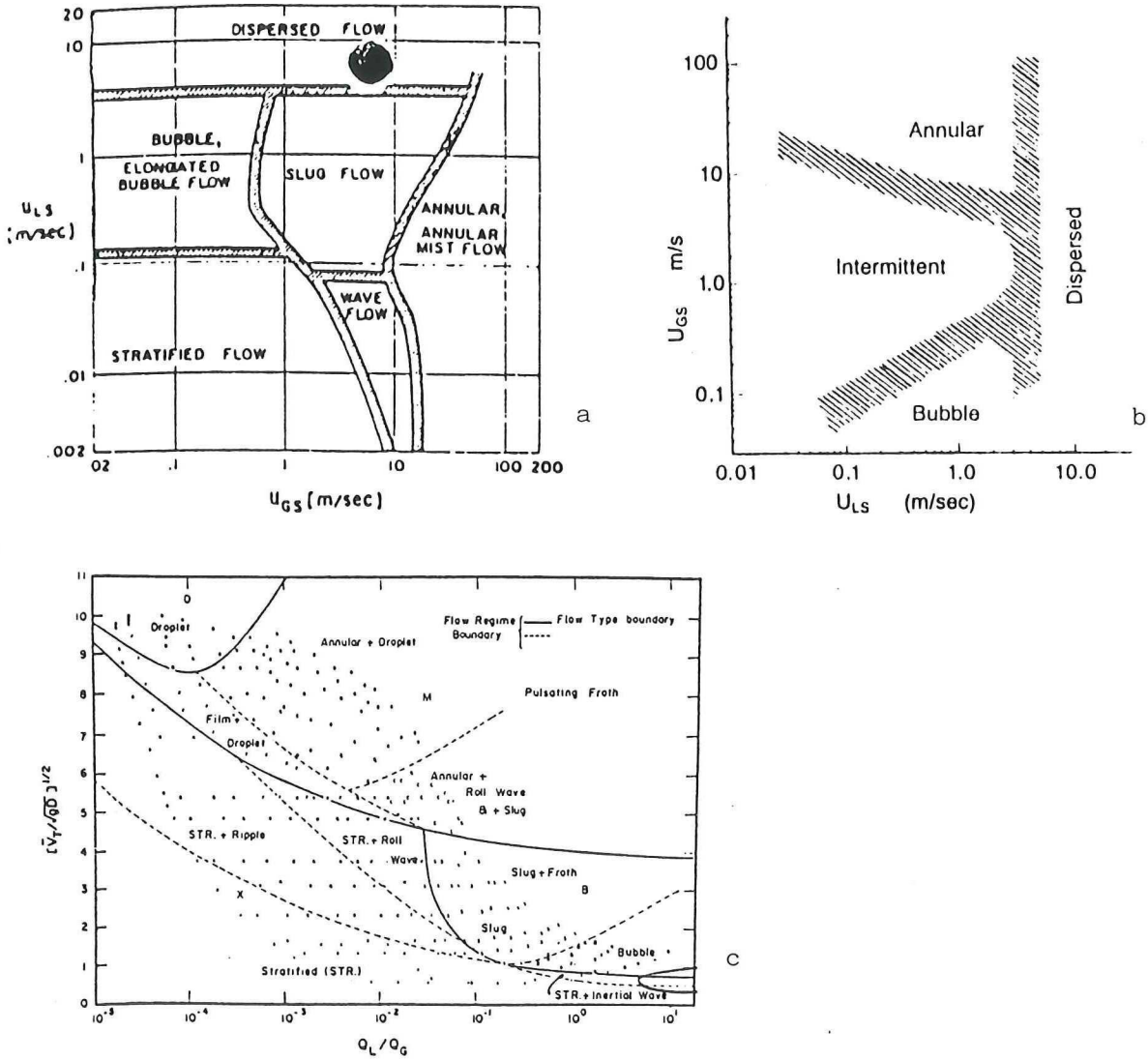

Figure 2.4. *Different kinds of flow maps: (a) horizontal flow, (b) vertical flow, (c) a more 'complex' flow map for horizontal flow*

In a *vertical* pipe, usually a classification into four flow regimes is made, as depicted in figure 2.2. The different regimes appearing are (in order of increasing gas fraction):

- Bubbly flow: the gas phase is distributed in the form of bubbles, more or less uniformly over the area of the tube.
- Slug flow: due to bubble coalescence larger 'bubbles', called slugs, comprehense the major part of the gas phase. These slugs have a diameter almost equal to that of the pipe. A minor part of the gase phase still travels in the form of bubbles.
- Churn flow: quite similar to slug flow, but more chaotic. No distinct slugs or bubbles can be observed anymore.
- Annular flow: the gas travels as the continuous phase, in the centre of the pipe. The liquid travels as a film attached to the pipe wall, and partly as drops, in the gas phase.

In *horizontal* flow, equivalent regimes can be observed, but one extra flow regime can be distinguished (see figure 2.3):

- Stratified flow: the gas and liquid phase are separated, possibly having quite a different velocity. Stratified flow can be classified further into stratified smooth and stratified wavy flows.

Each flow regime differs from all the others in hydrodynamics, transport quantities, momentum exchange mechanisms, and so on. So, for designing purposes, it is quite useful to know or to be able to predict the flow regime in a pipeline. The transitions between the different flow regimes are however not very well known or predictable. Several models do exist (see [2] for a review on these), but none of them is generally applicable over a wide range of parameters.

Another way of predicting the flow regime is to make use of co-called flow maps. These indicate in which a given two-phase flow can be expected to be, as a function of two or more parameters. These parameters can be quite simple, like liquid and gas superficial velocity, but difficult combinations of quantities do occur as well, in an attempt to generalize the map. Some examples are given in figures 2.4 a to c.
However, all known flow maps can only be used within certain limits. None of these has been proved to be generally applicable yet.

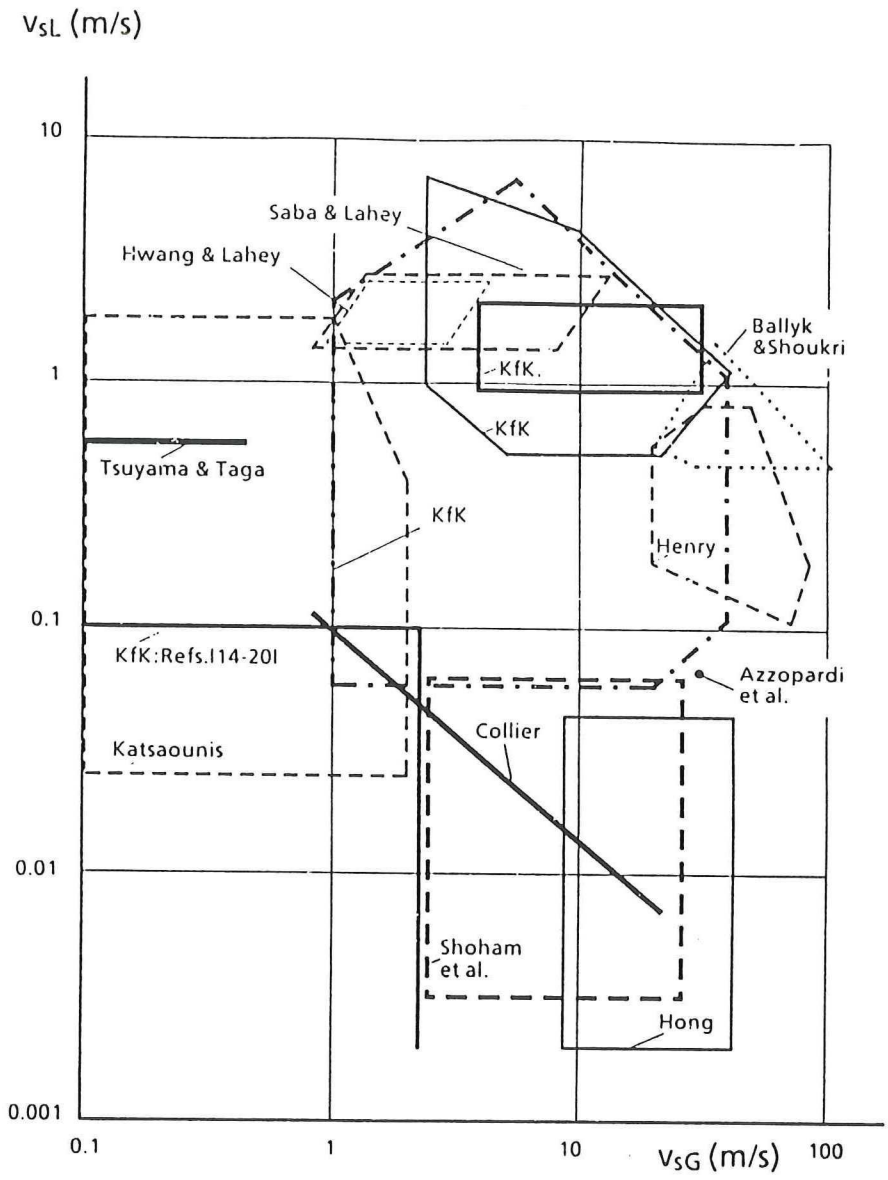

Figure 2.5. Overview of earlier research: experimentors and their areas of interest

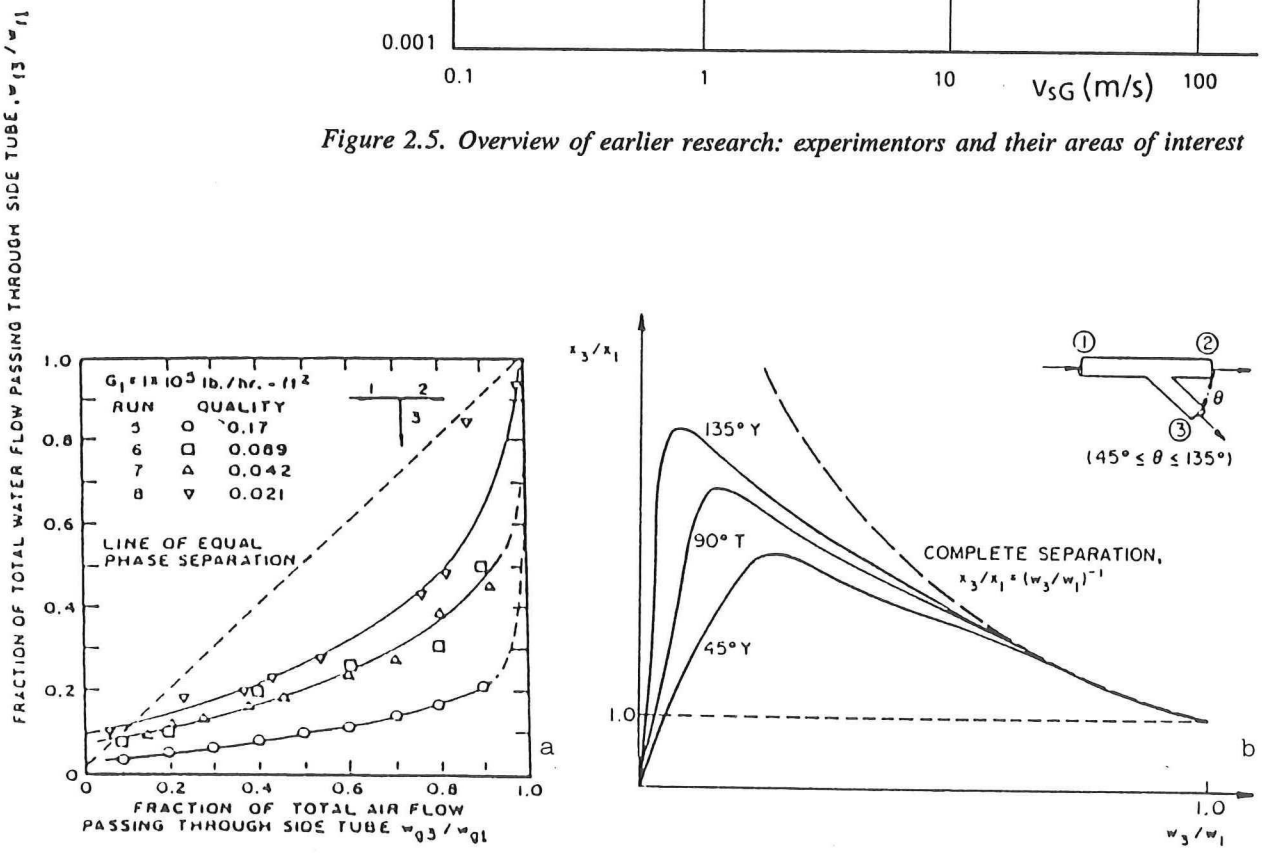

Figure 2.6. (a) a 'fraction plot', (b) a 'phase separation plot'

2.3. Phase separation phenomena

Phenomena surrounding flow split in a dividing junction have already been investigated quite widely, by a lot of authors. Figure 2.5 (taken from [3]) shows an overview of the different authors and their areas of interest, given in the form of a flow map. Their findings are summarized in this section.

2.3.1. Qualitative description and explanation of phenomena

As mentioned in the introduction, the flows entering the branch and the run hardly ever have the same composition as the inlet flow, i.e. a phase redistribution takes place.
The most common ways to describe the flow split graphically are shown in figures 2.6 a and b. Figure 2.6 a represents a so-called fraction plot, in which the fraction of gas extracted into the branch is given vs. the fraction of liquid extracted. Phase redistribution can be seen in this plot by comparing the curve with the line of equal flow split, i.e. the 'y = x'-line, where the fraction of gas extracted equals the fraction of liquid extracted.
Another, probably the most widely used type of graph is given in figure 2.6 b, this one is called the phase separation curve. It represents the ratio of qualities of the branch and the inlet, vs the mass extraction rate. The advantage of this graph is that very easily can be seen to what extent the phase separation takes place. To see if the phase separation is total, one draws the so-called total phase separation curve. By using a gas phase mass balance, this curve is easily derived as:

$$\frac{x_3}{x_1} = \left(\frac{w_3}{w_1}\right)^{-1} \tag{2.6}$$

One warning should be given: in this area the term 'total phase separation' does *not* mean that the phases do get totally separated. The only condition for using the term 'total' phase separation is that all the gas enters the branch. The amount of liquid entering the branch as well, is of no importance for this term.

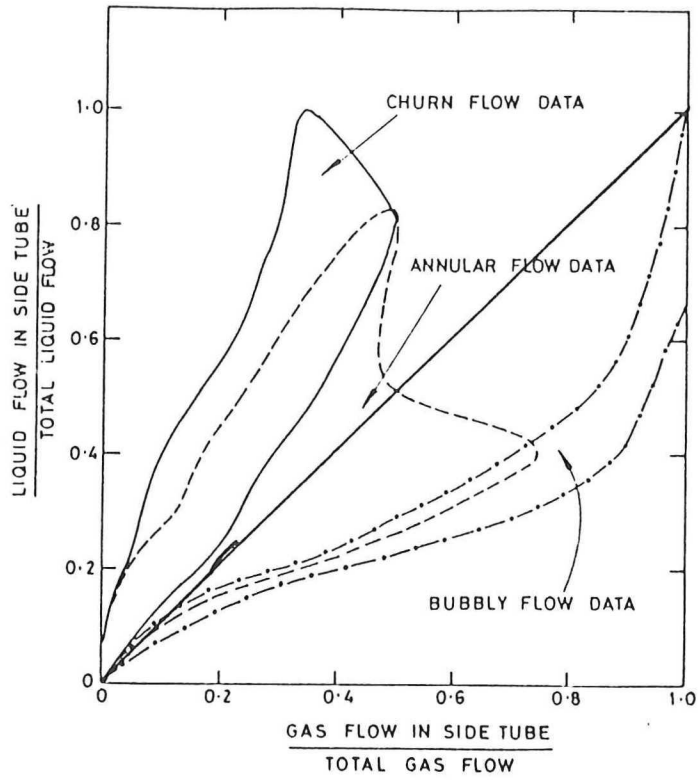

Figure 2.7. Effect of the inlet flow regime on the flow split

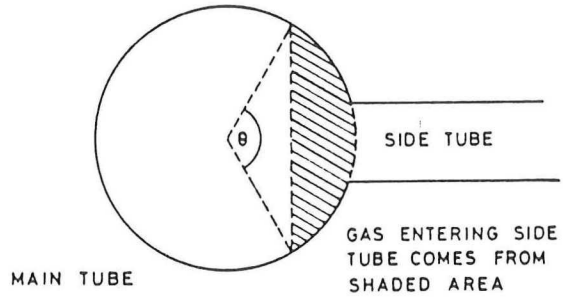

Figure 2.8. Impression of a 'zone of influence'

Phase redistribution phenomena surrounding the flow split are described by many authors, and can be summarized as follows:

At bubbly and churn flow regimes, the gas is preferentially removed into the branch, except at low mass extraction rates, where the liquid is preferentially removed. At annular and slug flow regimes, the liquid is preferentially extracted over a considerable range of the mass extraction rate, but at high mass takeoff rates more gas is removed.

In the case of stratified flow, initially only gas or liquid (depending on the branch orientation being upward or downward, respectively), enters the branch. With increasing superficial velocities, a point is reached where the other phase is pulled through into the branch. This point is referred to as 'point of liquid/gas carryover', 'point of pull through' or 'gas/liquid fraction threshold', the latter meaning the fraction of the not-pulled-through fluid that is extracted as entrainment begins.

The degree of phase separation is mainly influenced by three effects (as mentioned by for instance Seeger, Reimann and Müller [4]):

- inertia differences of the phases,
- gravity effects,
- the distribution of the phases over the area of the inlet, mainly caused by the flow regime present.

Taking these three effects into account, several flow split phenomena can be explained.

The fact that the phase split is dependent on the flow regime is hardly surprising, as the regime determines the distribution of the phases over the area of the pipe. Azzopardi and Whalley [5] investigated the influence of the flow regime on the split for different orientations and a couple of flow regimes. The results of this investigation are given in figure 2.7.
As to the dependence on the flow regime, several phase redistribution phenomena can be described by defining a so-called 'zone of influence' of the branch. Such a zone of influence is sketched in figure 2.8. The two-phase flow that enters the T-junction through this zone is expected to enter the branch. The distance this zone reaches into the inlet is mainly determined by the

pressure drop between the branch and the inlet and so depends on the mass extraction rate. This idea was originally developed by Azzopardi for annular flow, but, by defining an equivalent zone of influence for other flow regimes at least phase separation phenomena in the lower mass extraction region can be predicted for churn and bubbly flow.

The influence of gravity is quite comprehensible as well, the liquid generally having a much higher density than the gas. Gravity 'wants' the liquid and gas to separate.

At bubbly and churn flow conditions, the velocities of the gas and the liquid are more or les equal. Generally, this means that the gas has far less momentum than the liquid, and thus is converted into the branch more easily. The fact that initially more liquid is removed is explained using the knowledge that the gas preferentially resides in the centre of the tube, in the so-called 'bubble street'. At low mass extraction rates, the zone of influence of the branch does not reach as far as this bubble street. Of course, this bubble street is much more pronounced in a vertical flow then in a horizontal flow.
At annular and slug flow conditions, the velocity differences are much larger, the momentum of the gas and the liquid being about the same order of magnitude. The phase separation phenomena can then be understood by the distribution of the phases over the pipe area and by using an equivalent zone of influence.
In the case of stratified flow, initially only the phase adjacent to the branch is extracted. The pressure drop over the inlet-to-branch requires a certain minimum to start entrainment of the other phase. This explains the occurence of the 'point of pull through'.

2.3.2. Parametric dependence

Several authors have investigated the parametric dependence of the flow split in the T-junction. In his Ph.D. thesis, Zetzmann [6] summarizes these findings and concludes that the parameters that most strongly influence the flow splits are the mass extraction rate, w_3/w_1, the ratio of the branch and inlet diameter, D_3/D_1 and the inlet flow regime. For low extraction rates, the angle ϕ between the inlet and branch has some influence, too. Honan and Lahey [7] reported that, within the same flow regime, the flow split is hardly depending on the inlet mass flow, but the pressure drop is.

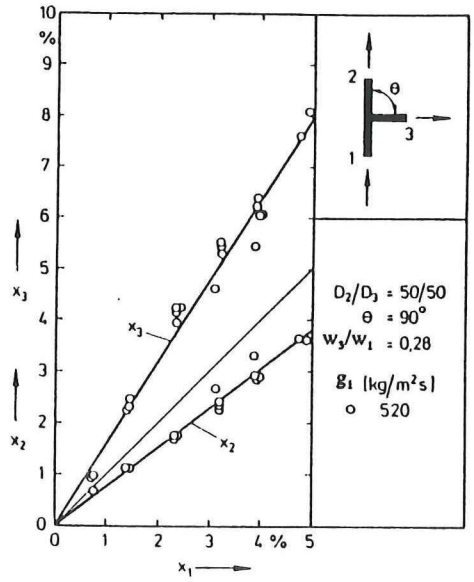

Figure 2.9. Proportionality of x_2 and x_3 to x_1, as reported by Zetzmann

As has already been mentioned, the dependence of the phase redistribution on the mass extraction rate can be explained in terms of a 'zone of influence'. The fact that the phase separation is better at higher extraction ratios seems somewhat trivial, because it is more or less incorporated in the term 'total phase separation' (see the warning several paragraphs above). At high mass extraction ratios, most likely all the gas is extracted into the branch. This especially holds for a horizontal upward T-junction.

The dependence of the phase redistribution on the ratio of diameters of branch and inlet has been reported quite often. The diameter ratio was one of the main parameters in Zetzmann's Ph.D. research project. Other authors have published papers on this subject as well, mostly differing in the flow regime investigated [8, 9, 10]. All conclude that the phase separation is much more pronounced when a reduced T-junction is involved. This effect is however much smaller at stratified and annular flow conditions [11].
Lahey [12] gives the following explanation for this effect: when the cross sectional area of the branch is reduced, a larger pressure drop is required to reach the same mass extraction rate. This larger pressure drop results in a larger zone of influence of the branch, into which generally more gas, having less momentum, will be extracted.
It seems, however, that the important parameter in this is the *ratio* of the diameters, and not the absolute values. So a T-junction with $D_1 = 100$ mm and $D_3 = 50$ mm should render the same separation results as a T-junction with $D_1 = 50$ mm and $D_3 = 25$ mm. This example is explicitly reported by Zetzmann.

The dependence on the angle ϕ can be explained by taking inertia effects into account, the gas turning the corner more easily. The higher the angle, the better the phase separation is.
Zetzmann investigated the dependence on the inlet quality. He concluded that, for qualities beneath 5 %, the run and branch quality are directly proportional to the inlet quality, as is illustrated in figure 2.9.

Several authors noticed that the orientation of the T-junction does not show a strong influence on the separation process. Seeger, Reimann and Müller [4] as well as Hwang, Soliman and Lahey [13] mention that measurements made by Saba and Lahey [14] in a horizontal T-junction, quite

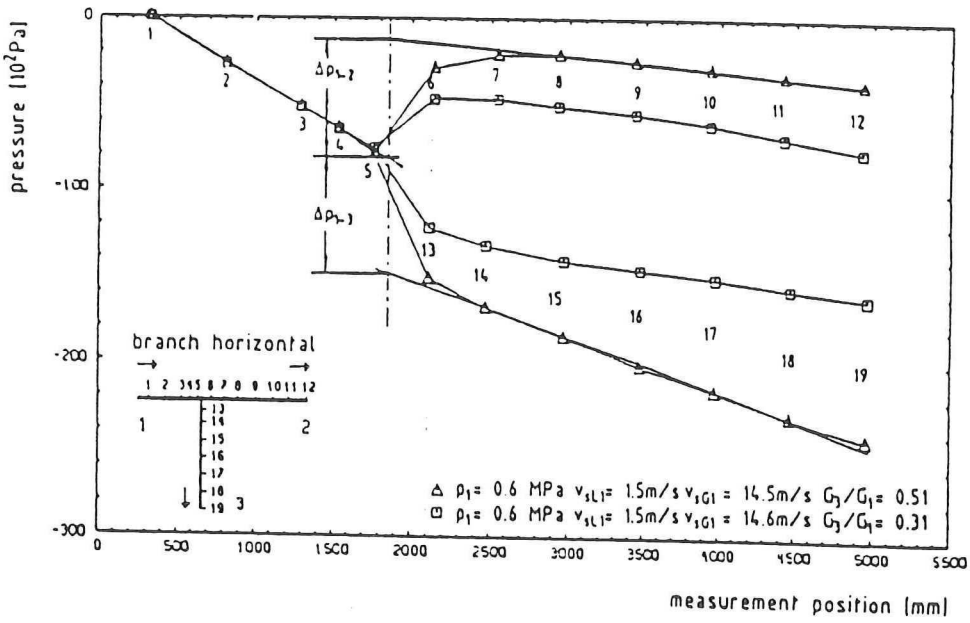

Figure 2.10. Typical pressure profile over a T-junction

closely resemble those made by Honan and Lahey in a vertical T-junction, under essentially the same circumstances [7]. Apparently the inertia effect is stronger than the gravity effect.

2.4. Pressure drop phenomena

Pressure drops induced by a flow splitting in a T-junction are induced by several different effects. These can be divided into gravitational effects, effects because of velocity changes and effects due to the flow turning the corner or the like. Because the first two effects mentioned can be reversed, these are referred to as *reversible* pressure changes (sometimes called Bernoulli effects), the last ones are called *irreversible*. Apart from these changes, in all three legs of the T-junction pressure decreases slowly because of wall friction effects.

When a flow is split in a T-junction, the part of the flow that enters the run mainly experiences a pressure rise because of the decrease in velocity. The fraction diverting into the branch undergoes a pressure change as well (the pressure falling or rising depending on the flow accelerating or slowing down, respectively). Both split flows can undergo pressure drops due to hydrostatic effects. This of course depends on the orientation of the T-junction and the branch. The inlet-to-branch flow undergoes an extra pressure drop because it costs energy to force the fluid to turn the corner. The irreversible pressure drops the inlet-to-run flow experiences are mostly quite low, if not neglegible. These phenomena cause the pressure drop to look as given in figure 2.10.
The pressure drops due to the T-junction, $(\Delta p_{12})_J$ and $(\Delta p_{13})_J$, can be obtained graphically by extrapolating the wall friction dominated pressure loss curves in the arms of the junction, as is shown in this figure.

2.5. Modeling flow split and pressure drop

To mention al models published on this subject would go too far. In this section the models used in this project to compare the measurements with are treated rather concisely. As mentioned at the beginning of this chapter, a more comprehensive and deeper treatment of the different models can be found in my literature review essay [1].

2.5.1. General remarks on modeling

Several models to predict the flow split and the pressure drop over the T-junction have been derived, developed and proposed. These models differ in many ways, but have one thing in common: they are -again- only applicable within a small range of parameters. All models have been derived and tested using small diameter T-junctions, and it is not known if they are applicable as well for larger scales, because of the simple fact that no large-scale measurements have been performed so far.
Models that have been derived so far, can be distinguished into three categories (see Lahey [12]): theoretical, empirical and phenomenological, flow regime based models. Theoretical models are based upon physics as much as possible and use empirical correlations only when physical knowledge is missing. Phenomenological models start from merely describing what happens. Empirical models are essentially fits that are laid through measurements.

2.5.2. Description of the problem

The problem on flow split and pressure drop in a T-junction is governed by eight parameters: three mass flows w_i, three qualities x_i and the inlet-to-run and inlet-to-branch pressure drops Δp_{12} and Δp_{13}. Generally, three of them can be specified, w_1, x_1 and for instance Δp_{13} (the latter by changing the friction coefficient of the branch valve). This leaves five unknown variables, requiring five independent equations. Four of these are quite easily obtained by the total mass and momentum balance and the mass and momentum balance for one of the phases. Some of the models published are essentially a way to obtain the fifth equation.
The model presented by Saba and Lahey [14] is the only one up till now that eventually comes up with a fully defined set of five independent equations. Two models invoking geometry and flow regimes are the one developed by Hwang, Soliman and Lahey and the one of Shoham, Brill and Taitel [13, 15].
These models are not used however in this project to compare the results with, for the following reasons: first, the models are both developed for small scale apparatus and they are quite complicated, comprising a lot of equations. In this stage of research into scaling up rules it seems

Table 2.1. Limits in using Zetzmann's model

$\theta = 0$
$\phi = 45, 90$
$24 \leq d_1 \leq 100$ mm
$500 \leq \mathbf{g}_1 \leq 3.000$ kg/m^2 s
$0.005 \leq x \leq 0.035$
$0.1 < w_3, w_1 < 0.8$

to be rather overdone to immediately compare the measurements with these complicated models, while more simple models are available as well. Second, the modeling of an *upward* T-junction has been found most difficult of all. No model has been found capable of producing adequate predictions concerning an upward T-junction, as is reported by several authors. Expressions like 'for the upward branch all models fail', are no exception.

2.5.3. Models used to describe the flow split

The models used in this project are the following:

Zetzmann

In his Ph.D. thesis, Zetzmann [6] varied some parameters over quite a range of variables (see table 2.1). As for the inlet quality, the zone of interest of this project is not covered within this range, but Zetzmann comes closer than others.
He presented a completely empirical model using the following equations:

for $0 \leq w_3/w_1 \leq 0.12$:

$$\frac{x_2}{x_1} = b\left[\exp\left[-4\left(\frac{w_3}{w_1}\right)^{1.75}\right] - 0.147\left(\frac{w_3}{w_1}\right)\left(1-\frac{w_3}{w_1}\right)\right] \tag{2.7}$$

$$\frac{x_3}{x_1} = a\,\frac{\left[1-\left(\frac{x_2}{x_1}\right)\left(1-\frac{w_3}{w_1}\right)\right]}{w_3/w_1} \tag{2.8}$$

for $0.12 \leq w_3/w_1 \leq 0.5$:

$$\frac{x_2}{x_1} = b\left[\exp\left[-4\left(\frac{w_3}{w_1}\right)^{1.75}\right] - 0.147\left(\frac{w_3}{w_1}\right)\left(1-\frac{w_3}{w_1}\right)\right] \tag{2.9}$$

Table 2.2. Values for a and b in Zetzmann's model, depending on diameter ratio and inlet-to-branch angle

d_3/d_1	ϕ	a	b
50/100	90°	0.8	1.00
24/50	90°	1.35	0.75
24/50	45°	1.4	0.80
50/50	90°	1.05	0.90
24/24	90°	1.05	0.90
24/24	45°	0.9	0.98
50/50	45°	0.9	0.98

$$\frac{x_3}{x_1} = a\left[15.64\left(\frac{w_3}{w_1}\right)^{0.75}\exp\left[-2.75\left(\frac{w_3}{w_1}\right)\right] - 2.0\left(\frac{w_3}{w_1}\right)\left(1-\frac{w_3}{w_1}\right)\right] \tag{2.10}$$

and, for $0.5 \leq w_3/w_1 \leq 1.0$:

$$\frac{x_2}{x_1} = \frac{1}{1-w_3/w_1}\left[1-\left(\frac{x_3}{x_1}\right)\left(\frac{w_3}{w_1}\right)\right] \tag{2.11}$$

$$\frac{x_3}{x_1} = a\left[15.64\left(\frac{w_3}{w_1}\right)^{0.75}\exp\left[-2.75\left(\frac{w_3}{w_1}\right)\right] - 2.0\left(\frac{w_3}{w_1}\right)\left(1-\frac{w_3}{w_1}\right)\right] \tag{2.12}$$

The parameters a and b are dependent on the diameters of inlet and branch and on the angle ϕ between the branch and the inlet. In his thesis, Zetzmann only gives values for b. Table 2.2, taken from the Encyclopedia of fluid mechanics [2], gives values for a as well. For a further treatise on this model see section 2.6.

Seeger, Reimann and Müller

In two publications, essentially comprising his Ph.D. thesis [16], Wolfgang Seeger, together with several co-authors, presents some models to predict the flow split and pressure drop. The model on pressure drop is given in the next section, the (empirical) model on the flow split is treated here [4].

For a horizontal T-junction with an upward branch, Seeger reported that he could not find any real parametric dependence. For engineering purposes, he recommends the following expression:

$$\frac{x_3}{x_1} = \left(\frac{w_3}{w_1}\right)^{-0.8} \tag{2.13}$$

This expression may not be used at low values of w_3/w_1. In the publication Seeger uses the mass flux G_i instead of w_i, but as he was working with a *straight* T-junction and this project deals with a reduced one, things have to be transposed.

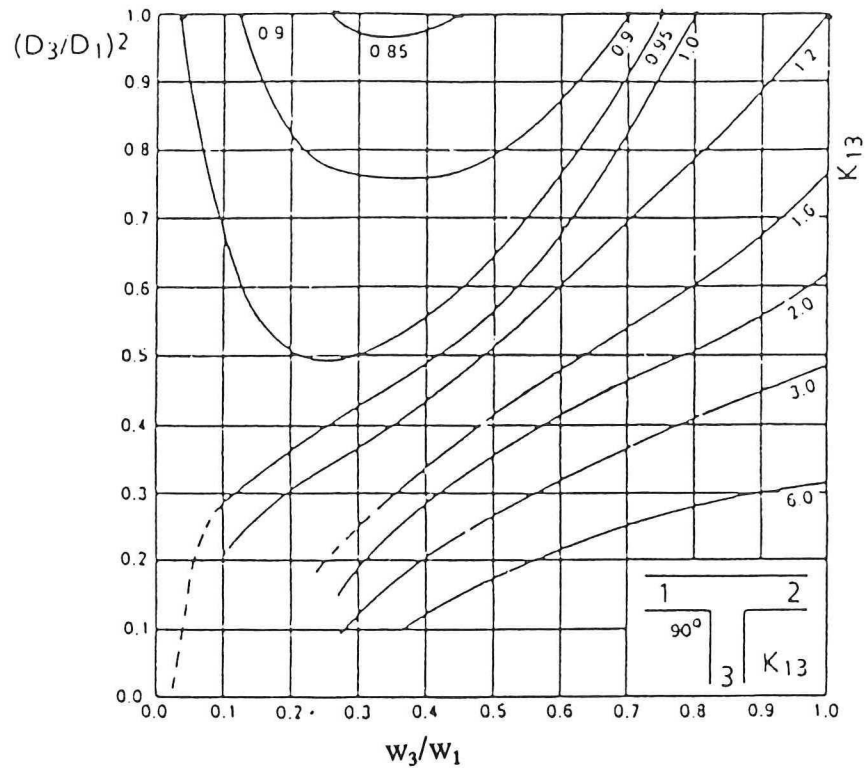

Figure 2.11. *Inlet-to-branch friction coefficient as a function of the mass extraction ratio and the branch-to-inlet diameter ratio, for single-phase flow*

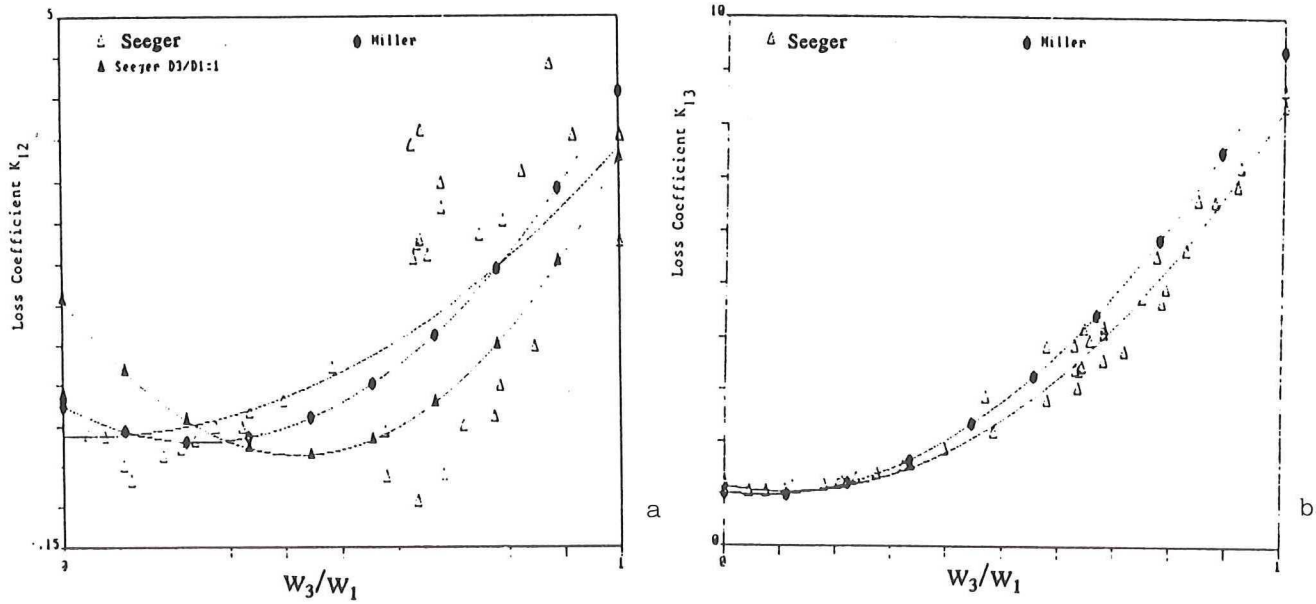

Figure 2.12. *Determination of friction coefficients as a function of the mass extraction ratio, for $D_3/D_1 = 0.52$, (a) inlet-to-run, (b) inlet-to-branch*

Seeger states that in the very low extraction region, the branch quality x_3 equals 1, even for bubbly flow, this is supported by Reimann, Brinkmann and Domanski [3]. The following equation is proposed to estimate the maximum value of g_3 where x_3 is still 1:

$$g_{3,max,where\ x_3=1} = A_G * 0.23(gD_3(\rho_L-\rho_G)\rho_G)^{0.5} \tag{2.14}$$

In this equation, $A_G = 0.5$ for bubbly flow in the inlet, and $A_G = 1$ for other inlet flow regimes.

2.5.4. Modeling the pressure drop

Pressure loss phenomena are quite hard to describe because theoretical models require *local* void fractions and velocities, which are very difficult to measure. Thereby, the flow mechanisms in the T-junction are very complex and poorly understood.

In modeling the pressure drop caused by a T-junction, this drop is usually split into a reversible and an irreversible part (as described in section 2.4):

$$(\Delta p_{1i})_J = (\Delta p_{1i})_{J,\ REV} + (\Delta p_{1i})_{J,\ IRREV} \tag{2.15}$$

For single-phase flow, these two pressure drops are calculated as follows:

$$(\Delta p_{1i})_{J,\ REV} = \frac{1}{2}\left(\rho_i u_i^2 - \rho_1 u_1^2\right) \tag{2.16}$$

and

$$(\Delta p_{1i})_{J,\ IRR} = K_{1i}\frac{1}{2}\rho_i u_i^2 \tag{2.17}$$

In one phase flow, generally $\rho_1 = \rho_i$. The loss coefficients K_{12} and K_{13} depend on D_3/D_1 and w_3/w_1. In figure 2.11 K_{13} is given as a function of these parameters [17]. In figures 2.12 a and b both friction coefficients are given as a function of w_3/w_1, for $D_3 = 0.52 * D_1$, which comes closest to the ratio involved in this project [3].

For two-phase flow, things are not so well known. Generally, a two-phase pressure drop is calculated as a derivation from the single-phase pressure drop, according to:

$$(\Delta p_{1i})_J = (\Delta p_{1i})_{J,\,REV} + K_{1i}\frac{1}{2}\rho_{L_1}\overline{u_1}^2 \cdot \varphi \tag{2.18}$$

Note that in the irreversible term, the mean *upstream* velocity is used instead of the *downstream* velocity which was used in the single-phase equation. The parameter φ is the so-called two-phase loss multiplier. For this multiplier several models exist.

Modeling the *inlet-to-branch* pressure drop the most simple model is acquired by assuming homogeneity in the inlet and branch. This model is termed the homogeneous model (hm):

$$(\Delta p_{13})_{J,\,REV} = \frac{1}{2}\overline{\rho_3}\left(\overline{u_3}^2 - \overline{u_1}^2\right) \tag{2.19}$$

and the homogeneous two-phase loss multiplier:

$$\varphi_{hm} = \frac{\rho_{L_1}}{\overline{\rho_1}} \tag{2.20}$$

The friction coefficient K_{13} is taken from single-phase flow measurements.

The Chisholm model (cm) is used quite often, for example in the model of Saba and Lahey. Chisholm uses the same expression for the reversible pressure drop as given above, but the following model for the two-phase loss multiplier:

$$\varphi_{cm} = (1-x_1)^2\left(1 + \frac{C_{13}^*}{X_{tt}} + \frac{1}{X_{tt}^2}\right) \tag{2.21}$$

in which X_{tt} is the so-called Lockhart-Martinelli parameter:

$$\frac{1}{X_{tt}} = \left(\frac{x_1}{1-x_1}\right)\left(\frac{\rho_L}{\rho_G}\right)^{0.5} \tag{2.22}$$

and

$$C_{13}^* = \left[1 + (C_3-1)\left(\frac{\rho_L-\rho_G}{\rho_L}\right)^{0.5}\right]\left[\left(\frac{\rho_L}{\rho_G}\right)^{0.5} + \left(\frac{\rho_G}{\rho_L}\right)^{0.5}\right] \tag{2.23}$$

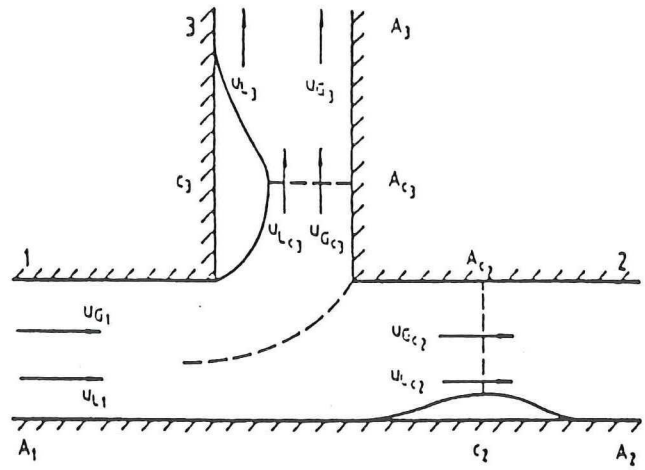

Figure 2.13. Illustration of the 'vena contracta' (c_2 and c_3) in Reimann's model

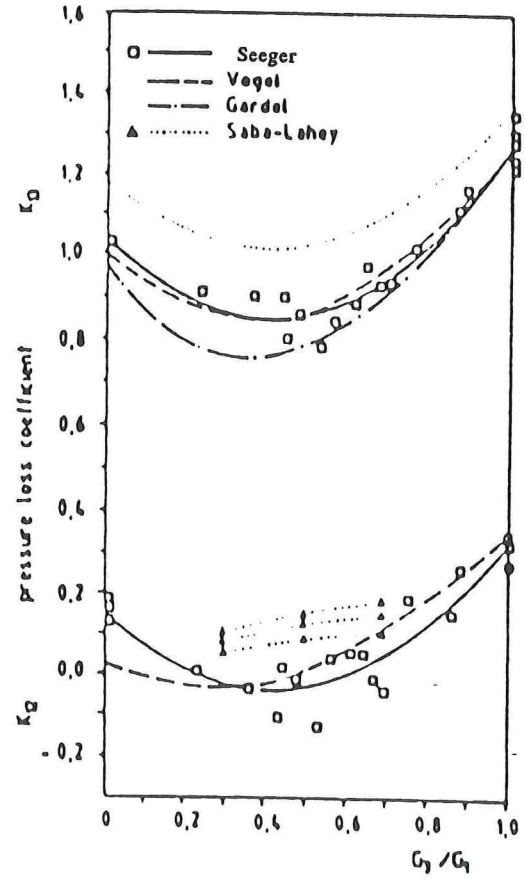

Figure 2.14. Polynomial determination of friction coefficients K_{12} and K_{13} as a function of the mass extraction ratio

C_3 has a value of 1.75 for stratified flow, and a value of 1 for homogeneous flow. Lahey uses these equations with the following polynomial expression of K_{13}:

$$K_{13} = \left[1.18 - 0.8\left(\frac{w_3}{w_1}\right) + \left(\frac{w_3}{w_1}\right)^2\right]\left(\frac{A_1}{A_3}\right) \tag{2.24}$$

Reimann and Seeger developed quite a complex model (the rsm) , assuming the inlet-to-branch flow passes a so-called 'vena contracta' first, before occupying the entire branch area [18]. This assumption is depicted in figure 2.13. The Reimann and Seeger model involves local slip (defined as gas velocity divided by liquid velocity) and local gas volume fractions. As these usually are quite hard to determine, finally quite rigid assumptions were made like homogeneity for all legs (so all slips equalled unity), resulting in an alternative expression for the two-phase loss multiplier:

$$\varphi_{rsm} = \frac{\rho_{L_1}\overline{\rho_3}}{\overline{\rho_1}^2} \tag{2.25}$$

K_{13} is determined using the following polynomial:

$$K_{13} = 1.0369 - 0.9546\frac{w_3}{w_1} + 1.2123\left(\frac{w_3}{w_1}\right)^2 \tag{2.26}$$

This polynomial is depicted in figure 2.14, together with a model for K_{12}, which Reimann and Seeger developed using quite a complex model they did not simplify.

For all the models mentioned, a correction factor K was proposed, determined from measurements at total takeoff. This resulted in an empirical model:

$$(\Delta p_{13})_J = (\Delta p_{13})_{J,\,REV} + K(\Delta p_{13})_{J,\,IRREV} \tag{2.27}$$

K equals 1.34 for the homogeneous model and 0.85 for the other models.

For the *inlet-to-run* flow one mostly assumes that the irreversible pressure drop is neglegible, so the pressure drop is mainly due to velocity changes. However, some pressure loss occurs, resulting from effects around the T-junction itself. This is accounted for in the so-called empirical pressure recovery coefficient K_{12} (determined from single-phase flow measurements), which is less then unity (in this case, the term *reversible* pressure drop is of course somewhat inaccurate):

$$(\Delta p_{12})_J = (\Delta p_{12})_{J,\,REV} = \frac{1}{2} K_{12} \left(\overline{\rho_2}\,\overline{u_2}^2 - \overline{\rho_1}\,\overline{u_1}^2 \right) \tag{2.28}$$

K_{12} is determined empirically by:

$$K_{12} = 0.11 + \frac{5.0}{\left[\frac{g_1 D_1}{\mu_{L_1}} \right]^{0.17}} \tag{2.29}$$

For the upward branch horizontal T-junction, the Reimann and Seeger model gives better predictions for $w_3/w_1 < 0.15$ then the homogeneous model and the Chisholm model. Above this value, all models give comparable results. The Reimann and Seeger model deviates from measurements at higher takeoff rates.

2.6. Expectations for this project

This graduation project deals with a horizontal upward reduced T-junction. In a horizontal T-junction, the orientation of the branch is of major importance. The phase separation is most pronounced when the branch is oriented upward, because the gravity effect and the inertia effect reinforce each other.

In horizontal flow, the majority of the gas resides in the upper part of the pipe, independent of the flow regime (this phenomenon is roughly sketched in figure 2.3). Thus it may be expected, that with an upward oriented branch, at very low takeoff rates, only gas is extracted ($x_3 = 1$). In the phase separation plot, this is shown by a horizontal line at $(x_3/x_1) = (1/x_1)$ -of course, the ratio of branch-to-inlet qualities can never exceed this value. At a certain takeoff rate, liquid will be extracted into the branch, and the curve will start to deviate from this horizontal line. This

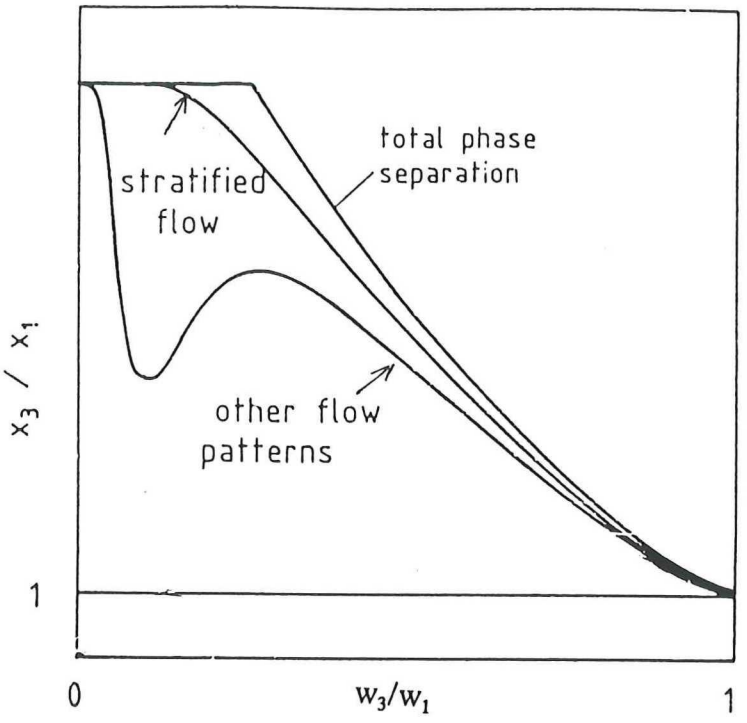

Figure 2.15. Different appearances of the phase separation plot due to different flow regimes

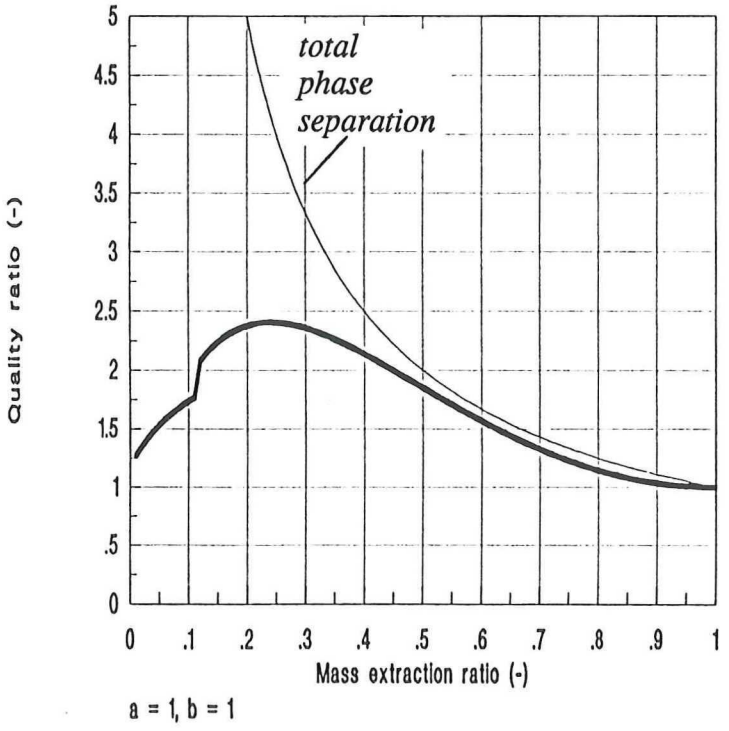

Figure 2.16. Graphical representation of Zetzmann's model

tendency is shown in figure 2.15. Of course, this effect is most pronounced at stratified flow conditions. At other flow patterns, several authors expect that the phase separation curve may yield another 'maximum' at $w_3/w_1 > 0$, as is measured many times in a horizontal *dividing* T-junction [e.g. 4]. This has not been proved yet, one can however expect that this maximum is that close to $w_3/w_1 = 0$, that it cannot be measured adequately enough, because of the slope of the curve being very steep in that region.

Mainly because in the upward oriented branch the liquid 'tries' to flow back into the run, due to the gravity effect, secondary flows can occur quite easily. This makes the flow split in a horizontal upward T-junction even more difficult to describe.

When invoking the model of Zetzmann, using the table presented in the Encycopaedia of Fluid Mechanics (table 2.2), one would take $a = 0.8$ and $b = 1$. However, this leads to strange results which do not satisfy boundary conditions. For instance, x_3/x_1 is less then 1 for higher extraction rates. As already mentioned, Zetzmann himself only mentions recommandation values of b. To me, it seems most reasonable to use $a = b = 1$, because in that case, boundary conditions at high and low mass extraction rates are satisfied. The Zetzmann model then looks as given in figure 2.16. However, in that case, the predictions for x_2/x_1 are rather bad.

As to phase separation, combining Seeger's empirical 'engineering' model with the fact that a reduced T-junction usually renders better phase separation than a straight one, leads to the expectation that the 'phase separation line', will lay between the total separation line and Seeger's model. Using Seeger's equation for the maximum branch mass flux without liquid entering the branch (equation), and estimating that the maximum density the air will obtain is 1.8 kg/m^3 (about 0.5 bar overpressure), the corresponding mass *flow* would be between about 30 and 80 g/s. This, taken into account that this mass flow should entirely exist of air, can be expected to be quite too much for this area of interest. Thus it might be expected that Seeger's equation does not apply to this field of interest.
A maximum in the phase separation curve (at $w_3/w_1 > 0$) might be present at higher superficial liquid velocity (i.e. bubbly flow), but this might fall outside the measurement range.

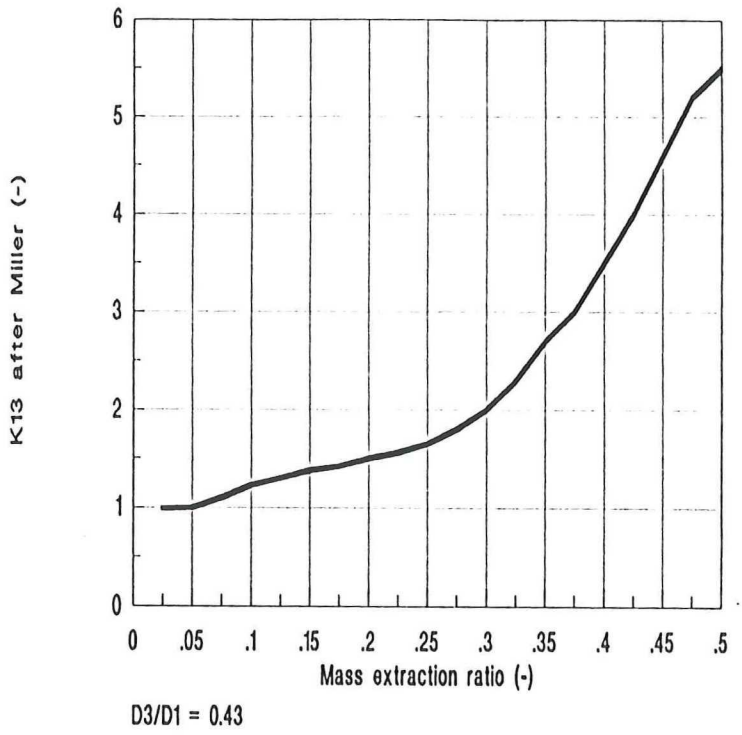

Figure 2.17. Prediction of K_{13} from Miller's graph, at present diameter ratio

The pressure drop of the inlet-to-run flow will be mainly reversible, caused by velocity changes. The pressure drop the inlet-to-branch flow experiences, will be caused by the flow 'turning the corner', by velocity changes and by height differences. So the reversible as well as the irreversible part will play a role. Using the picture of Miller (figure 2.11) for K_{13}, and combining this for the D_3/D_1 ratio for this project ($\{D_3/D_1\}^2 = 0.19$) the dependence of K_{13} on w_3/w_1 is as shown in figure 2.17.

Pressure drop in the T-junction due to friction will be quite neglegible, as can be understood using the Blasius equation [19], which gives the friction factor 4f for high Reynolds numbers Re (with μ = viscosity) for a single-phase flow:

$$4f = 0.316\ Re^{-0.25}\ ,\quad Re = \frac{\overline{\rho_1}\,\overline{u_1}\,D_s}{\mu_L} \tag{2.30}$$

which results in a pressure drop due to friction, calculated according to:

$$\Delta p = 4f \cdot \frac{1}{2}\,\overline{\rho_1}\,\overline{u_1}^2\,\frac{L}{D_1} \tag{2.31}$$

In these expressions D_s is a specific length scale of the system and L is the length of the T-junction. Thus, the pressure drop over the 2 meters of the T-junction is never above about 50 Pa, which is even less then the inaccuracy of the pressure transducers. This is mainly due to the relatively small L/D-ratio.

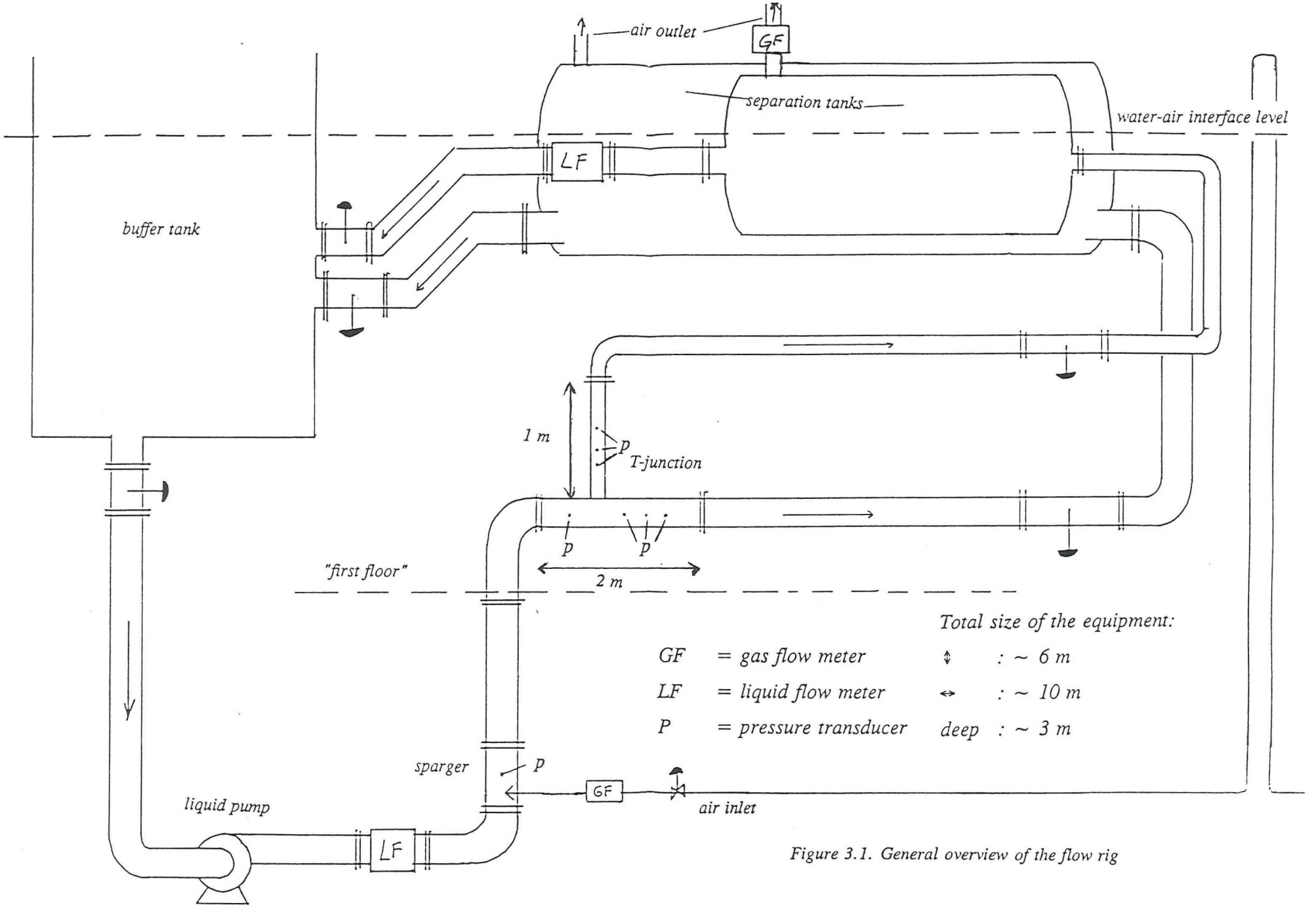

Figure 3.1. General overview of the flow rig

3. EXPERIMENTAL

3.1. Equipment

3.1.1 Flow rig

The equipment that was constructed for the project is shown schematically in figure 3.1.
The water was pumped out of the large buffer tank (see section 3.1.5) by means of a centrifugal pump. After having passed a liquid flow meter (sec. 3.2.1) the water entered a vertical section, in which the air was injected using a special sparger (sec. 3.1.3). The two-phase flow thus generated passed another bend, and immediately entered the T-junction (see next section). The purpose of the vertical section of the pipeline system is discussed in section 3.3.2.

After having split in the T-junction both the branch and the run flow passed a valve which were used to obtain a certain desired mass extraction rate. After this, each flow was brought into a separation tank (residence tanks, sec. 3.1.4), in which they were splitted in their respective liquid and gas flows. The branch liquid flow was measured after its separation tank. Using a steady state liquid mass balance, the run liquid flow equalled the difference between the total liquid flow and the branch liquid flow measured.
Both the branch and the run liquid flow back into the buffer tank again. In this section, no pump was used, the 'backstreaming' was only induced by the height difference between the water-air interface in the buffer tank and the separation tanks.

The inlet gas flow was measured before the air entered the equipment. On top of the two residence tanks a second gas flow meter was installed, to measure the branch or the run gas flow. By using two three-way valves it was possible to measure either of these using only one gas flow meter.

Several interesting sections of the pipeline system were made of perspex, to be able to watch things happen. Apart from the T-junction itself, the pipe immediately following the sparger and a -vertical- part of the run were made of perspex. Thus we could check if the mixing of the two

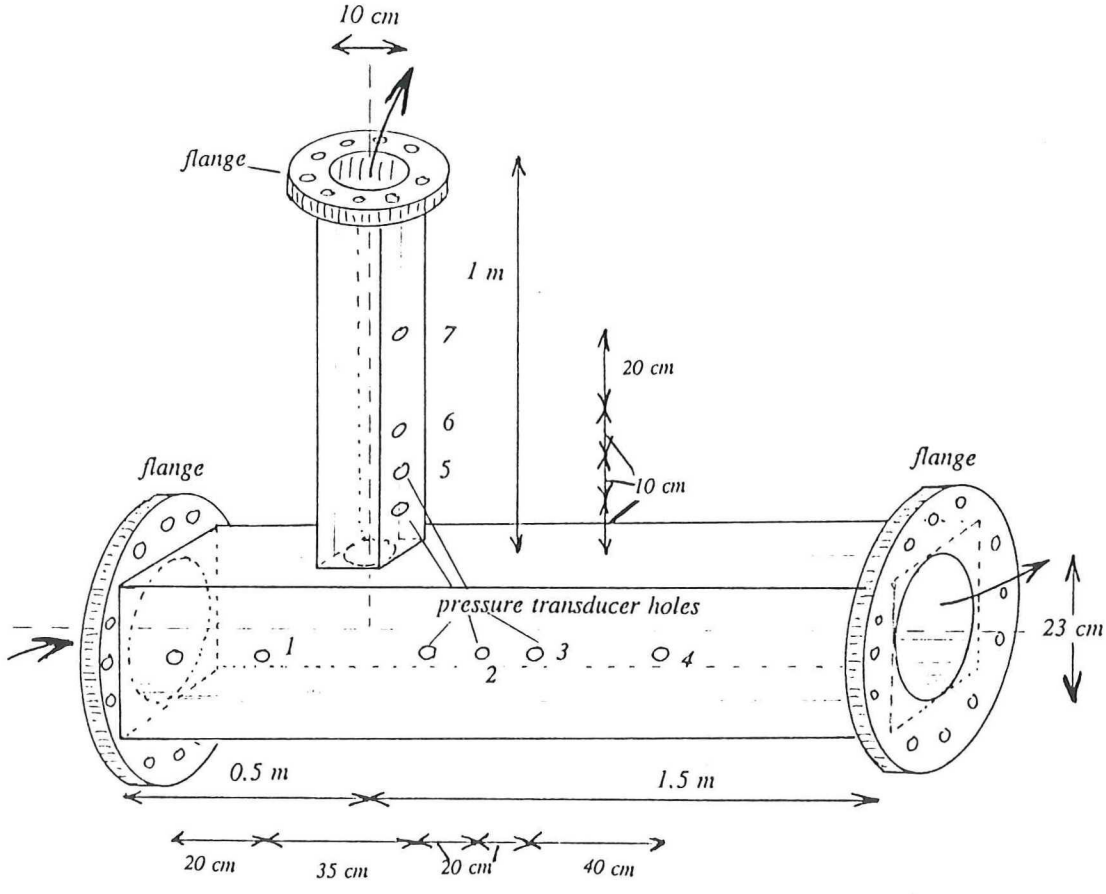

Figure 3.2. The T-junction

phases was well enough, and we could have a look at the flow regimes in the vertical section of the run. A major advantage of the perspex sections turned out to be that we could see pulses, induced by slugging in the branch, propagating through and appearing everywhere in the equipment. That this was quite an important aspect of this project will be become clear in chapter 4.

As this project dealt with industrial scale sizes and flows, the apparatus and other devices were rather big. The equipment was therefore built within a construction framework, the top of the equipment thus reaching two 'stocks' high (see sizes in figure 3.1). At the 'ground level', the pump, the inlet liquid flow meter and the air sparger were placed. The T-junction was built at the 'first floor', because of the vertical pipe having to precede it. At this same level, a 'control room' was arranged, in such a way that all important switches and valves, as well as the data acquisition computer (sec. 3.2.4), were all at that same level. The liquid pump was steered by a remote control unit. The 'second floor' contained the separation tanks and the two outlet flow meters. The large buffer tank comprised two stocks.

3.1.2. The T-junction

The T-junction is shown in figure 3.2. The junction was made out of perspex, in order to enable visualisation studies like photography and videorecording. The inlet-and-run consisted of a 2 meters long, 23.0 cm inner diameter pipe, the branch (10.0 cm inner diameter) was 1 meter long. The distance between the front end of the junction and the splitting point was 50 cm.
The junction was connected to the equipment with three flanges, also machined out of perspex, the branch was connected to the inlet-and-run using flanges as well. This was done to, in future projects, be able to disconnect and change the T-junction itself easily (e.g. turn it around or change its orientation), or to test various mechanical modifications inside the T-junction which might have serious impact on the phase separation.

To reduce distortion problems in observing the T-junction, the junction was put into a square-shaped box. The space between this box and the tubes of the junction was filled with water. Because perspex and water have approximately the same refractive index, distortion was

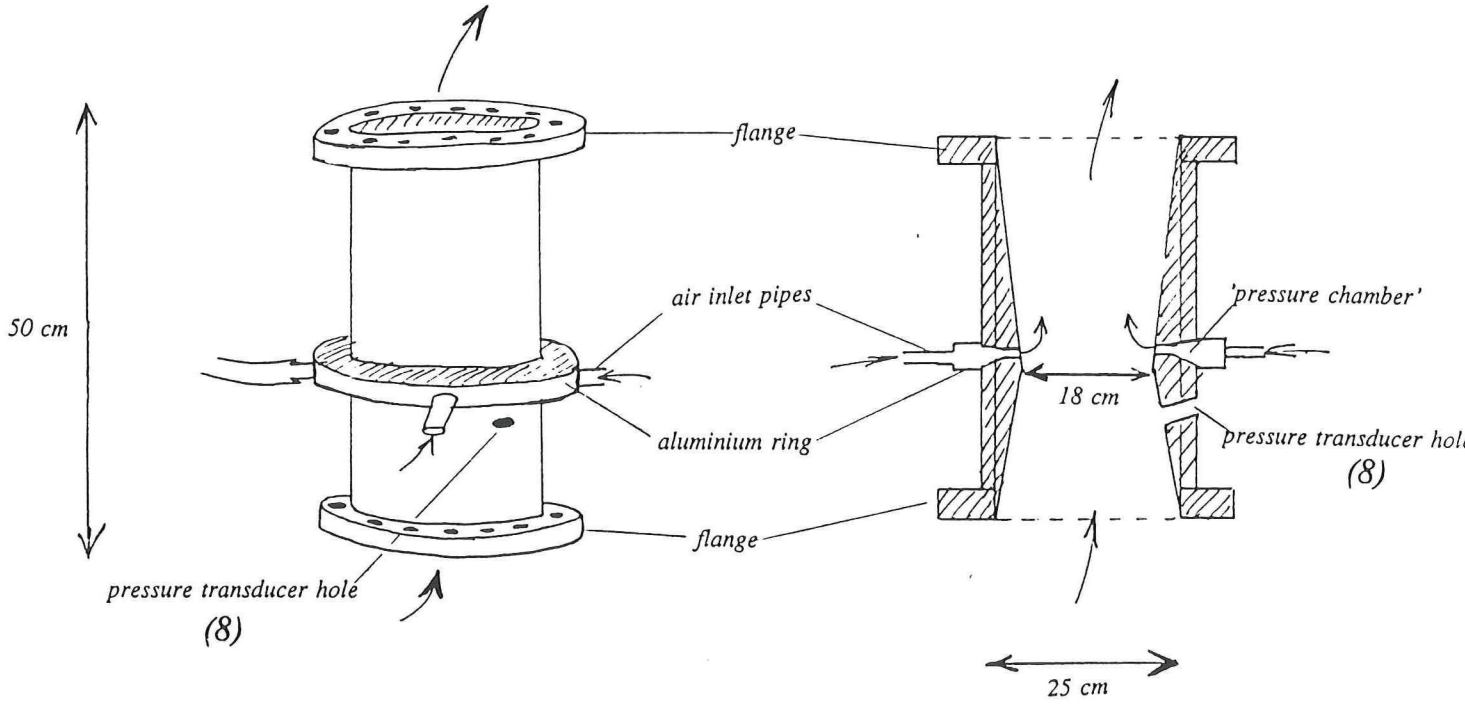

Figure 3.3. The air inlet sparger, general and technical view

diminished to an acceptable level. To minimize algae growth in this box, demineralized water was used. An anti-algae medicin could not be used, because of the danger it would dissolve the chloroform used to glue the perspex, and thus cause leakages.

To measure the pressure at various places over the T-junction, several holes were made at several places in the inlet, branch and run. Into each of these either a pressure transducer could be fixed, or it could be closed off by means of a screw-like cap. The holes were dimensioned in such a way, that the front end of the pressure transducers would be flush with the inner surface of the tube.

3.1.3. Air inlet

Special attention had to be given to the way in which the air could be brought into the water-flow. It had to be taken into account that, on the one hand, a large amount of air had to be injected (up to 60 Nm^3/h) and, on the other, the bubbles should not be too large, in order to prevent coalescence at large scale. Conventional ring spargers that could cope with both these requirements, however, appeared to be too large to fit in the piping network without demanding special modifications.

The sparger that was designed and built for this project is shown in figure 3.3. It was machined out of PVC, and, to promote the mixing of the air and water, it was made in a conical shape, like a venturi-tube. The diameter of the pipe decreased gradually until the point of air injection, where it would reach a minimum. By increasing the diameter slowly again, the air would not remain at the outer part of the tube, but spread over the tube area more or less homogeneously.

At the position of the diameter minimum, an 'air chamber' was made. This air chamber was closed off by an aluminium ring, containing four holes through which the air was blown in. The air used was taken from the laboratory network and was brought into the sparger by means of four equivalent PVC tubes, after having passed a reduction valve (which reduced the overpressure to approximately 1.5 bar) and a control valve. To prevent water entering the air pipeline system in

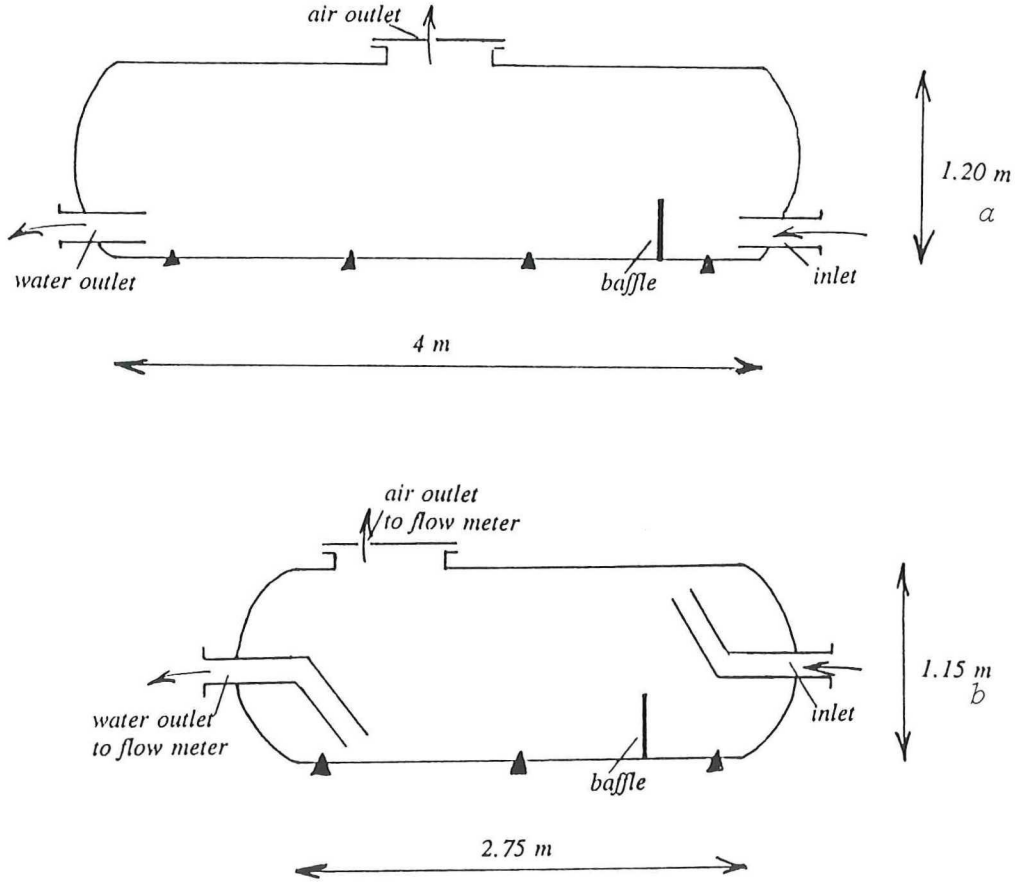

Figure 3.4. The separation tanks: (a), inlet-to-run tank, (b), inlet-to-branch tank

case of an accident, the air pipeline was first led above the highest possible water-air interface level, before actually entering the sparger (see also figure 3.1).

The air injection itself took place through 50 small holes (3 mm diameter), which were drilled around the tube periphery at the position of smallest diameter. In this way, the air was injected homogeneously across the periphery of the sparger, as could easily be observed in the perspex pipe immediately following the sparger.

3.1.4. Separation tanks

Figure 3.4 shows a sketch of the separation tanks.
Both the run and branch flow had to be separated into their gas and liquid phases, to determine the phase separation. This is done by using two 'knock-out' tanks, in which a two-phase flow is split by gravity. The volume needed in both tanks was estimated taking into account the magnitude and composition that the different flows were expected to have, and using simple stokes-like bubble rising and drop falling calculations as well as several corrections for this model (see e.g. [20]). Both tanks were overdesigned by approximately a factor two.
In both tanks, a baffle was fixed, to prevent air shortcut, i.e. air that would leave the tank through the wrong (liquid-) outlet, immediately after having entered the tank. In this way, the flow was forced to rise a small distance, hence a better phase separation could be expected.

The tank connected to the run (figure 3.4 a), had a volume of 5 m^3 (1.20 m diameter and 4 m long). It was made of 3 mm steel, and powder-coated against oxidation. As it was completely unprocessed when it arrived at the laboratory, it was easily modified to our wishes, the entrance and liquid exit being fixed as much to the bottom of the tank as possible.

The branch tank (figure 3.4 b), which had a volume of nearly 3 m^3 (1.15 m diameter and 2.75 m long), was made of stainless steel. It had already been used in another process, and thus had flanges and connecting points already attached to it. These were in the centre of both sides of the tank, so the inlet and outlet pipes had to be curved within the tank. This arose another problem: at slugging flow conditions in the branch, the slugwise entering of the water resulted in a trembling

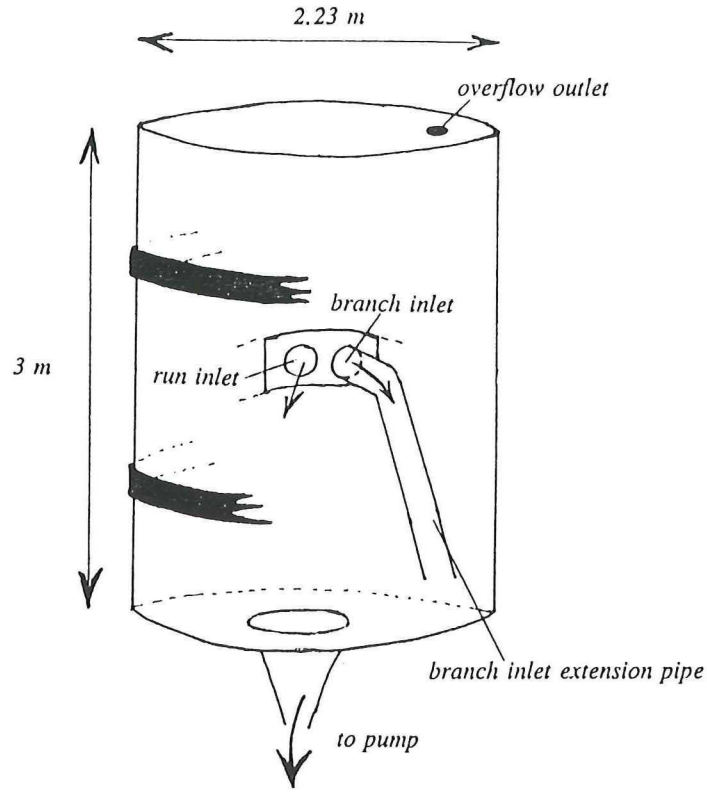

Figure 3.5. The buffer tank

and shaking of the tank, that could be felt throughout the entire equipment and construction framework. This appeared to be rather dangerous. By turning the entering pipe up, this problem was solved, although now the baffle, of course, was of little use.
This tank had two small windows in it, which enabled us to observe the process of flow separation in the tank.

3.1.5. Buffer tank

The buffer and storage tank that was used (figure 3.5) contained 12 m^3 of water (2.23 m diameter and 3 m high). This tank was already present at the laboratory and could be used without large modifications.
About half-way the project, one modification was made: at high liquid flows the height of the water in the tank would get below the pipe inlets coming from the separation tanks. This resulted in air entering the pipe between the branch tank and the buffer tank, making accurate measurements of the branch liquid flow quite impossible.
By attaching a curved pipe to this inlet, which reached to the bottom of the buffer tank, the liquid level of the tank could get lower, without endangering the measurements. This resulted in a significant increase of the amount of water that could be pumped around without problems, and thus in a larger parameter area that could be investigated.

3.1.6. Process safety

The equipment is 1 to 1 to industrial scale. This results (apart from large diameters and tanks) in a very large amount of water present in the system (about 20 m^3). Hence we were obliged to take several precautions against possible accidents with large amounts of water coming down. One of the safety precautions has already been mentioned in section 3.1.3, preventing the water in the system entering the air inlet pipelines.

The pump that was used was a centrifugal pump. When one of the valves would accidentally be closed while the pump was switched on, this kind of pump (being a non-displacement type pump)

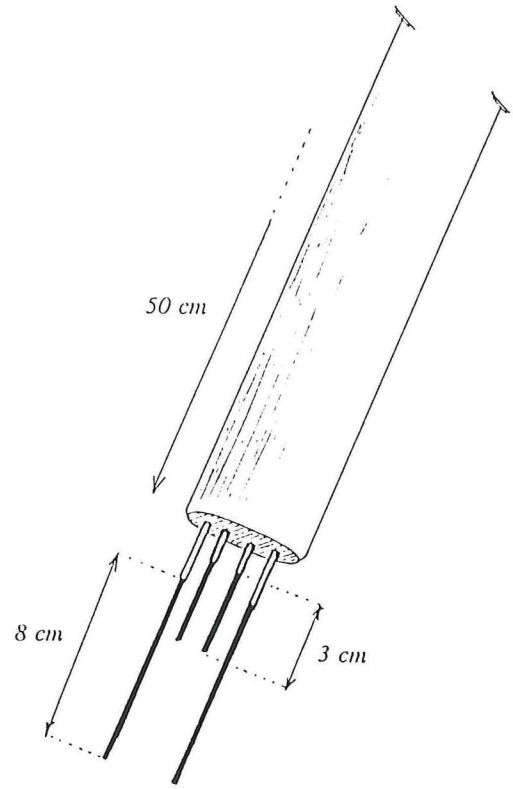

Figure 3.6. Level switch

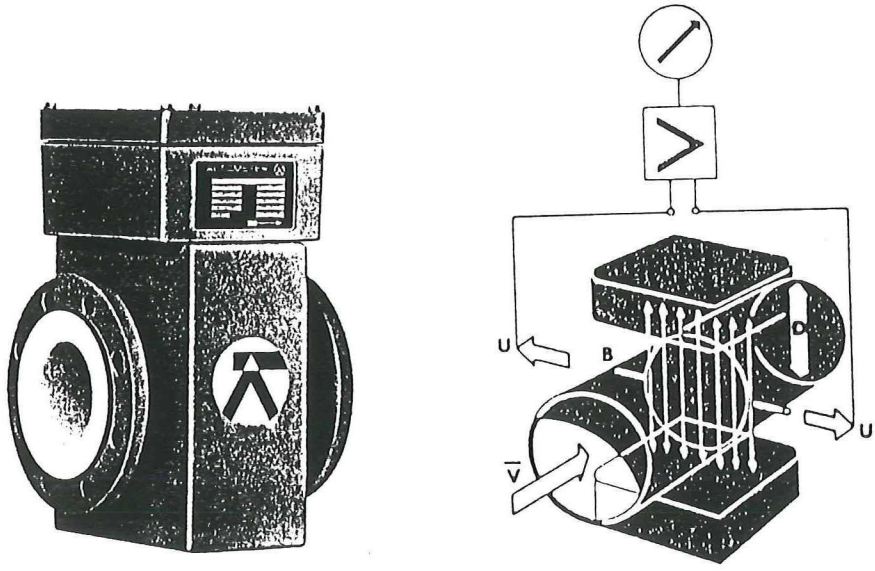

Figure 3.7. Picture and principle of operation of a liquid flow meter: B = magnetic field strength, U = induced voltage

could end up rotating in the same small amount of liquid, and damaging itself quite severely. To prevent this, a simple measure was taken using the liquid flow meter directly following the pump: when this flow meter measured a flow below a certain critical setpoint for more then 30 seconds, the pump was switched off automatically.

Another safety measure that had to be taken was due to underestimation of the height differences between the water-air interface levels that were needed to let the water flow back to the buffer tank, in order to reach a steady state. At high volume flow, these differences could become that large, that one of the separation tanks could overflow. At one of the first test-runs, this had appeared to be quite possible.

To prevent such thing to happen again, which would cause severe damage to either the measuring equipment or the data acquisition unit, level switches were placed in both tanks. Such a level switch is shown in figure 3.6. When the water level would reach the longer contact pins, a warning signal was given. When the shorter pins contacted the water, indicating things were really getting critical, an alarm sound was heard, and the pump was shut off immediately. This system was directed within a small box, containing a green, an orange and a red LED, these of course representing the safe, warning and critical situation.

3.2. Measuring equipment and techniques

3.2.1. Liquid flow meters

The inlet and branch liquid flow were measured using magnetically inductive flow meters. The measurement is based on Faraday's law of induction, which states that when a conducting medium flows through a magnetic field, an electrical potential difference is generated over this medium, which is strictly porportional to the *average* velocity of the medium (see figure 3.7). By measuring the voltage induced at known magnetic field strength, this velocity can be calculated. By simply multiplying by the area of the pipe, the flow is known. The only condition to use this technique is that the medium should be conductive, other properties of the fluid like density or

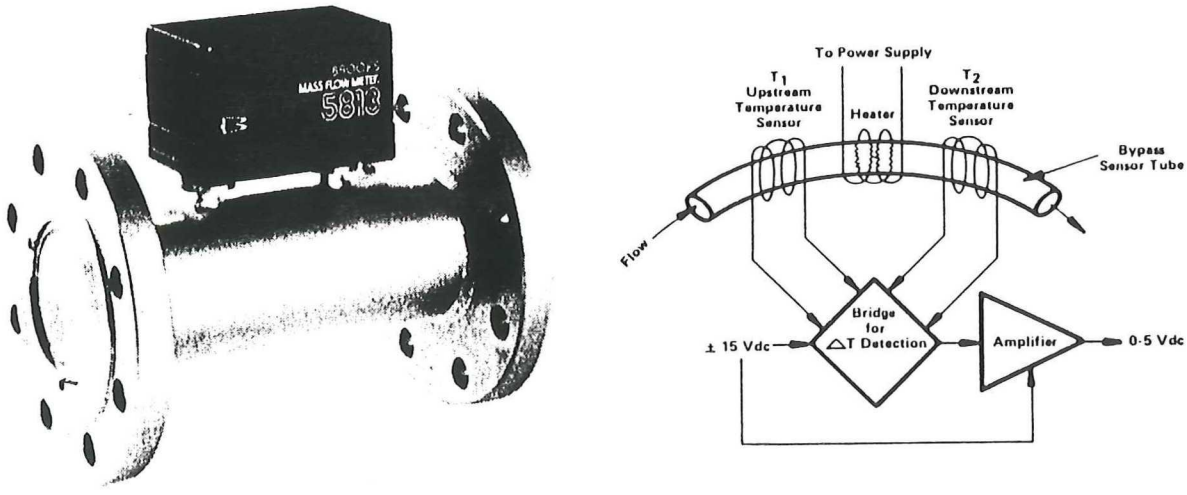

Figure 3.8. Picture and principle of operation of a gas flow meter

viscosity or even the flow profile across the area do not influence the measurement. This makes this technique quite generally applicable.

The flow meters used in this project generate an alternating magnetic field, thus inducing an alternating voltage across the area of the pipe, which gives a more accurate measurement. The potential is measured by two platinum electrodes.

Both liquid flow meters were designed to accurately measure velocities up to 2.00 m/s. As the diameter of the inlet liquid flow meter was 20 cm, this meant volume flows up to 226 m^3/h. The branch liquid flow meter was 15 cm diameter, so this one could cope with 127 m^3/h.
According to the calibration certificates accompanying the liquid flow meters, the measurement inaccuracy of both was beneath 0.4 % of the measured value, for measurements between 20 and 100 % of the full scale value. For measurements under 20 %, the inaccuracy could get as much as 0.2 % of the maximum value (that is, 0.45 and 0.25 m^3/h, respectively).

3.2.2. Gas flow meters

The inlet and outlet (branch *or* run) gas flows were measured using gas mass flow meters (figure 3.8). These flow meters separate a well defined portion from the gas flow that enters the meter, and put a well known amount of energy into this side-flow. By measuring the temperature rise and using the specific heat of (in this case) air, the part separated, and thus the total amount of gas flowing through, is known. This value is processed to a signal, indicating the amount of *normal* cubic meters per hour (Nm^3/h). This value can, of course, be corrected for the local pressure in order to obtain the local gas volume flow.
The advantage of this method is that it is independent of the pressure and temperature of the gas flowing through, as *mass* flow is measured. The specific heat (per unit mass) of a gas is, within limits, independent of pressure and temperature.

Both gas flow meters were arranged to measure flows of up to 60 Nm^3/h accurately. The calibration certificate said that, over the total range of calibration, the measurement inaccuracy was never over 0.75 % of the maximum value.

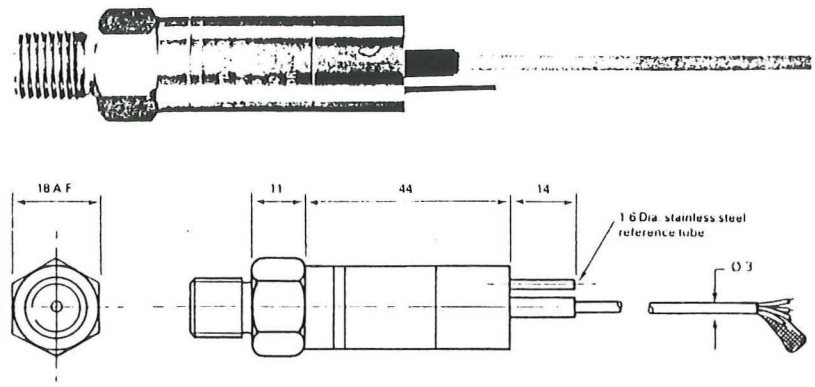

Figure 3.9. Picture and schematic view of a pressure transducer

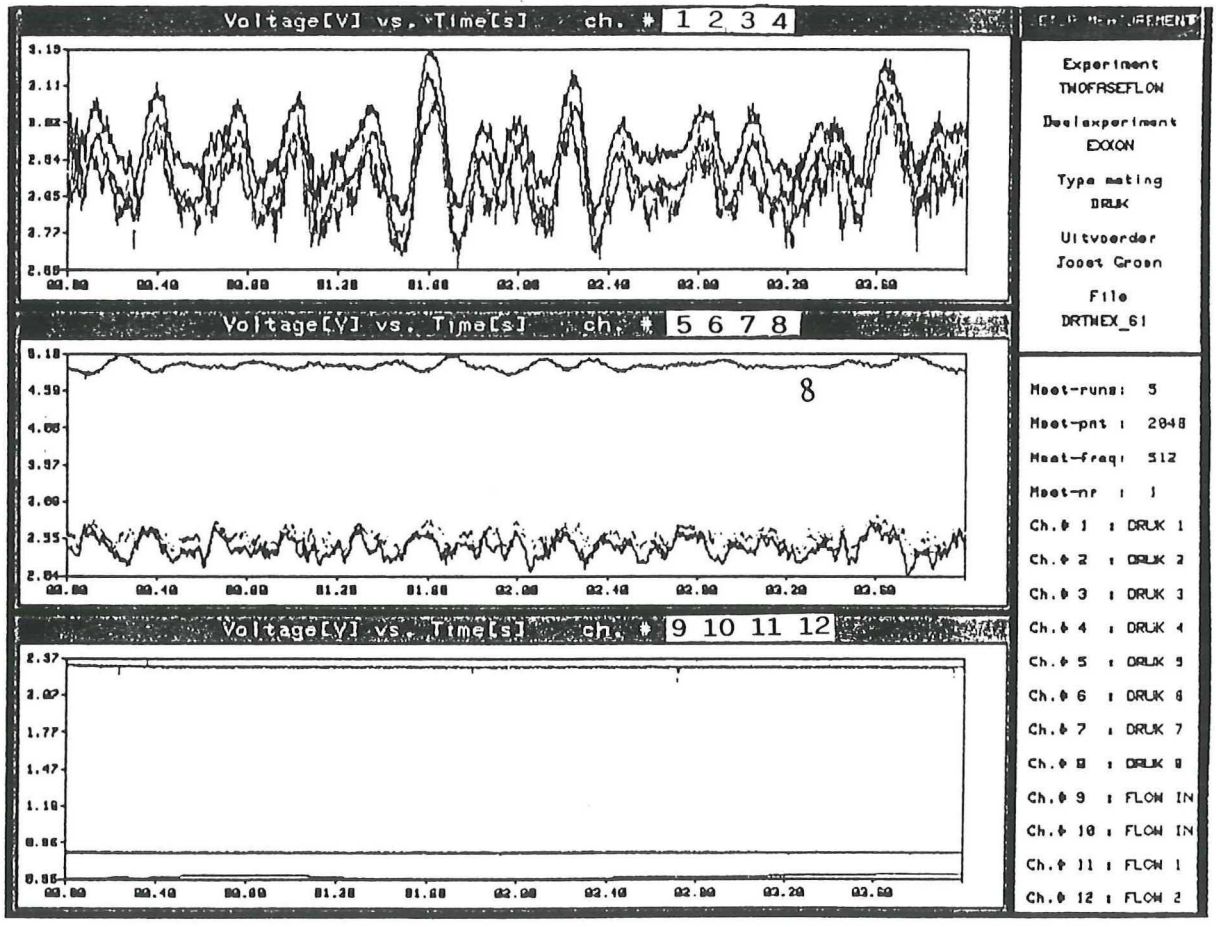

Figure 3.10. The monitoring screen as presented by the data acquisition program

3.2.3. Pressure transducers

The pressure transducers used are shown in figure 3.9. The method is based on change of resistance of a compound caused by deformation. Because of the pressure difference (with respect to the pressure outside the equipment) the silicon 'window' is deformed, resulting in a change of resistance of this window. So from the measured value of the resistance, and processing this to a voltage the pressure difference can be calculated.

Eight pressure transducers were available, of which seven were positioned in the T-junction: one in the inlet and three in the run as well as in the branch. The eighth pressure transducer was placed in the sparger. This one was used for monitoring whether the pressure of the water in the sparger wouldn't get too high. If that would happen, the pressure drop between the air inlet and the water flow could get that low, that the reduction valve had to be adjusted in order to maintain a desired inlet air flow.
The transducers were able to measure pressure differences between -1.5 and +1.5 bar. The measurement inaccuracy was claimed to be lower than 0.5 % of the maximum value, over the total range of calibration.

3.2.4. Data acquisition, monitoring and processing

The eight pressure transducers, two gas flow meters and two liquid flow meters resulted in twelve signals to be measured, preferably simultaneously. This was accomplished using a Hewlett Packard HP 3852A data acquisition and control unit, and a Hewlett Packard HP 340/9000 workstation. Simultaneous measuring was made possible using a HP 44711A high speed FET multiplexer, which can switch at a maximum frequency of 100 kHz. This provided a maximum sampling frequency of over 8000 Hz, which was quite sufficient.

Software for measuring the signals and showing the measured signals on screen was already present in the laboratory and had only to be modified slightly to be able to cope with twelve channels at a time. An example of the screen is given in figure 3.10. As this program did not

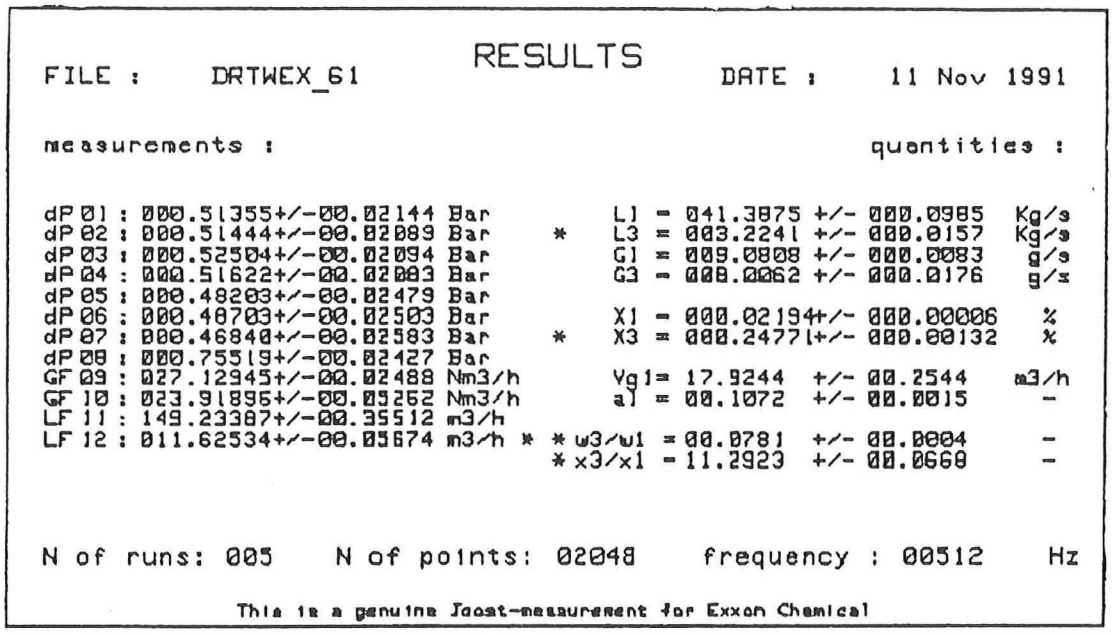

Figure 3.11. Appearance of the result-window

provide continuous monitoring, the most important signals (i.e. the four flow meter signals) were monitored using a control unit containing four voltmeters. This enabled us to detect disturbances in the steady state (for instance when the liquid pump was developing its own will) and to nullify these more easily.

To process the measured data a procedure was incorporated in the data acquisition program. This procedure calculated the flows and pressure drops from the measured voltages as well as several quantities deduced from these data, like mass flows, flow qualities, the mass extraction rate, etc. Thereby, it calculated the deviation in the measurements and the accuracy of the derived quantities. This was all brought on screen in a result-window, of which an example is given in figure 3.11.
The processing procedure contained several safety precautions, indicating when (unawarely) measurements were taken outside the calibration area of the different equipment. These 'questionable' measurements, as well as quantities that were calculated using these, were indicated in the results window by an asterisk (see figure 3.11).

To determine the measuring frequency and time necessary to get representative signals, the various signals were first investigated using a transiscope which could calculate the fourier spectrum of a measured signal. The maximum frequency present in the pressure transducer signals appeared to be approximately 200 Hz. The signals of the gas and liquid flow meters did not contain any frequencies higher then this. As both the sampling frequency and the measuring time should be powers of two, a sampling frequency of 512 Hz was used.
To determine the time needed for a representative signal, measured values made at different measuring times were compared. It appeared that the measured values did not change significantly at measuring periods of four seconds or larger. Thus a measuring time of four seconds was used in the project. Every measurement was done five times and the results were averaged.

3.3. Area of interest

3.3.1. Parameter space

The indications for the area of interest of this project were given by Exxon Chemical. The focus was put to a liquid superficial velocity of about 0.5 to 1.0 m/s, whereas the gas superficial velocity should be covering the area between 0.05 and 0.15 m/s.
The phase separation behaviour should be investigated within the region of 'interesting' takeoff-rates, which in practice meant at mass extraction rates up to about 50 %.
All experiments were performed at room temperature and no special higher-pressure conditions were required. Thus, the slight overpressure in the system was due to the flow being pumped around.

3.3.2. Flow regime requirements and consequences

Using the flow map given in figure 2.4 a, it could be expected that the inlet flow regime would be stratified (either smooth or wavy) in the lower liquid velocity region, and bubbly in the higher liquid velocity region. However, Exxon Chemical wanted bubbly flow to be investigated as much as possible. To cope with this requirement, a vertical pipe (see sec. 3.1.1) was built in the setup, just preceding the T-junction.
As can be seen from the flow map of figure 2.4 b, when the 'flows of interest' would be sent through a vertical pipe, almost certainly bubbly flow would occur. Because it takes a two-phase flow about ten pipe diameters to establish a new flow regime, it could be expected that when the vertical bubbly flow suddenly turned the bend and immediately entered the horizontal T-junction, at least at the junction itself the flow regime would *still* be bubbly.

3.4. Measuring program setup

3.4.1. Measurement series

A measurement series was executed at constant inlet liquid and gas flows. This because changes in these caused a long period of waiting until the rig was in steady state again. A certain mass extraction rate could be established by varying the position of the two valves in the run and the branch. The value of the mass extraction rate due to the position of the valves turned out to be quite independent of the inlet liquid or gas flow. Thus a desired mass extraction rate could be quite easily accomplished.

A measurements series started with establishing the desired liquid flow by means of the liquid pump. When the flow rig was in steady state (which could take over two or three hours), the desired amount of gas was injected using the inlet gas control valve. This was done with the run and inlet valves completely opened, inducing a mass extraction rate of about 28 %.

When the equipment had reached steady state again, measurements were started. First, a series was made while gradually closing the branch valve, thus gaining a series covering the mass extraction area between 0 % and 28 %. After this, the branch valve was opened again and a second series was started while gradually closing the run valve. This last series was continued until a measurement in the mass extraction region between 40 % and 50 % was made. Between two measurements mostly only about a quarter of an hour had to be waited, as the changes in the flows induced by changing the position of the valves were relatively small and thus a new steady state was reached quite quickly.

In this way series of about ten measurements were made. As the most interesting extraction area is that beneath 25 % takeoff, most of the measurements were performed in that area, and only two or three were made in the 30 to 50 % takeoff area, to make the picture complete.

3.4.2. Program setup

To be sure the area of interest was investigated representatively enough, the first thing to do was to make a flow map covering the parameter space. This was done by varying the gas and liquid flows within the area of interest, with the branch valve closed, so that the two-phase flow was enabled to fully develop, with as little influence of the T-junction s possible.

After the flow map had been made, measurement points were set out in such a way, that every occuring flow regime would be investigated and that the influence of the various variables, as well as those of possibly occuring flow regime transitions would be investigated.

The results calculated by the data acquisition unit were written down in an observation journal. The phase separation was represented by making separation plots and fraction plots (see sec. 2.3.1). The pressure drop over the junction was merely recorded and used to calculate the resistance coefficients K_{12} and K_{13} (see chapter 2).

During the project photographs were taken of interesting occurrences in the behaviour of the two-phase flow. These were meant merely to illustrate what was happening.

3.5. Error consideration

The accuracy of the quantities calculated is determined by several different sources. The measurement accuracy has already been mentioned in section 3.2. Reading errors or adjustment errors in the measured quantities do not occur mentionably, because the accuracy of the computer is quite high. Errors due to small variations in the measured signals during one measurement are taken into account by the processing program.

The main source of errors, is the fact that it is only possible within limits to check if the equipment is really in steady state. As mentioned, the steady state is believed to have appeared when the four volt meters indicating the four flow signals do not change significantly anymore. Thus the 'steady state error' *is* due to a reading error. This error is estimated to be two times the 'least digit' of the voltmeter. Within the region of interest this results in a maximum relative error of about 3 %.

In chapter 4 the errors will be treated further.

4. RESULTS AND DISCUSSION

Note: all the lines drawn between the measurements in the graphs in this chapter are strictly meant for *'guiding the eye'*. No prediction or interpolation properties whatsoever should be attributed to or gained from these.

4.1. Observations, trouble shooting

4.1.1. Problems in operation, trouble shooting

As already mentioned in chapter 3, the most important problem of operating the equipment was getting the rig in steady state and keeping it there. After the desired liquid and gas flow were set in, it could take over three hours to reach a steady state, especially when dealing with low inlet flows. During this period, both inlet flows had to be adjusted several times, so that eventually the desired steady state was reached. That this took so long was mainly caused by the fact that the liquid flows from the separation tanks to the buffer tank were entirely induced by gravity. Thus, the two height differences between the air-water interface levels should match these flows.
When this had been established, measurements were started. The relatively small changes in the flows between consecutive measurements resulted in intervals of 15 to 30 minutes between these measurements.
Problems in maintaining the steady state were reinforced by two reasons. First, because of other researchers extracting large amounts of air out of the same pressured air network sometimes a very sudden collapse of air inlet flow occured and second, because the liquid pump sometimes was developing a will of its own. By constant monitoring of the inlet flow signals, these unwanted changes could be nullified quite quickly, thus reducing the time needed to establish steady state again as much as possible. Still, something like this could easily cost another hour.

The gas flows were subject of trouble shooting more than once. The capillary tube of the outlet gas flow meter got choked several times, because of small rust-parts entering the meter together

with the air stream. This was repaired quite easily by using pressurized air to blow the capillary through. After several of these operations, it appeared that this flow meter had to be re-calibrated. A major question mark during the first half of the project was the fact that, at complete takeoff, always more air seemed to come out of the equipment than was put in. This turned out to be due to the fact that the air entering the sparger was practically dry, and the air leaving the separation tanks could be assumed to be saturated with water vapour, because of severe mixing of the two phases in the equipment. This phenomenon was then accounted for in the data processing program. It appeared that the outlet gas mass flow had to be divided by a factor of 1.02 to correct for water vapour. The calculation used to obtain this factor is given in appendix I.

Because the liquid flow meters operate by measuring a velocity, care should be taken not to let any air get caught in the pipe leading from the branch separation tanks to the buffer tank. As mentioned in section 3.1.4, the liquid outlet pipe did not enter this separation tank at the bottom, but in the centre, and it curved towards the bottom inside the separation tank (see figure 3.4.b). At very low extraction rates, it could happen that the air-water interface level in this tank could get that low, that air entered this pipe, thus spoiling the experiments. This problem was solved by, at lowering takeoff rates, gradually closing the valve in this pipeline. This increased the flow resistance of this pipe, requiring a larger height difference to maintain steady state. In this way the air-water interface level could be maintained above the entrance of the liquid exit pipe. As the branch separation tank contained two windows, this requirement was easily monitored, using a lamp shining through one window, and watching through the other. In the pipeline two small valves were made, to let entrapped air out of the equipment.
Another measure to prevent air entrapment in this pipeline has already been mentioned in section 3.1.5: the extension of the inlet pipe in the large buffer tank.

In section 3.1.6 already has been mentioned that, at higher flow rates, the run separation tank could overflow. This could lead to incomplete measurement series, or to the fact that no measurements could be taken at very high superficial velocities. This was remedied by simply attaching a PVC tube to the gas outlet of this tank, so that any overflowing water would be led to the buffer tank. This was referred to as 'controlled overflow'.

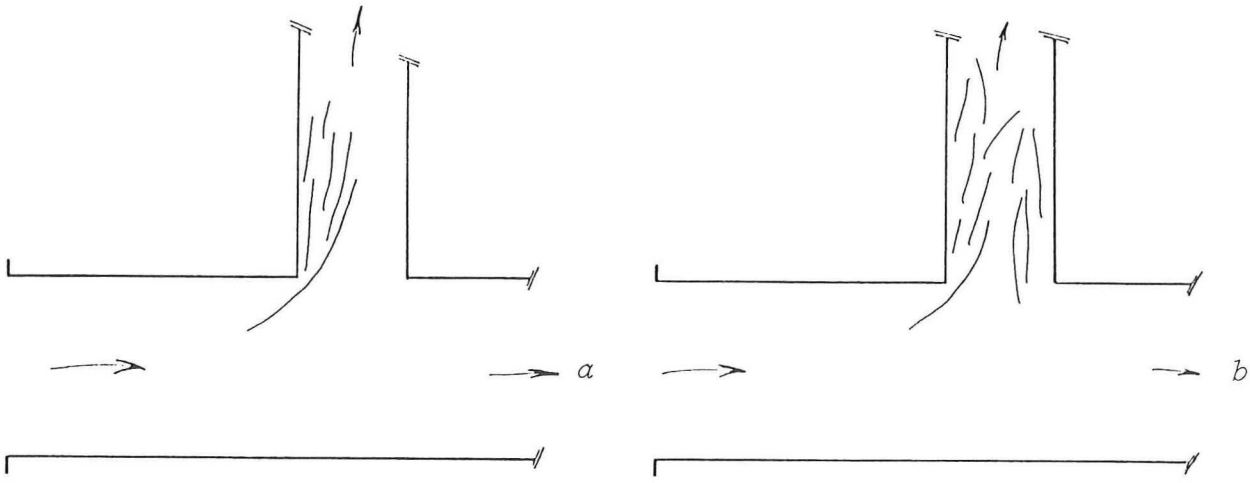

Figure 4.1. Gas intake into the branch: (a), at low takeoff, (b) at high takeoff

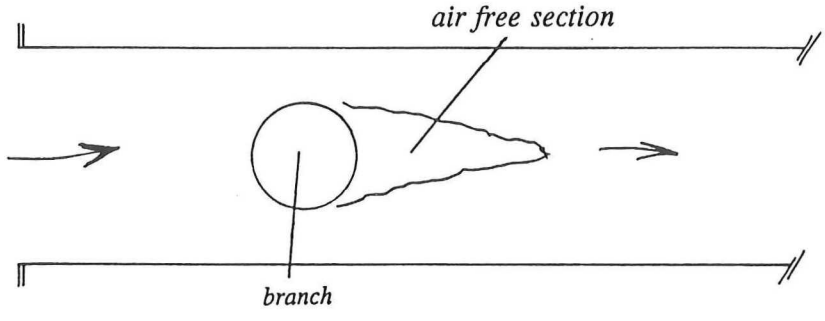

Figure 4.2. Impression of the observed 'zone of influence' (top view)

4.1.2. Observations of phenomena

As expected, the flow regime in the inlet was stratified or bubbly. The transition between these took place rather gradually, more and more gas entering the T-junction in the form of bubbles at increasing superficial velocity. This process continued until finally a stratification layer was hardly visible. The flow regime in the vertical section preceding the T-junction was bubbly over the entire range of measurement.
The regime in the branch was churn flow at higher takeoff rates, and slowly became slug flow at decreasing takeoffs. At low mass extraction ratios, the gas takeoff mainly took place at the 'beginning' of the branch. When the takeoff was large, the gas intake took place over the whole area of the branch. This phenomenon is sketched in figures 4.1 a and b.

In the stratified flow regime (especially at stratified smooth conditions), the T-junction almost acted as a perfect separator, only very small amounts of gas entering the run. At increasing 'bubbly character' of the inlet flow, more and more bubbles passed the branch undisturbed and entered the run.

At several different moments, a 'zone of influence' could be observed, as in the zone of the run that directly followed the branch no gas was present, as sketched in figure 4.2. Apparently all the gas in the corresponding section in the inlet was extracted into the branch.

The transition from churn to slug flow appeared to be quite interesting. Slug flow present in the branch resulted in a phenomenon in which bubbles, that had already entered the branch, were 'pumped' back into the main pipe because of the up-and-down movement of the slugs and were finaly entrapped in the inlet-to-run flow. Thus this resulted in a higher flow of gas into the run. This phenomenon, that was named the *'slug-pump effect'*, could be observed very clearly by, at branch slug flow conditions, suddenly switching off the pump. At these circumstances quite a large amount of bubbles were pumped back into the main pipe.
This effect might contribute considerably to the decrease of gas intake into the branch. It is treated further in section 4.3.

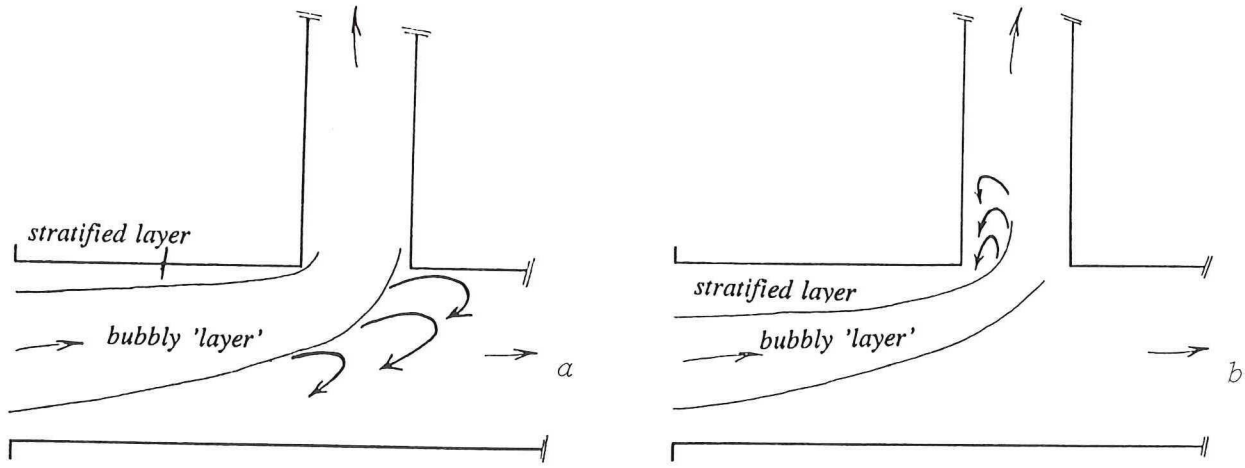

Figure 4.3. (a) and (b), Impression of two frequently occurring secondary flows ('fat' arrows)

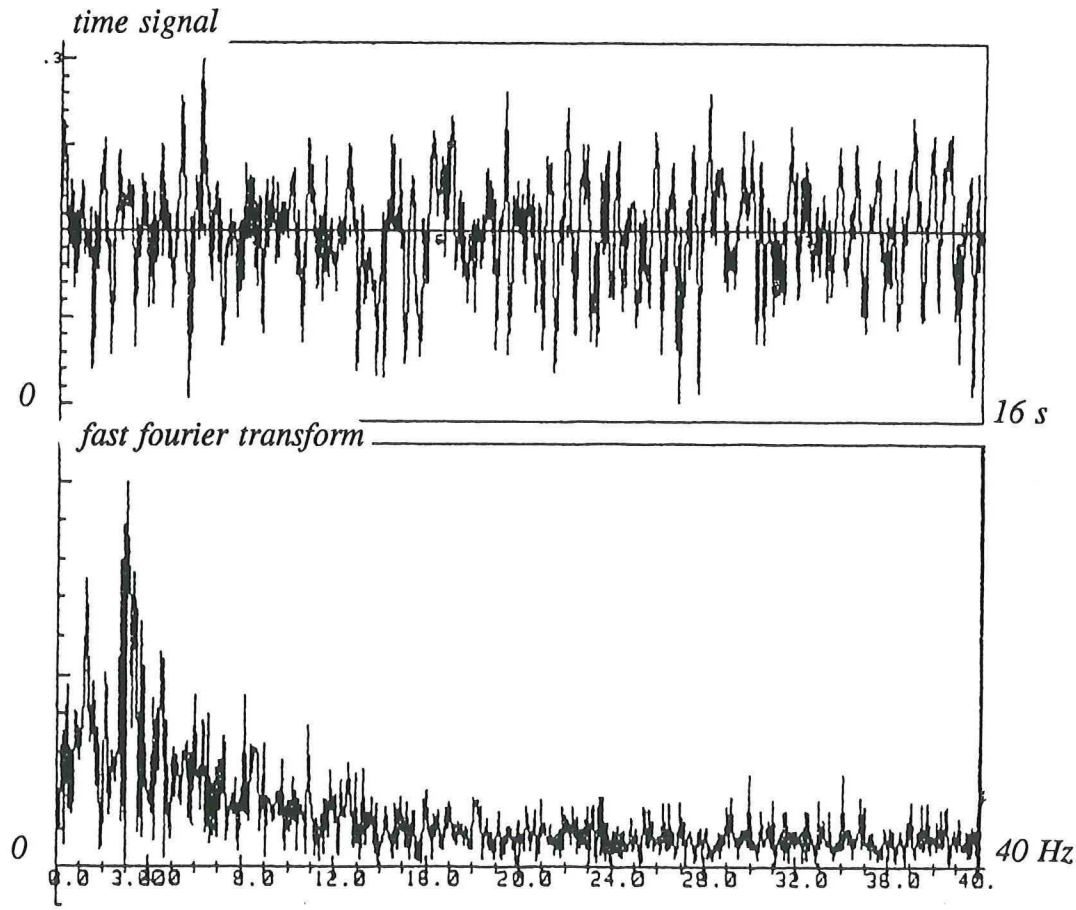

Figure 4.4. Typical time signal and fast fourier transform of churn flow, as measured in the branch

A quite interesting remark can be made already right now: it could happen that in the inlet, run and branch three *different* flow regimes were present. For instance, bubbly flow in the inlet, churn or slug flow in the branch, and stratified flow in the run.

Around the T-junction itself several secondary flows were observed, mostly because the bubbles made some additional movements. Two of these flows were present quite pronouncedly. They are depicted in figures 4.3 a and b. A 'vena contracta' in the branch was not detected distinctly, but neither can be claimed explicitly that it wasn't there.

4.1.3. Description of the signals

The twelve signals were, as mentioned, monitored using the HP workstation. By merely watching these signals, some valuable things could be remarked.

The signals of the pressure transducers were the most interesting ones, because they contain quite a lot of information, especially when comparing signals of different transducers present in the equipment.
Again, one of the most striking features was the transition from churn to slug flow in the upward branch. This transition could be monitored very well using the pressure signals. First, because when slugging started, the standard deviation of the pressure signal would increase by a factor up to about three. And second, because the signal itself changed quite specifically. At churn flow conditions, the signal was rather chaotic, and frequencies all over the sampling frequency interval (this was not te 512 Hz as used in the project, but 16 Hz for slug flow and 64 Hz in the churn flow case) were present, as was easily seen by calculating the fast-fourier transform (fft) of the signal. The time signal of a representative churn flow and its fft signal are given in figure 4.4. The slugging of a two-phase flow causes pressure pulses, which are registrated by the pressure transducers. A typical slug time signal and its fft are given in figure 4.5. The periodicity of the signal, coming from the slugging up and down, is quite striking. This 'heartbeat' signal results in two very pronounced frequency peaks in the fft signal. This 'slugging frequency' roughly coincides with that of the visually observed slugging. This slugging frequencies can be considered as eigenfrequencies of the system, and these thus depend on the physical properties of the fluids,

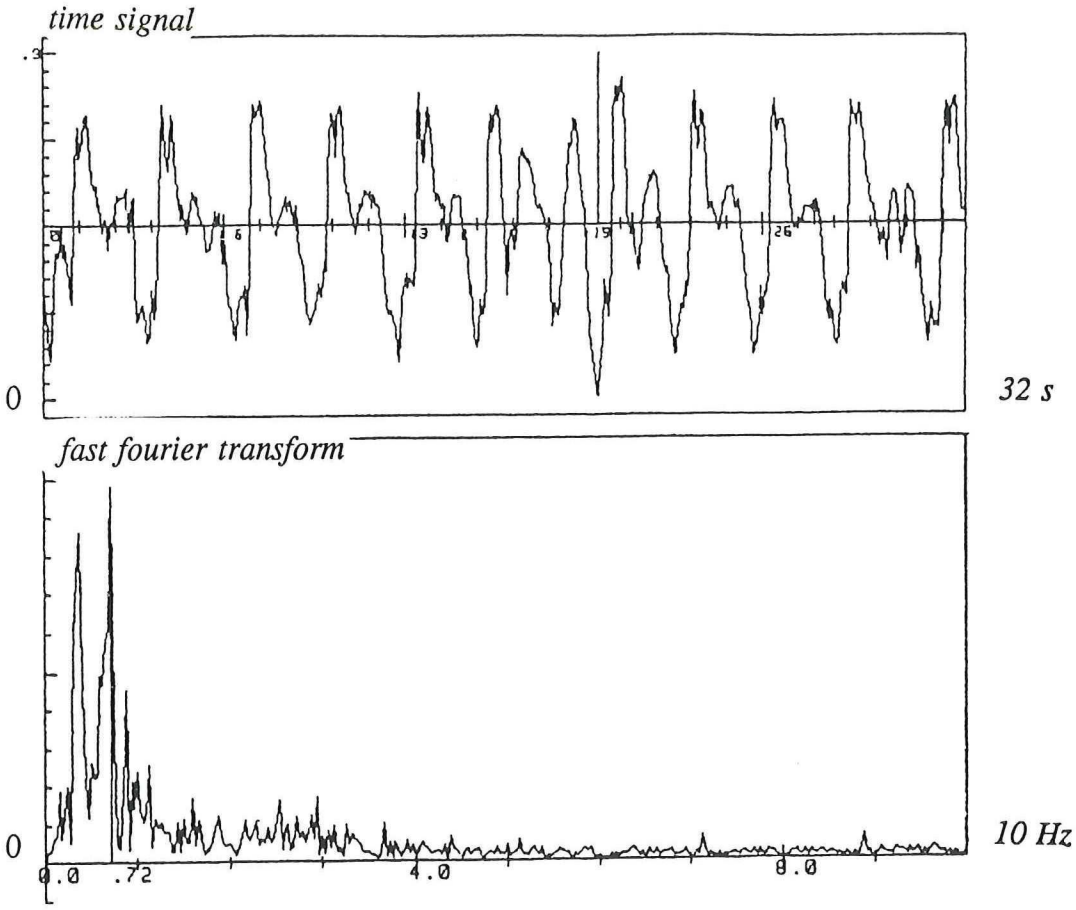

Figure 4.5. Typical time signal and fast fourier transform of slug flow, as measured in the branch

on the geometry of the T-junction and the surrounding equipment (e.g. the bend directly following the branch). The 'heartbeat' signal could be heard as well, mainly at the branch valve, as the flow pulsated its way through.

The pulses induced by the slugging in the branch propagate throughout the equipment (in the same as well as in opposite direction of the flows) and can thus be registrated with a pressure transducer anywhere in the system. That this is true is illustrated most clearly with the signal of the pressure transducer in the sparger, so several meters *upstream* of the T-junction. In the monitoring screen given in figure 3.10 this can be observed (the signal of this pressure transducer is marked *8* in this figure). If these registrations were done accurately, by using the offset between two signals (or correlating them), an estimation of the speed of sound in the two-phase flow could be made. A first estimate for this velocity, as determined from these graphs is about 30 m/s, which does match literature values (see e.g. [22]).

The influence of the slugging could be observed not only by pressure signals, but also by merely watching the perspex parts of the equipment. At slug flow conditions in the branch, bubbles would enter the T-junction and flow through the run in a pulsating way (with the slugging frequency, of course). A very clear illustration of the pulses propagating in the upstream direction was the fact that, at slug flow conditions, the air brought into the flow in the sparger entered the water flow in quite a pronounced pulsating way as well.

Compared to all this, the gas and liquid flow signals could hardly be called interesting. They were relatively stable and no high frequencies were present in the signals. No striking effects of the slugging on these signals were observed, this is most likely due to the fact that the separation and buffer tanks have a smoothing effect.

4.2. Construction of a flow map for the horizontal tube

By keeping the branch valve closed and varying the inlet superficial gas and liquid velocity over the range of interest, a flow map for the horizontal inlet-and-run was constructed. For this construction, about 50 measurements were made, and the flow regime at the end of the run was

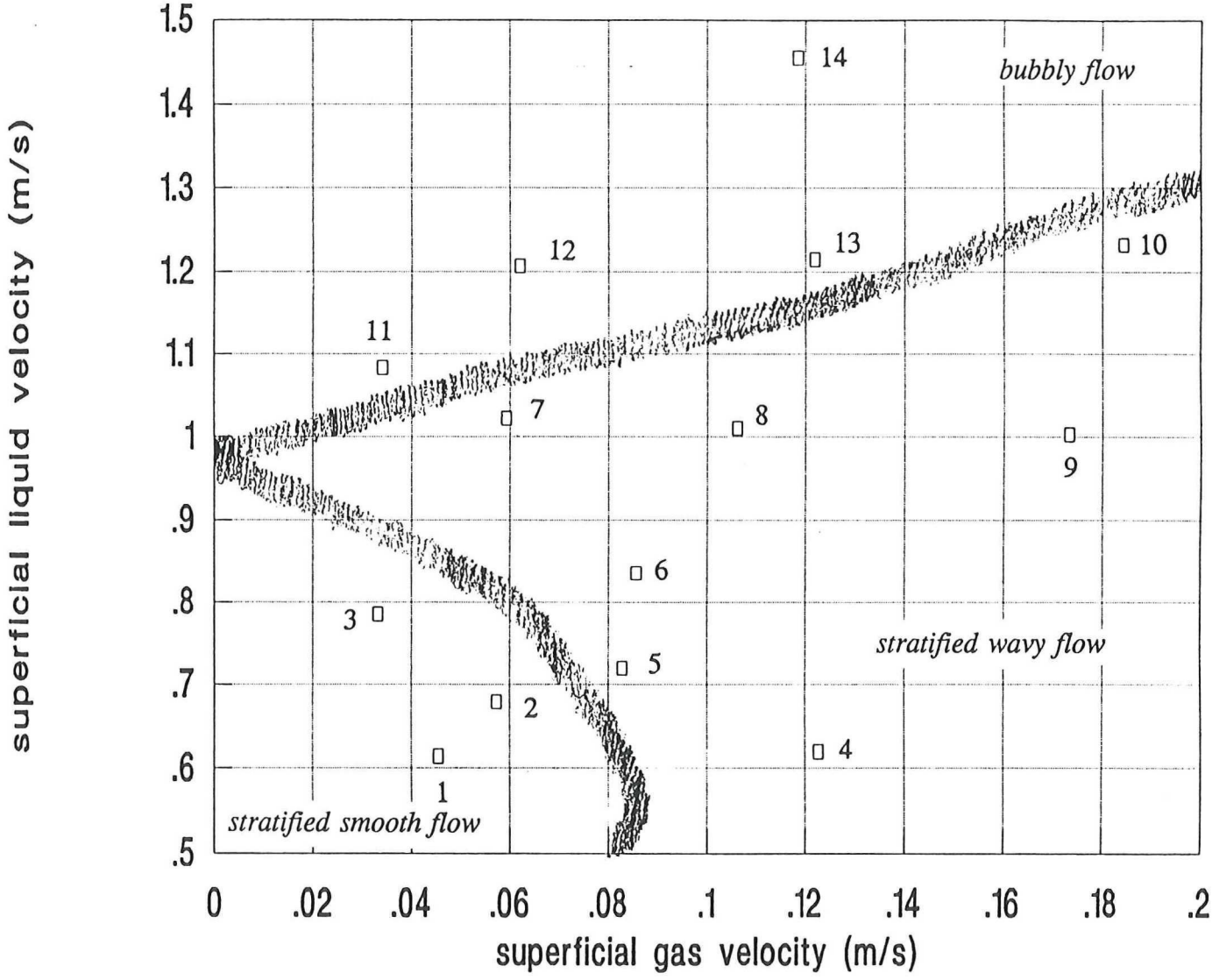

Figure 4.6. Flow map for the inlet-and-run, as obtained from observations

considered to be fully established. This might have been slightly on the optimistic side, since a two-phase flow requires at least about ten pipe diameters (2.3 meters in this case, whereas the T-junction is 2 meters long) to fully establish the regime. However, the measurements performed can be taken as good estimations.

The flow map that followed from the measurements is given in figure 4.6. Three regimes are present: stratified smooth, stratified wavy and bubbly flow. As mentioned in the last section, especially the transition from stratified wavy to bubbly flow is not a very sharp one.

When comparing this flow map with the ones given in figures 2.4 a and c, one sees that the form of the stratified-to-bubbly transition is the same, but that the transition in this project takes place at a much higher liquid velocity. Apart from the fact that the literature flow map might not be valid for the pipes used in this project, the following explanation might account for this difference: When the two-phase flow passes the bend just before the T-junction, the 'centrifugal' force wants the liquid to move to the outside of the bend, but gravity wants the opposite. In the area of velocities used in this project, gravity has more influence than the centrifugal forces. This can be explained with the Froude number (Fr):

$$Fr = \frac{\bar{u}^2 / R}{g} \tag{4.1}$$

In the case of the project, R, the radius of the bend, equals 0.625 m, and the maximum velocity is in the order of magnitude of 1 to 1.5 m/s. This means that the Froude number will be much less then unity throughout the project.
So, whereas the bend was meant to 'extend' the bubbly flow regime area (see section 3.3.2), it might have turned out to work as a stabilization factor for stratified flow.

By monitoring the transition from churn to slug flow in the branch, it might be possible to acquire a flow map for the vertical section as well. This is treated in section 4.3.

To cover the area of interest as representative as possible, measurements were taken in all three different flow regimes, and several pairs of measurements were performed near to each other, at 'opposite sides' of flow regime transitions. The measuring points are indicated in the flow map.

The numbers attached to these in the figure correspond to the numbers given in the graphs and tables in the rest of this report.

4.3. Phase redistribution experiments

Fourteen measurements series were performed, each existing of about ten measurements. Three measurement series took place in the stratified smooth regime, four in the bubbly regime and seven under stratified wavy circumstances. The series were continued with decreasing takeoff rate, until adequate measurements were impossible because of disturbances of the steady state or air entrapping complications. This point mostly laid between 2 % and 5 % takeoff.
The inlet and branch quality, the mass extraction ratio, the quality ratio and several other quantities were determined from the flow measurements. The measured and calculated quantities are given in appendix II.
At various different moments, the *run* gas mass flow was measured, to verify the gas mass balance. Within a range of about 1 % to 2 %, the mass balance was satisfied.

The measurements were converted to phase separation curves and fraction plots. The phase separation plots are given in figures 4.7 a to n, together with the total separation curves and the curve given by the Seeger model. The explanations of the arrows present in the pictures will follow in due course.

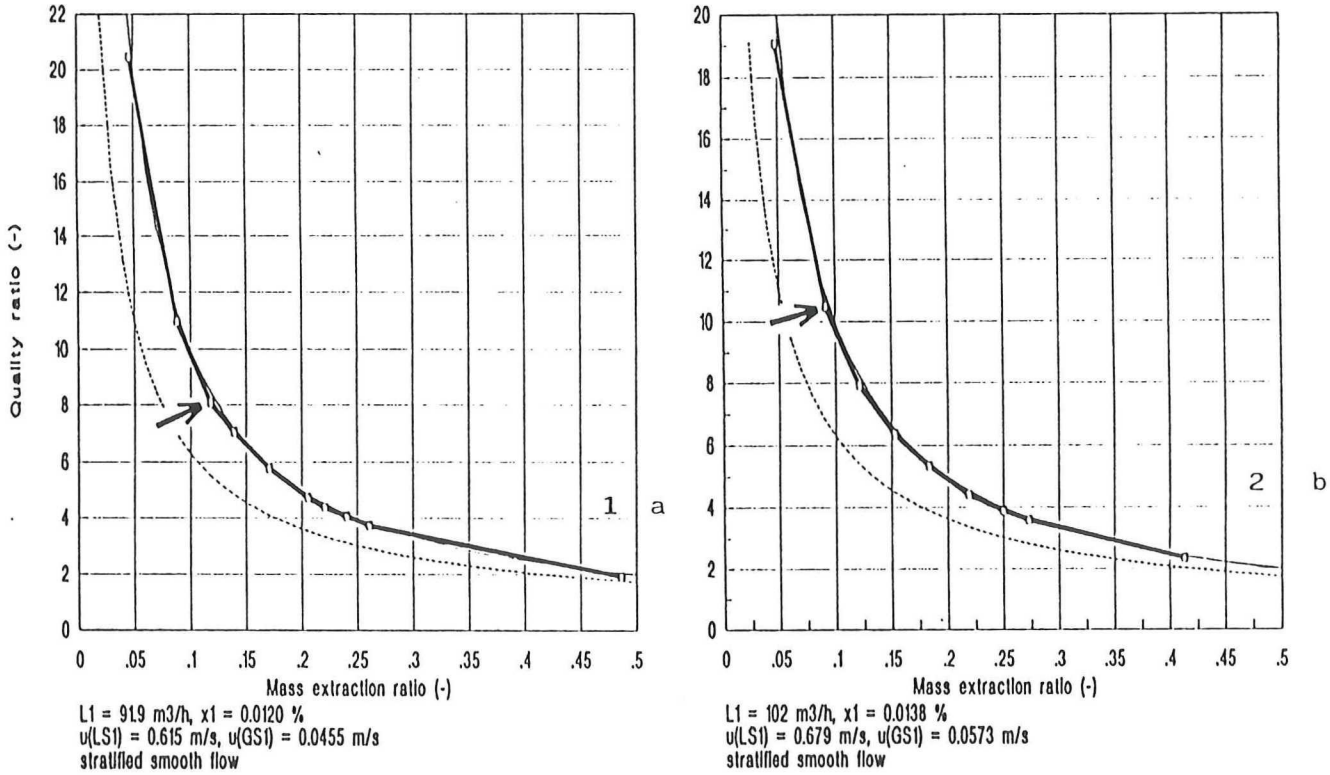

Figure 4.7. (a) to (n), Phase separation plots, as followed from the measurements
legend: ——□——: measurements, ————: total phase separation, -----: Seeger model

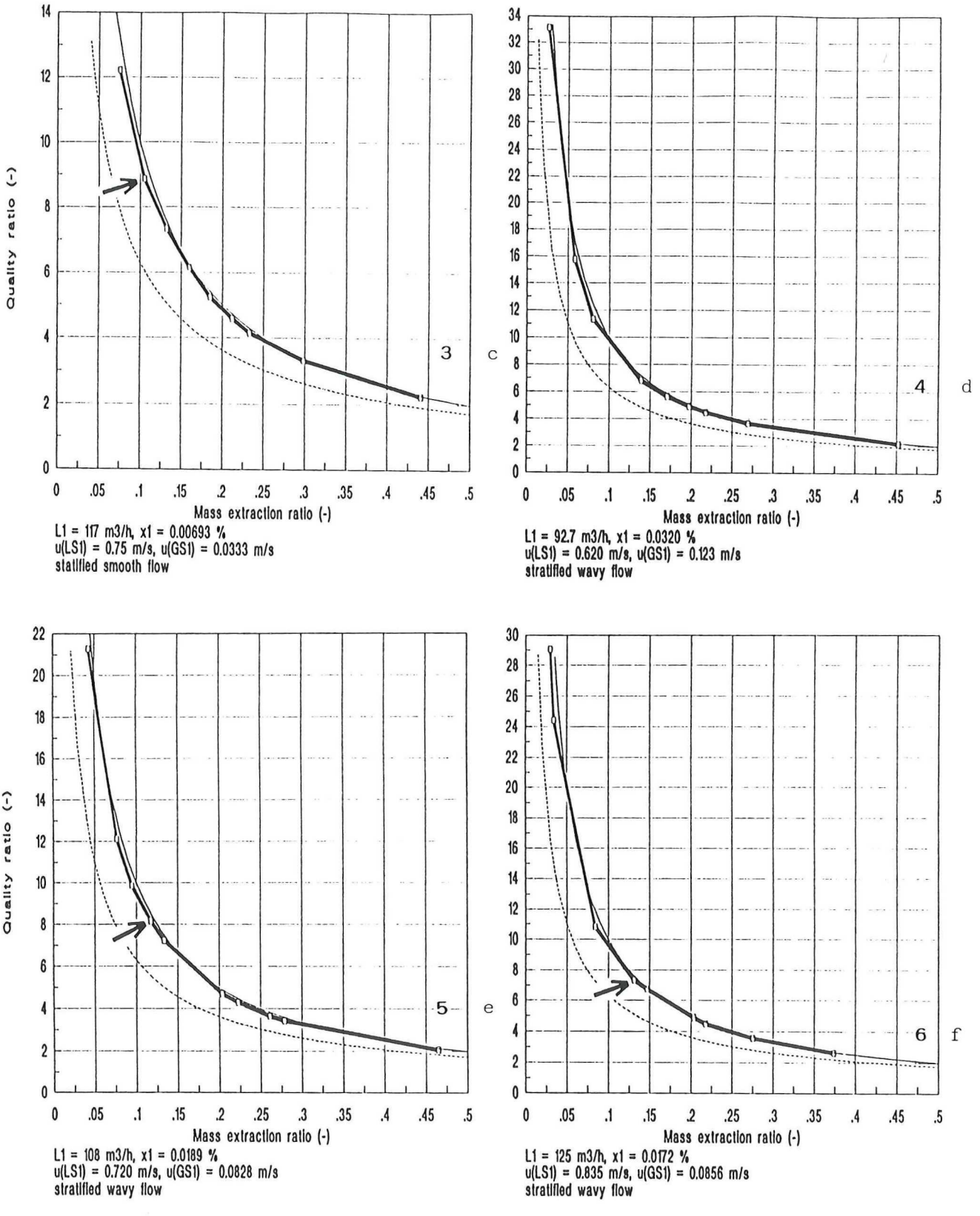

Figure 4.7. -continued- (a) to (n), Phase separation plots, as followed from the measurements
legend: ——□——: measurements, ————: total phase separation, -----: Seeger model

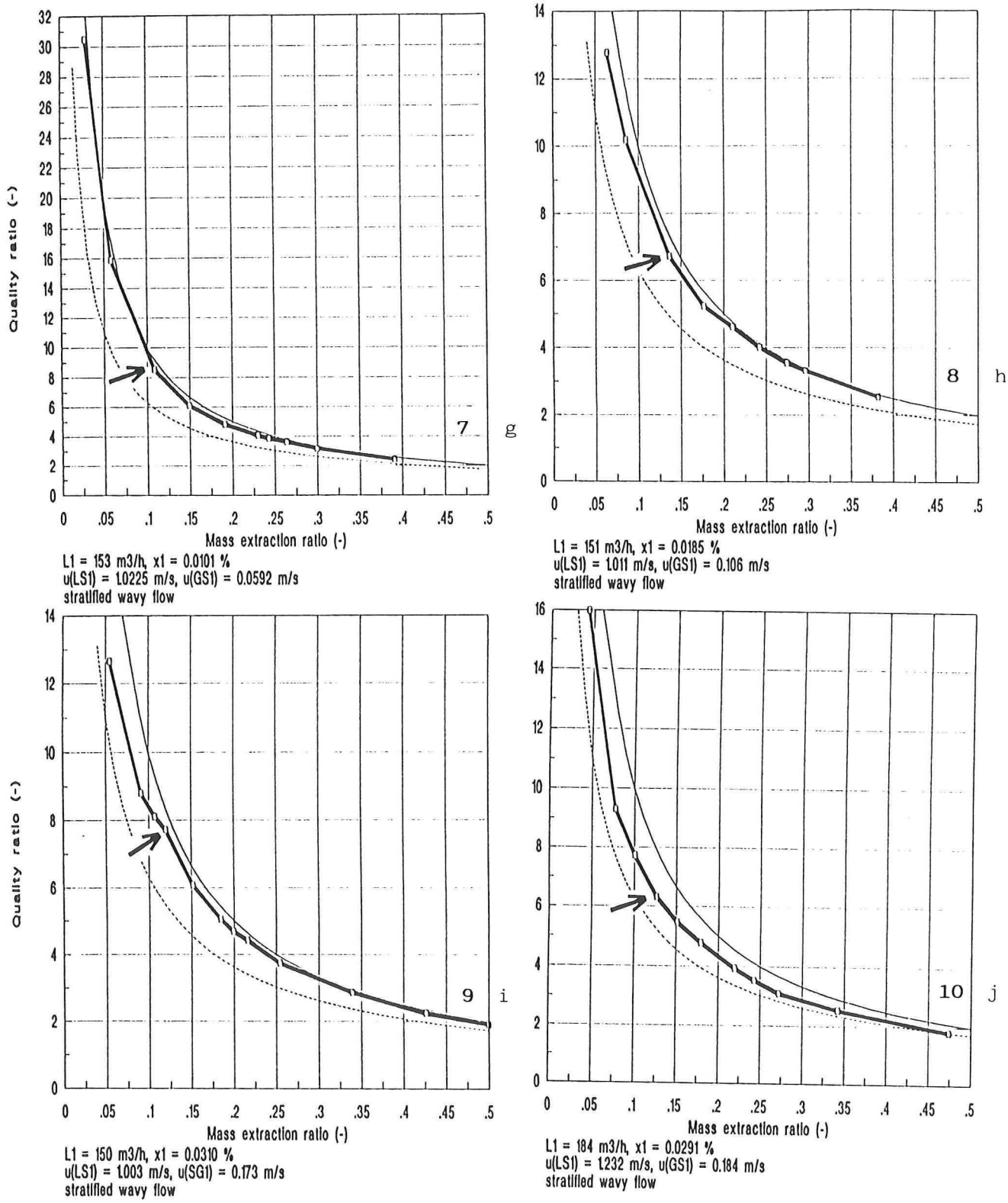

Figure 4.7. -continued- (a) to (n), Phase separation plots, as followed from the measurements
legend: ——□——: measurements, ————: total phase separation, -----: Seeger model

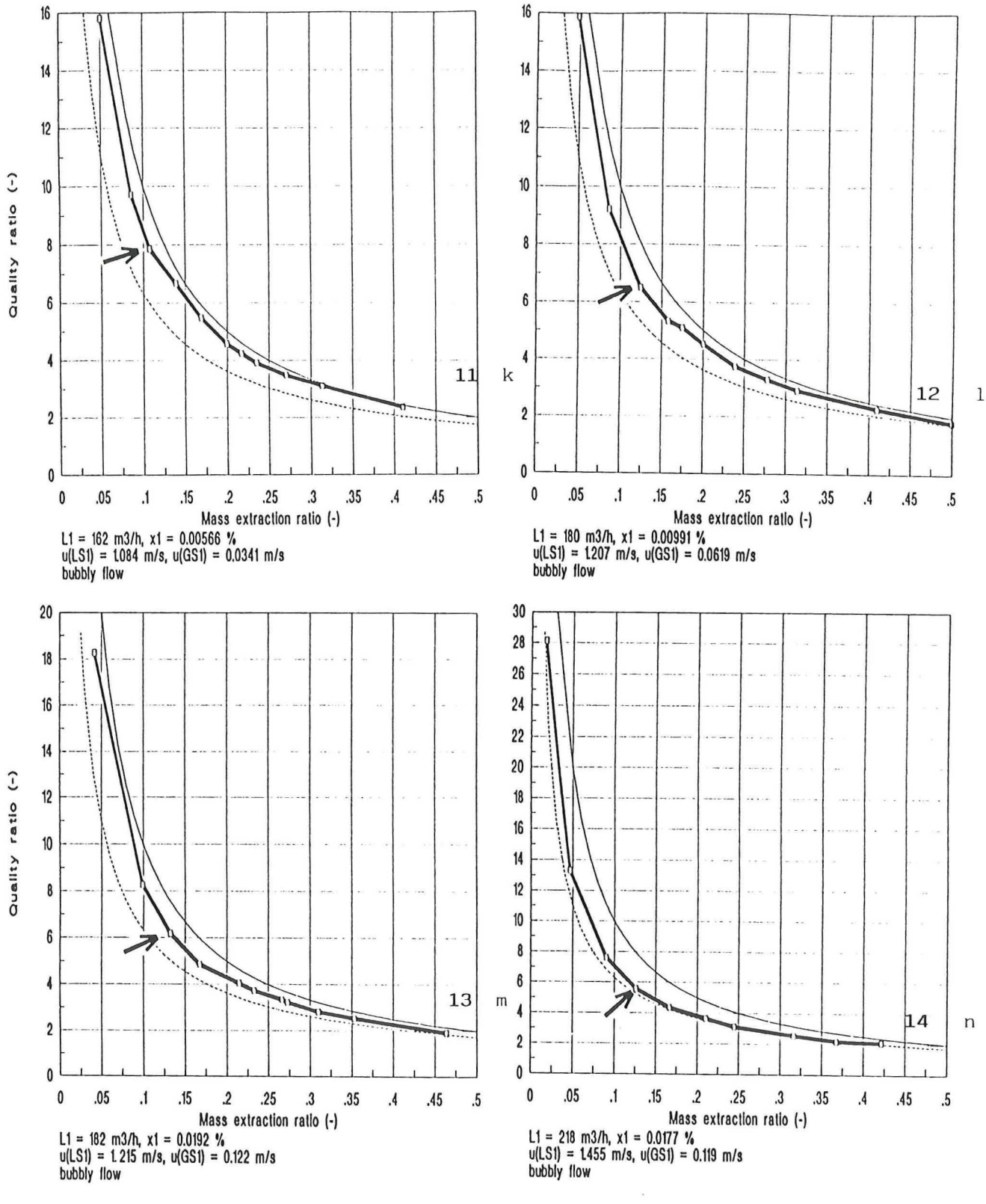

Figure 4.7. -continued- (a) to (n), Phase separation plots, as followed from the measurements
legend: ——□——: measurements, ————: total phase separation, -----: Seeger model

It is easily seen that, in the stratified flow regime (i.e. at low inlet superficial velocities), the measurements quite closely follow the total separation line. At stratified wavy flow conditions, at increasing inlet velocities, the measurement curve 'creeps away' from the total separation line. In the bubbly flow region, this 'creeping' goes on, and at the measurement at highest velocity, the measurement curve is almost exactly described by the Seeger equation. This 'creeping' phenomenon seems to be mainly dependent on the superficial liquid velocity, and not on the flow regime present. So the expectation that the T-junction will act better than Seegers 'engineering model' is confirmed.
A maximum in the phase separation curves was not detected, neither at $w_3/w_1 \approx 0$, nor at $w_3/w_1 > 0$. The occurence of the first mentioned maximum is no wonder, since the value of that maximum (at $x_3/x_1 = 1/x_1$), would be at least 3000. This was of course far beyond our possibilities. A maximum at takeoff rates above zero might appear at higher liquid velocities then reached in this project.

Without trouble it can be seen that the model of Zetzmann (see figure 2.16) with the parameters a and b both equalling one, does not apply to the measurements performed in this project. Apparently, the model is too empirical to have validity within the range of this project.

One should be careful using phase separation curves, because the deviation from the total separation line is of course in vertical direction. So, a curve might look as 'quite closely following the total phase separation line', but the deviation from it can still be considerable.
Another way of representing the phase redistribution, which does not have this problem, is the construction of the fraction plots. These are given for the experiments in figures 4.8 a to n, together with the line of equal separation, i.e. the curve given by the fraction of gas removed equalling the fraction of liquid removed. In these plots, the deviation from the total separation line (in this case the 'gas extraction fraction = 1' line) is much easier observed.

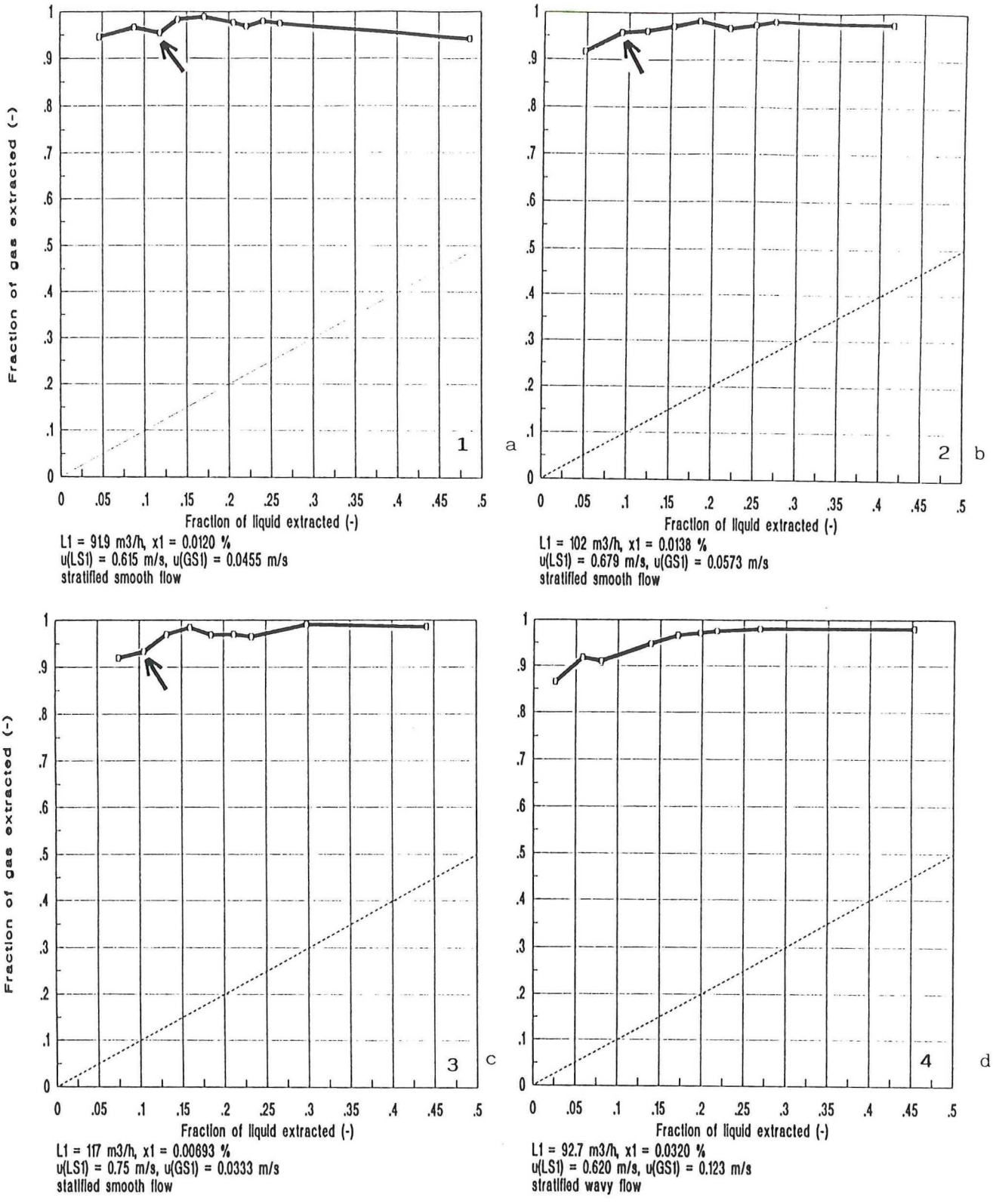

Figure 4.8. (a) to (n), Fraction plots, as followed from the measurements legend: ——□——: measurements, -----: equal phase separation

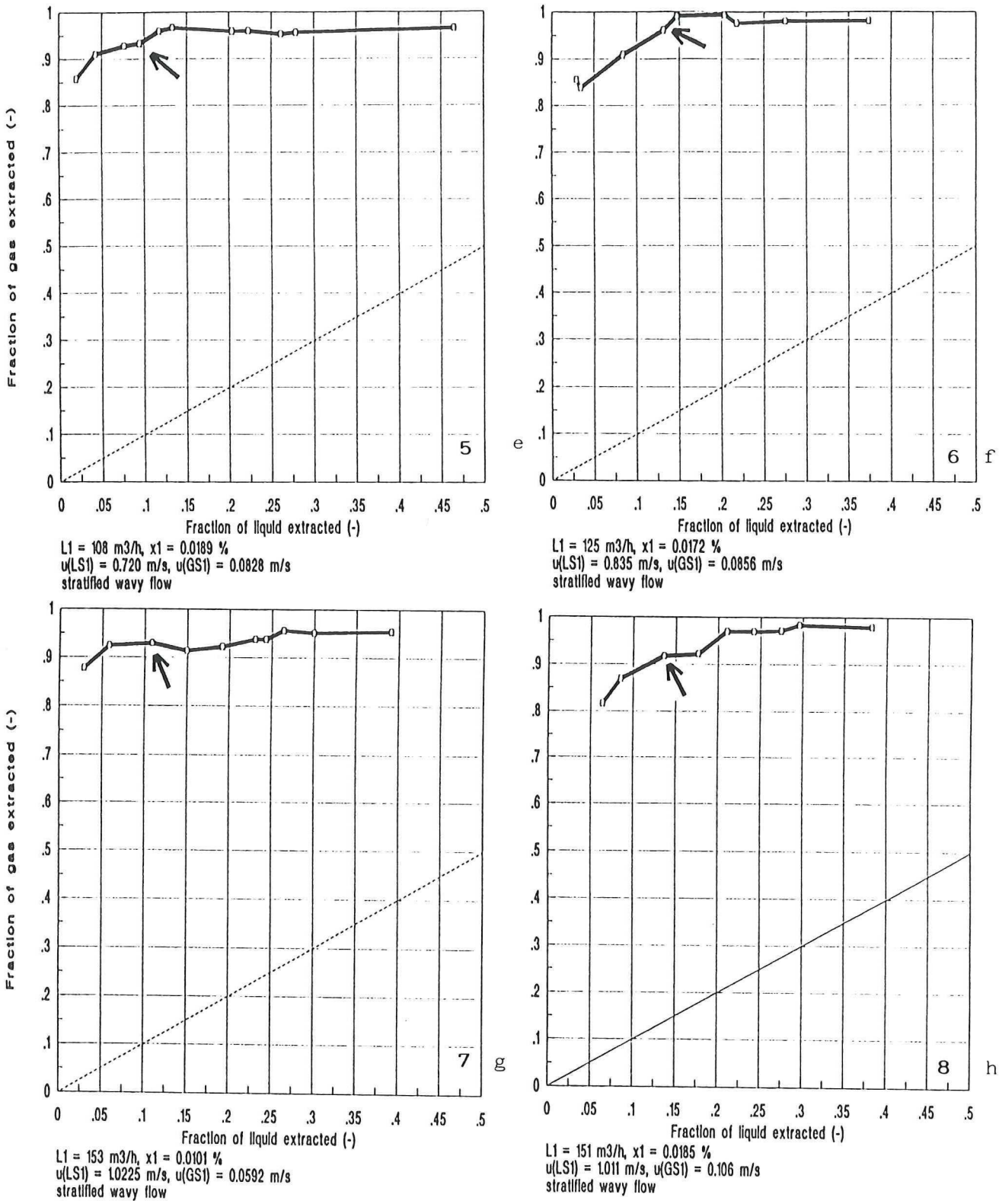

Figure 4.8. -continued- (a) to (n), Fraction plots, as followed from the measurements
legend: ——□——: measurements, -----: equal phase separation

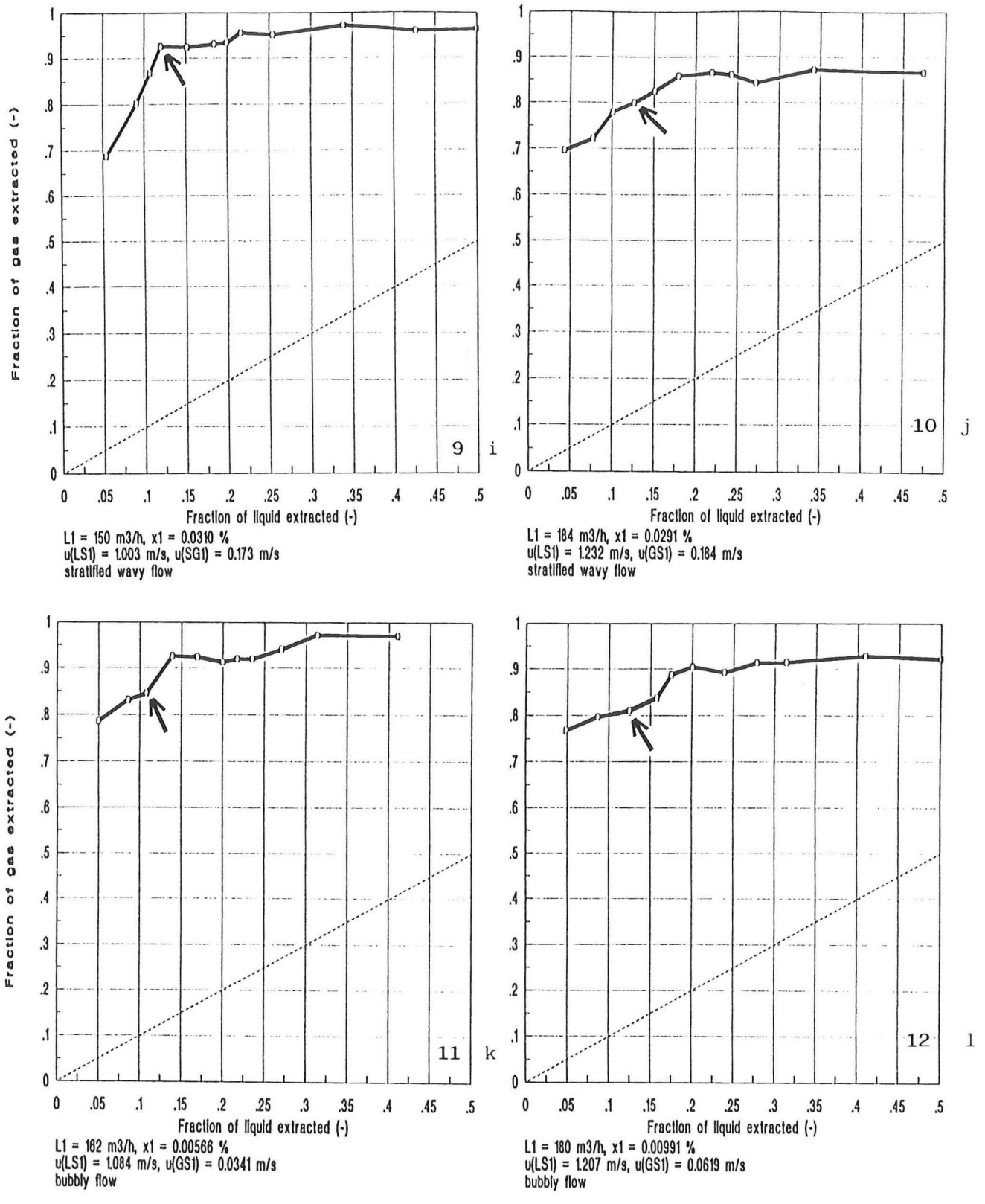

Figure 4.8. -continued- (a) to (n), Fraction plots, as followed from the measurements legend: ——□——: measurements, -----: equal phase separation

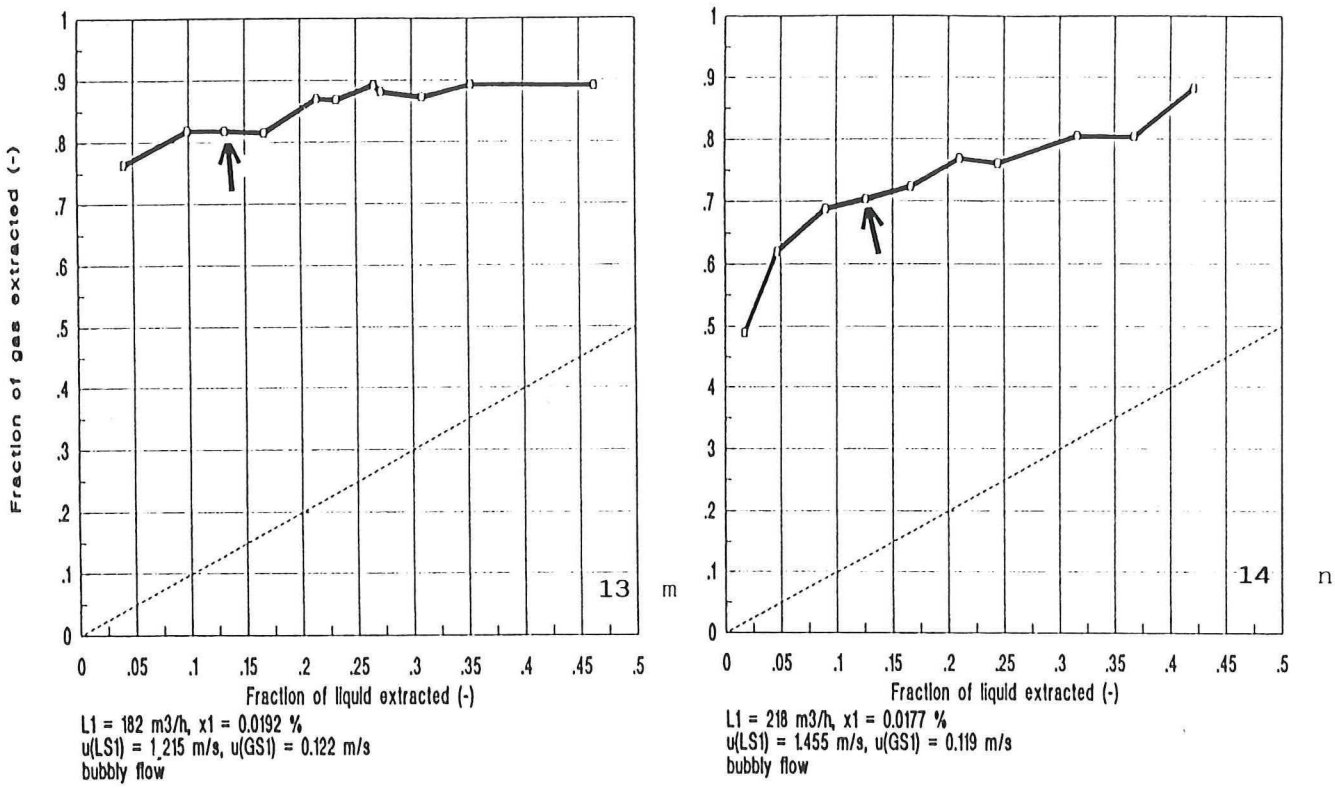

Figure 4.8. -continued- (a) to (n), Fraction plots, as followed from the measurements legend: ——□——: measurements, -----: equal phase separation

In the fraction plots it can be observed that, while lowering the takeoff rate (≈ the liquid extraction fraction), at a certain takeoff rate, the deviation from the total separation line starts increasing quicker then before. In some cases, this happens rather gradually, but in some series, this 'bend' occurs quite suddenly. The latter case, however, coincides quite neatly with the transition of churn flow to slug flow in the branch. The 'slug pump effect', as introduced in section 4.1.2 might be a considerable contribuant to this. In the phase separation plots and the fraction plots, the first measurement at which slugging occured, is indicated with an arrow. The criterion used for the occurence of the transition was the earlier described increase in inaccuracy of the pressure signals. In this case, the inaccuracy of pressure transducer number 7 was used, because it could be expected that the slugging was most 'severe' at that transducer.

In most cases, the measurement where slugging begins coincides more or less with the beginning of the kink in the fraction curve. That the determination of this transition cannot be done very accurately can be seen in figure 4.9, where a flow map for the branch is presented, over the area of superficial phase velocities occuring in the branch during the project. The measurements that

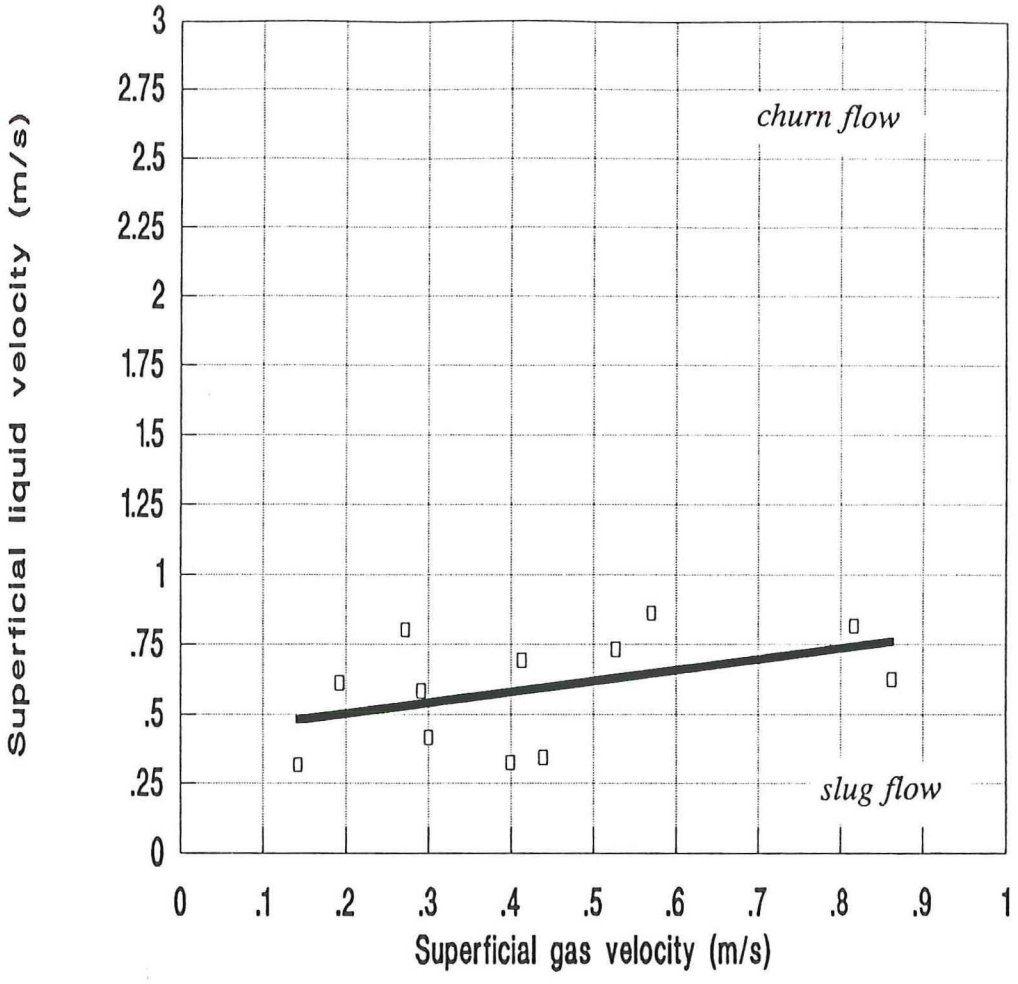

Figure 4.9. Flow map for the branch, as obtained from pressure measurements

first showed the occurence of slugging (in a measurement series at decreasing mass extraction ratio) are given in this graph, together with their best linear fit.
With some care can however be concluded that not only the flow regime present in the inlet of the T-junction does influence the flow split (as stated before by other authors), but that the influence of the regime in the other legs (presumably mainly the branch) may not be neglected either.

The claim of Zetzmann, that the run and branch quality are direct proportional to the inlet quality, could be verified because several series had been made at fixed liquid inlet velocity and increasing inlet quality. This was the fact for L_1 = 90 (two series), 150 (three) and 180 (three series) m^3/h. For each of this liquid inlet velocities these 'Zetzmann plots' were constructed for three different values of the takeoff rate. These are given in figures 4.10 a to i, together with the line of equal phase separation. The run quality curve lays of course unther this line, the branch quality curve above it.
Clearly is seen that the claim of Zetzmann holds for this T-junction at these low inlet qualities as well.

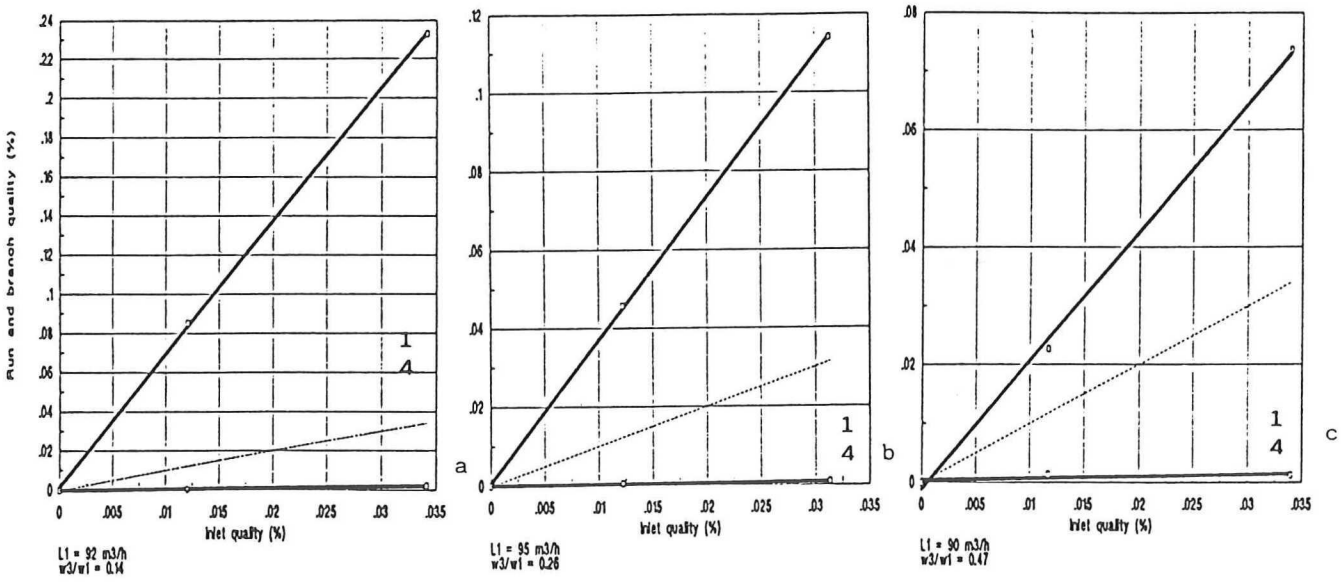

Figure 4.10. (a) to (i), 'Zetzmann plots', as followed from the measurements
legend: ——□——: measurements, -----: equal phase separation

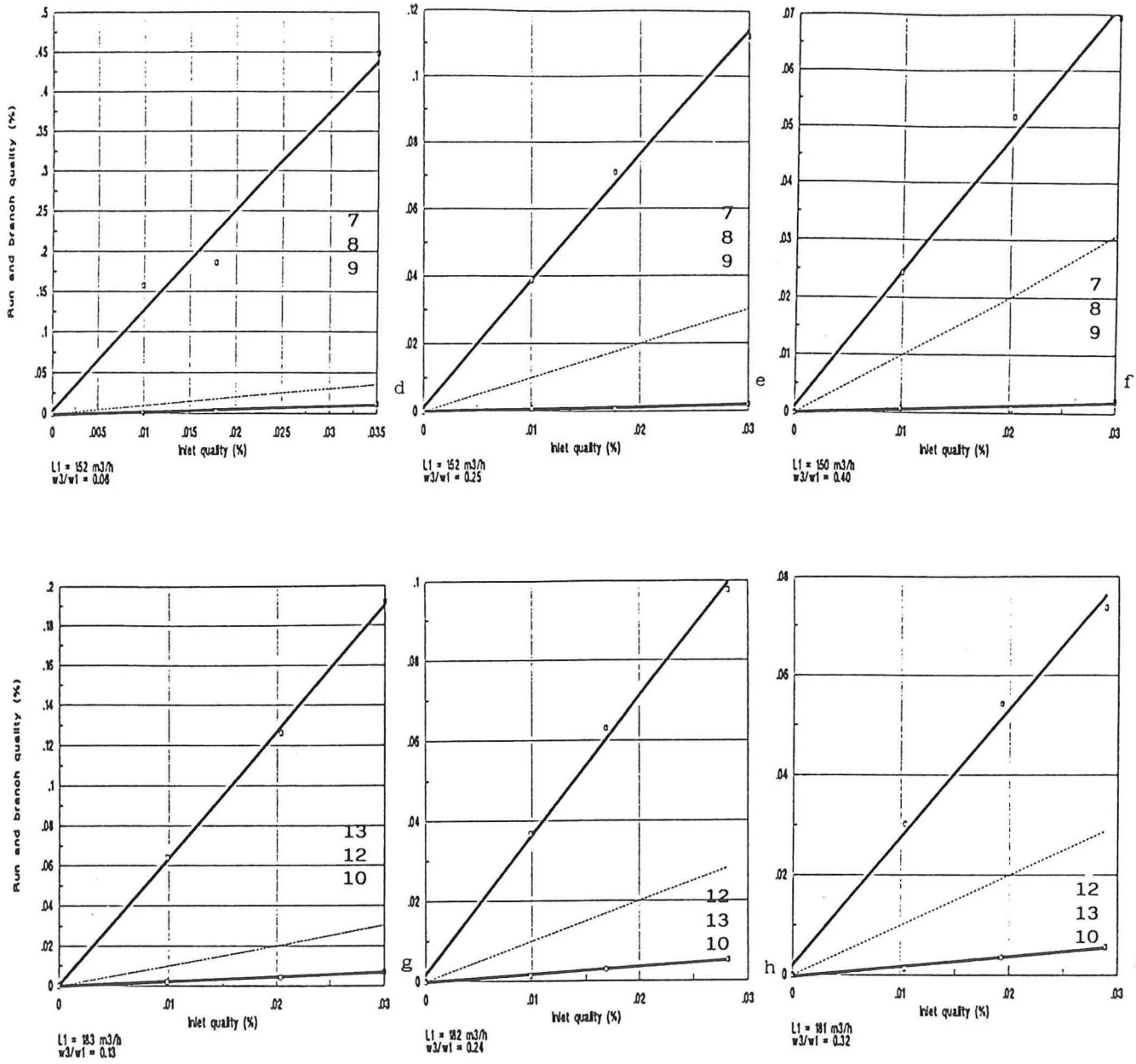

Figure 4.10. -continued- (a) to (i), 'Zetzmann plots', as followed from the measurements legend: ——□——: measurements, -----: equal phase separation

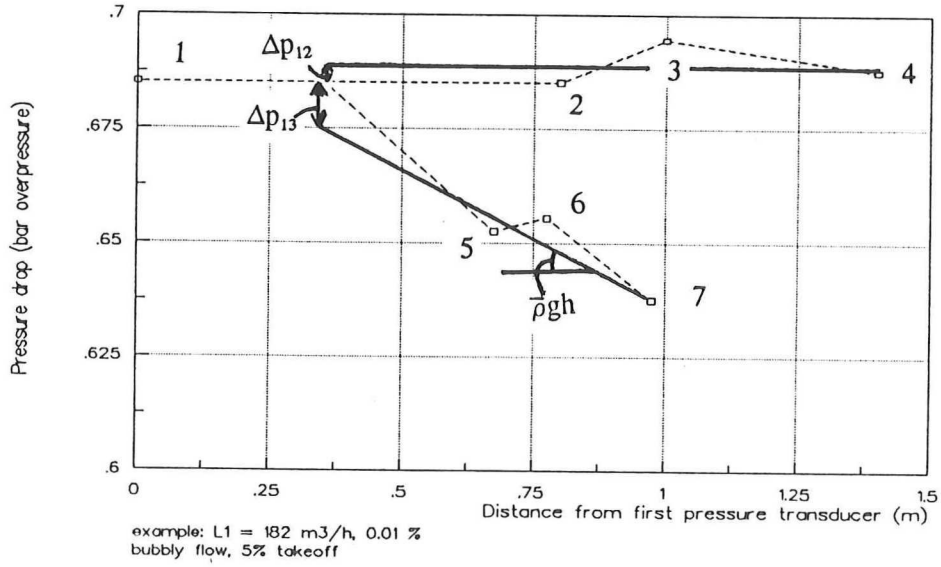

Figure 4.11. General appearance of the pressure profile accross the T-junction

4.4. Pressure drop experiments

At the same fourteen points in the flow map, the pressure drops of the inlet-to-run and inlet-to-branch flow were measured. Over the measured mass extraction range the pressures of the seven pressure transducers were monitored. The inlet-to run and inlet-to branch pressure drops due to the junction, so $(\Delta p_{12})_J$ and $(\Delta p_{13})_J$, were calculated and compared to several models. The inlet-to-branch pressure drop was compared to values that were predicted by the homogeneous, the Chisholm and the Reimann and Seeger models, all three with or without involving the correction factor K. The inlet-to-run pressure drop was compared to the nameless model that is mentioned in chapter 2 as well.
Because in several early measurement series, not the total pressure profile was recorded, these measurements cannot be compared to the models.

About half-way the project, it was found out that the run and branch were by far not long enough to assume wall friction dominated flow at the end of them. This means that the run and branch flows were not fully developed at the position of the 'last pressure transducers'. So the question is if the values of the 'last pressure transducers' are correct. Seeger states a pipe length of up to fifty diameters might be needed for fully developed branch and run flow. To illustrate what the pressure profile accross the T-junction looked like, an example is given in figure 4.11. As expected, the flow flowing into the run experiences a (small) pressure rise due to the decrease of the velocity. The inlet-to-branch flow undergoes a pressure drop because of the height difference and because of 'turning the corner', together with a pressure drop or rise due to velocity changes. An explanation of the 'wobble' in the branch pressure profile might be a decrease in flow velocity. This decrease could be caused by the flow occupying the total area of the branch, after having passed a 'vena contracta'.

As a best estimate, the following procedure was followed: The value of pressure transducer 4 (see figure 2.2) was taken as the final value of the run pressure drop, and compared to the value of the first transducer (the one in the inlet). As stated in section 2.6, the friction pressure loss in the T-junction may be neglected, so no correction was needed for these values.
The value of pressure transducer 7 was taken as best estimate for the eventual branch pressure. This value was corrected for the hydrostatic pressure drop.

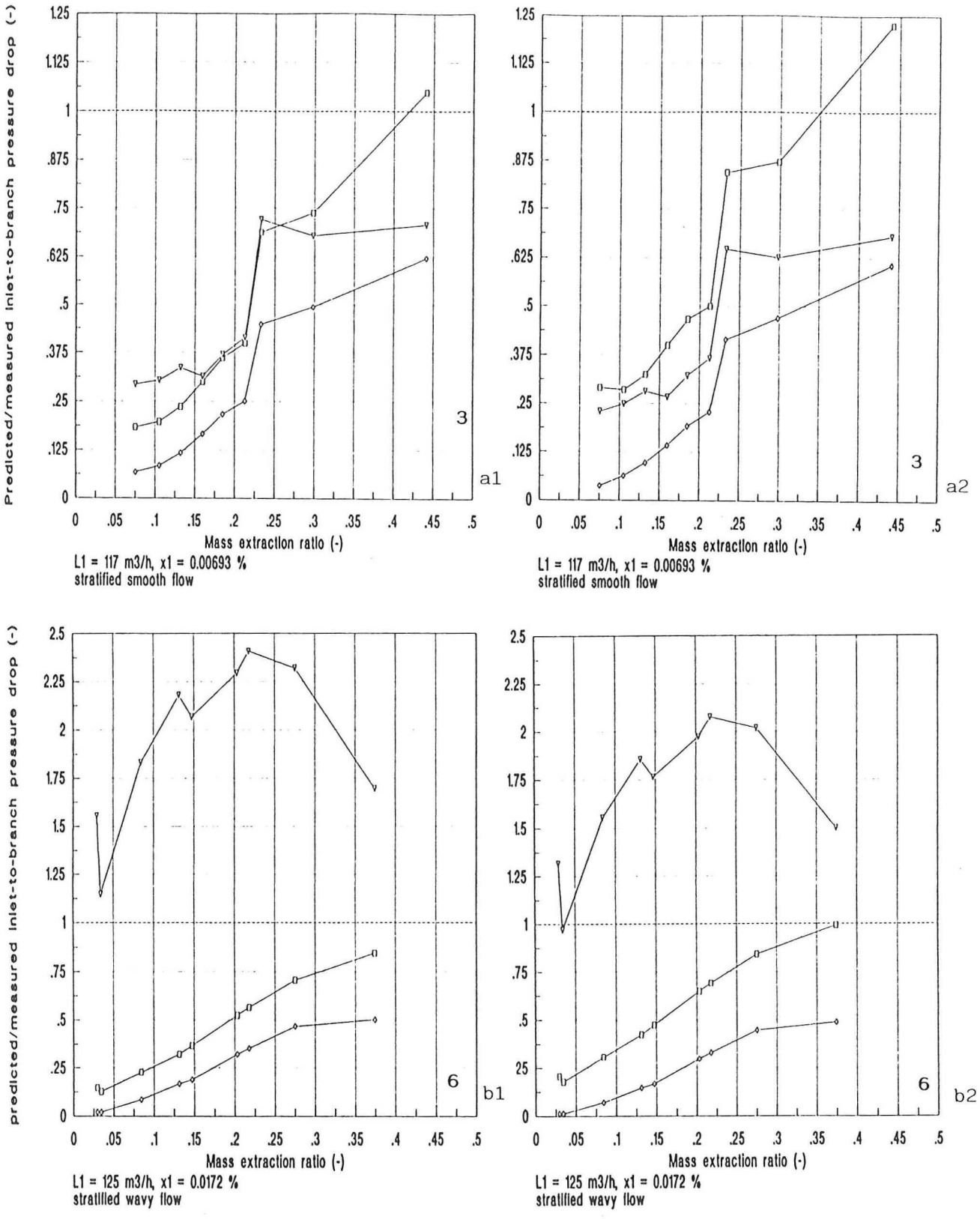

Figure 4.12. (a1) to (f2), Comparison of measured and predicted pressure drops (inlet-to-branch)
legend: ——□——: homogeneous model, ——▽——: Chisholm model, ——◇——: Reimann and Seeger model

As some of the pressure profiles looked rather similar, only six of the fourteen measured comparisons, chosen representatively over the area of interest, are represented graphically in this chapter. In appendix III all the measurements are given in tables.
In figure 4.12 a1 to f2, the predictions of the three models for the inlet-to-branch pressure drop is compared to the measurements. The y-axis comprises the ratio of predicted pressure drop over the measured pressure drop, as a function of the mass extraction ratio. The '1' graphs are the uncorrected values, in the '2' graphs the correction factor K is used.

Some of the 'peaks' that are present in all three plots within one graph, are most probably due to too low (peaks) or too high (dips) measurements. This indicates that the pressure drop measurements are not too accurate.
As can be seen, no model really 'outclasses' the other two over the entire area of interest.
The Reimann and Seeger model gives too low predictions for all the flow regimes. This might be explained by the fact that the version of the rsm that was used was quite a simplified one. In calculating the two-phase loss multiplier for this model, the assumption of homogeneity is quite important, as it is present in both the numerator and the denominator (to the power two) of the equation. As this assumption might be somewhat optimistic, this model can produce larger deviations than the homogeneous model, which invokes the question of homogeneity only once.
In the stratified smooth regime all models give too low predictions. In the wavy and bubbly flow regime the results of the Chisholm and the homogeneous model are comparable. Generally, with some caution can be said that the homogeneous model is slightly better then the Chisholm model.
There is no real indication that the K-corrected models are better then their uncorrected equivalents. In some cases, the corrected predictions are better, but sometimes they are worse. This does not seem to be flow regime dependent.
At lower takeoff rates all three models tend to give too low results. At increasing takeoff rates, all models, the uncorrected as well as the corrected ones, seem to head for unity, indicating that they will render better results in that region.

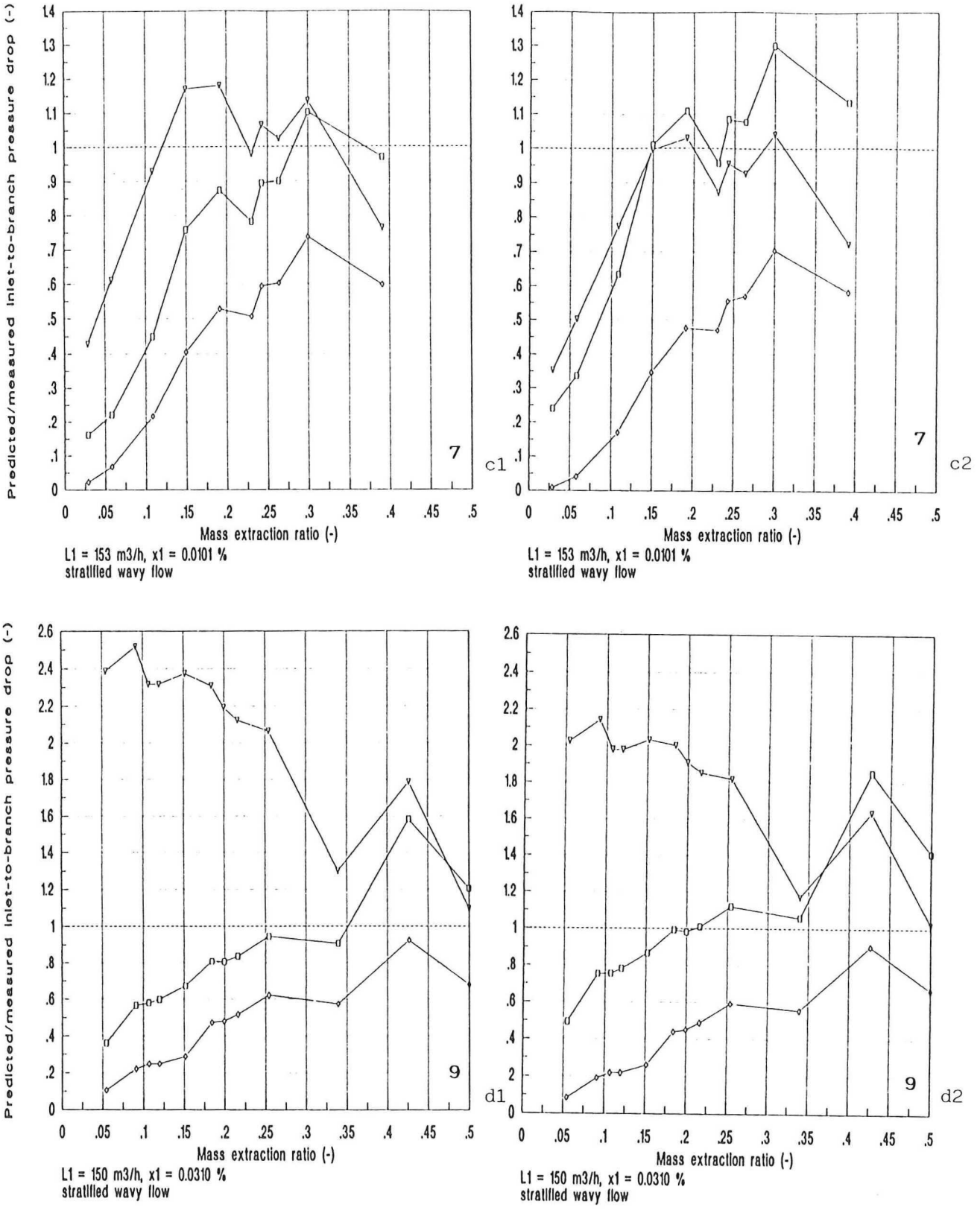

Figure 4.12. -continued- (a1) to (f2), Comparison of measured and predicted pressure drops (inlet-to-branch)
legend: ——□——: homogeneous model, ——▽——: Chisholm model, ——◇——: Reimann and Seeger model

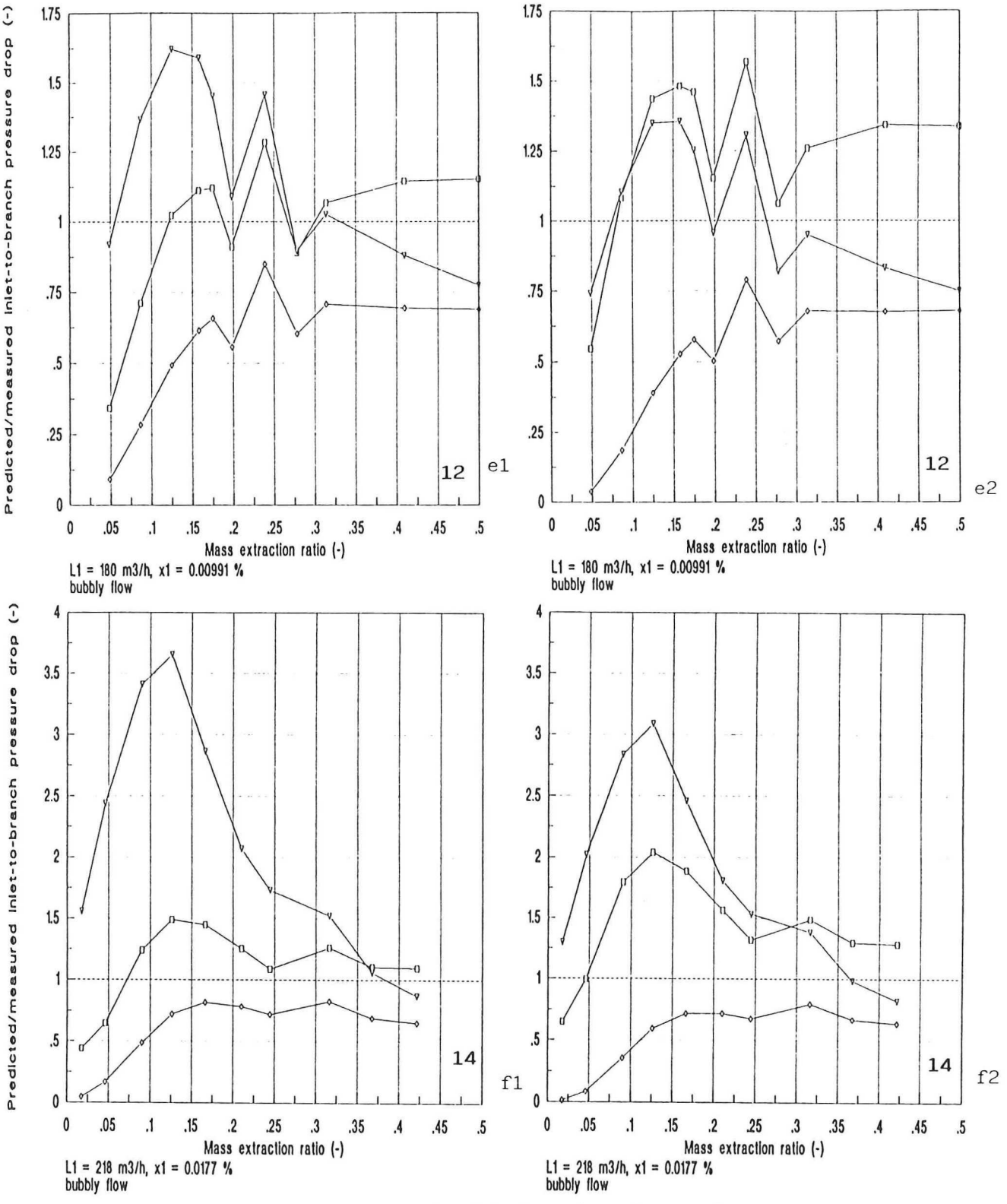

Figure 4.12. -continued- (a1) to (f2), Comparison of measured and predicted pressure drops (inlet-to-branch)

legend: ——□——: homogeneous model, ——▽——: Chisholm model, ——◇——: Reimann and Seeger model

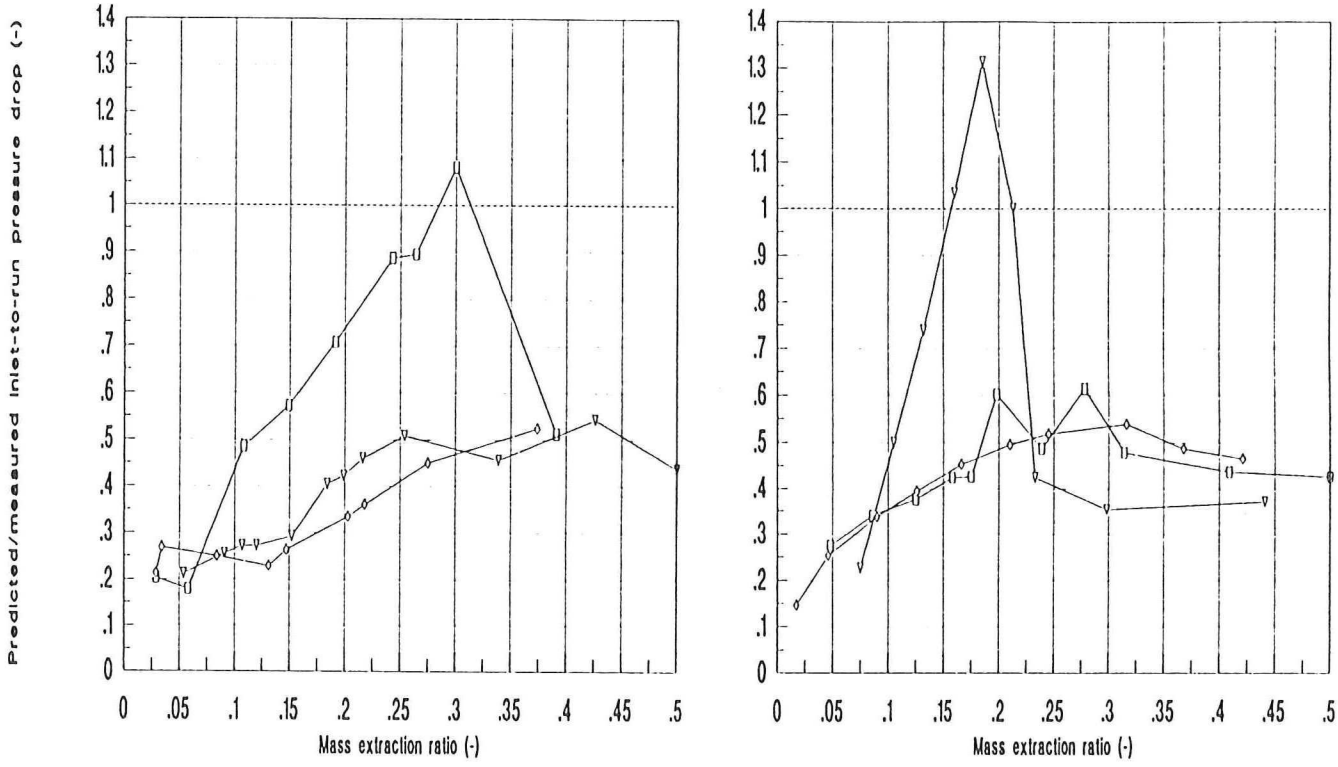

Figure 4.13. (a) and (b), Comparison of measured and predicted pressure drops (inlet-to-run)
legend (a): ——□——: 7, ——▽——: 9, ——◇——: 6
legend (b): ——□——: 3, ——▽——: 12, ——◇——: 14

From the fact that the predictions are rather adequate, one can conclude that the branch at least is not *far* too short for the pressure drop measurements. This was rather surprising. However, the most important conclusion of this section has to be that, generally, at larger scale the same pressure drop models may be used (with the same predictive qualities) as the ones used for the small-scale experiments.

The inlet-to-run flow was compared to the model involving the pressure recovery coefficient, for the same six measurement series as above. These results are given in the same predicted/measured way as the inlet-to-branch measurements. In appendix III, the results of these comparisons are given as well. The results are represented graphically in figures 4.13 a and b.
The pressure recovery coefficients K_{12} calculated are less than unity, as was expected. But, as can be seen quite clearly, the model gives too low results. This does not depend on the flow regime or any other parameter. It can be expected that this deviation is due to the fact that the run pipe is too short for the flow to have fully developed. The order of magnitude of the predictions is the same as that of the measurements, but it seems rather premature to connect any conclusions about the applicability of the inlet-to-run model for larger scale to this measurements.

4.5. Error consideration

The inaccuracy of the pressure signals in churn flow conditions did hardly ever exceed 1 %. When slug flow occured, as mentioned this inaccuracy could be about three times higher, so up to about 3 %. The inaccuracy of the flow measurements were under 1 % (with a small number of exceptions).

It is quite hard to determine the error in the measurements, as the expected largest source of error, the flow rig not-being-in-steady-state, is quite hard to determine, as was already argumented in section 3.5, where an error of up to about 3 % was assumed. Thus the majority of the measurements will have an error of between 2.5 % and 5 %.

However, some errors can have considerable consequences. When a small error is made in determining for instance the mass extraction rate, in the low extraction region the error in for instance the quality ratio can be quite large. This is due to the fact that in the low extraction area, the phase separation curve and the fraction curve have a rather steep slope. So a small error in the 'x-coordinate' can have severe impact on the 'y-coordinate'. The magnitude of such an error is very hard to tell. But one should keep this in mind while considering the errors made in the measurements.

The errors in the pressure measurements are somewhat larger. From the peaks and dips in the pressure drop prediction curves, one can determine a relative error of up to about 10 %. This error can most likely be mainly attributed to casual errors.

5. CONCLUSIONS

Generally can be said that the phase separation and pressure drop at large scale qualitatively act in the same way as those at smaller scale.

At low inlet liquid velocity, the T-junction acts as an almost perfect phase separator, in the sense that hardly any gas enters the run. With increasing inlet velocities this effect decreases. A maximum in the phase separation curves has not been found.
Graphically, the phase separation takes place between the total separation line and the empirical 'engineering model', proposed by Seeger. His estimation of the maximum branch mass flux at which no liquid entrainment occurs however does not fit.
Zetzmann's empirical model does not hold for the T-junction and area of interest. The claim of Zetzmann, of proportionality of branch and run quality to the inlet quality is true for this project as well.

A new aspect in the separation theory might be the fact that it appears that not only the inlet flow regime, but the branch flow regime as well, does influence the phase separation. This has been shown by means of the *'slug-pump effect'* in the branch, which seems to increase the amount of air entering the run. It has not been proved definitely, but at least strong indications exist into that direction.

The three inlet-to-branch pressure drop predicting models that have been investigated render predictions as good as in the case of smaller scale junctions, for which they were developed. The homogeneous and Chisholm model give slightly better predictions than the simplified Reimann and Seeger model. The most commonly used inlet-to-run model does not apply, but this might mainly be due to the run being not long enough to reach stabilized, friction dominated flow.

6. RECOMMENDATIONS

In order to get better insight in the flow split phenomena occurring at this larger scale, it is inevitable that many more measurements are performed.
These new measurements should focus on higher liquid superficial velocities, to determine if the inlet flow will behave even more 'bubbly', which eventually could result in a maximum in the phase separation curve at non-zero mass extraction rates.

Special attention should be attributed to the transition of churn to slug flow, as occuring in the branch. In this way the influence of the flow regime of the branch on the phase separation behaviour can be more accurately investigated. If this statement is true, it might be of interest to investigate other flow regime transitions in the branch as well.

Several modifications of the existing flow rig could increase the area of variables that can be covered with the equipment. One could think of several possibilities:
The area of superficial liquid velocities could be increased considerably by skipping the branch separation tank and putting the run separation tank in its place. In this case, the run two-phase flow would not pass a separation tank, but would be directly brought into the buffer tank again. Of course, one would have to assume that the mass balance is always satisfied, i.e. what flows through the run equals the inlet minus the branch mass flows.
By 'turning the T-junction around', i.e. swapping the inlet and the run, the new inlet would be longer and so the flow regime in this inlet would get more opportunity to fully develop. In this way the supposed stratification-stabilizing effect of the bend will be annihilated, which might lead to a better insight in the dependence on the flow regime.

Now several models have proved to be applicable to this scale as well, one could consider trying other, more difficult models. Especially the Saba and Lahey model, which is most of all based on physics, could be used to compare the measurements with. The total Reimann and Seeger model might render better results than its simplified equivalent.

One could think of adding a third, bubble promoting, agent like a detergent, to the system. This would lead to an increase of the bubbly flow area, which, for the chemical industry, is most likely the most interesting regime. Another possibility for achieving this might be to promote bubbly flow in a mechanical way, for instance by using an impeller upstream of the junction.

The separation itself might be influenced by several modifications *inside* the T-junction. Trying some existing ones like screens and small pipes, and maybe designing some ourselves might be an interesting project in order to reach a phase separation as complete and efficient as possible.

REFERENCES

[1] Groen, J.S., *Phase separation and pressure drop of two-phase flow in a dividing T-junction*, literature research essay, Delft University of Technology, (1991).

[2] Cheremisinoff, N.P. (Ed.), *Encyclopedia of fluid mechanics, volume 3: gas-liquid flows*, Gulf Publishing Co., Houston (1986).

[3] Reimann, J., Brinkmann, H.J., Domański, R., *Gas-liquid flow in dividing tee-junctions with a horizontal inlet and different branch orientations and diameters*, KfK 4399, Karlsruhe, (1988).

[4] Seeger, W., Reimann, J., Müller, U., *Two phase flow in a T-junction with a horizontal inlet, part I: phase separation*, Int. J. Multiphase Flow, **12**-4, (1986), 575-585.

[5] Azzopardi, B.J., Whalley, P.B., *The effect of flow patterns on two-phase flow in a T-junction*, Int. J. Multiphase Flow, **8**-5, (1982), 491-507.

[6] Zetzmann, K., *Phasenseparation und Druckabfall in zweiphasig durchströmten vertikalen Rohrabzweigungen*, Ph.D.-thesis, Hannover, (1982).

[7] Honan, T.J., Lahey, R.T. Jr., *The measurement of phase separation in wyes and tees*, Nucl. Eng. Des., **64**, (1981), 93-102.

[8] Azzopardi, B.J., *The effect of the side arm diameter on the two-phase flow splt at a T-junction*, Int. J. Multiphase Flow, **10**-4, (1984), 509-512.

[9] Azzopardi, B.J., Smith, P.A., *Two-phase flow split at T-junctions with horizontal and vertically upward side arms*, UK AEA report ?, (1989).

[10] Shoham, O., Arirachakaran, S., Brill, J.P., *Two-phase flow splitting in a horizontal reduced pipe tee*, Chem. Eng. Sci., **44**-10, (1989), 2388-2391.

[11] Azzopardi, B.J., Patrick, L., Memory, S.B., *The split of two-phase flow at a horizontal T-junction with a reduced diameter side arm*, AERE R13614, (1990).

[12] Lahey, R.T. Jr., *Current understanding of phase separation mechanisms in branching conduits*, Nucl. Eng. Des., **95**, (1986), 145-161.

[13] Hwang, S.T., Soliman, H.M., Lahey, R.T. Jr., *Phase separation in dividing two-phase flows*, Int. J. Multiphase Flow, **14**-4, (1988), 439-458.

[14] Saba, N., Lahey, R.T. Jr., *The analysis of phase separation phenomena in branching conduits*, Int. J. Multiphase Flow, **10**-1, (1984), 1-20.

[15] Shoham, O., Brill, J.P., Taitel, Y., *Two-phase flow splitting in a splitting in a tee junction - experimenting and modeling*, Chem. Eng. Sci., **42**-11, (1987), 2667-2676.

[16] Seeger, W., *Untersuchungen zum Druckabfall und zur Massenstromumverteilung von Zweiphasenströmungen in rechtwinklichen Rohrverzweigungen*, Ph.D.-thesis, KfK 3876, Karlsruhe (1985).

[17] Miller, D.S., *Internal flow, a guide to losses in pipe and duct systems*, BHRA, Cranfield, Bedford (U.K.), (1971).

[18] Reimann, J., Seeger, W., *Two-phase flow in a T-junction with a horizontal inlet, part II: pressure differences*, Int. J. Multiphase Flow, **12**-4, (1986), 587-608.

[19] Bird, R.B., Stewart, W.E., Lightfoot, E.N., *Transport phenomena*, Wiley, New York, (1960), chapter 6.

[20] Barnea, Mizrahi, Chem. Eng. J., **5**, (1973),171,

[21] Janssen, L.P.B.M., Warmoeskerken, M.M.C.G., *Transport phenomena data companion*, Edward Arnold & Delftse Uitgevers Maatschappij, (1987), 19.

[22] Wood, A.B., *A textbook of sound*, G. Bell and Sons Ltd., London, (1941).

ACKNOWLEDGEMENTS

At the closing of this project I would like to express my thanks to several persons, without whom I wouldn't have come where I am now.

First of all, I would like to thank Ron Garton and Jan de Rijke of Exxon Chemical International, for providing me with such an interesting and enterprising project and for the nice conversations, discussions and lunches we have had.
The supervision of Professor Van den Akker and Rob Mudde was enormously helpful, in technical and scientific as well as in correcting and educational sense.
Without the help of all the workers and the staff at the Kramers Laboratorium voor Fysische Technologie the realization of this project would not have been possible. Especially those who helped me building the flow rig and getting it started and Karin Westra I thank explicitly.
The company of my fellow students (and future fellow-Ph.D.-students) has always been very comfortable. I wish to thank them for having coffee, beer or a laugh quite a lot of times, or for just annoying me or providing the possibility of being annoyed by me.

APPENDICES

APPENDIX I. CALCULATION OF THE CORRECTION FACTOR FOR WATER VAPOUR PRESENT IN THE OUTLET AIR FLOW

All values and formulas used in this appendix are gained from the Transport Phenomena Data Companion [21].

The way of operation of the gas mass flow meters has been described in section 3.2.2. The 'input variable' of the meter is the specific heat per unit mass of the gas passing (in this case air). So this is the variable that has to be modified.

The saturated pressure of water vapour in air at 25°C is about 2500 Pa. That means that the water vapour mass fraction in saturated air is slightly less than 1 %.
The specific heat per unit mass (C_p) of humid air is given by

$$C_p^{humid\ air} = C_p^{dry\ air} + H_{abs}\, C_p^{water\ vapour} \qquad (I.1)$$

in which H_{abs} is the absolute humidity of the air at pressure p, given by

$$H_{abs} = 0.622 \frac{p_v}{p - p_v} \qquad (I.2)$$

In this, p_v is the partial pressure of the water vapour. At p = 1 bar, H_{abs} is about 0.016 kg water/kg dry air. The specific heat of dry air is 1.00 kJ/kg K, teh specific heat of water vapour equals 1.87 kJ/kg K. So the specific heat of water saturated air equals 1.03 kJ/kg K. This value indicates that the mass flow meter, using the specific heat of dry air, calculates a mass flow that is a factor 1.03 too high. So, dividing the flow calculated by the flow meter by 1.03, one obtains the mass flow of humid air. The mass fraction of dry air in this mixture is, as argued, 99 %. So to obtain the actual mass flow of dry air, one has to divide the value calculated by the mass flow meter by a factor 0.99 * 1.03, which is 1.02.

APPENDIX II. TABLES CONTAINING THE FLOW SPLIT DATA

The numbers given at the top left hand corner of the tables correspond to the numbers in the flow map (figure 4.6).

1

L_1	L_2	L_3	G_1	G_2	G_3	x_1	x_2	x_3	L_3/L_1	G_3/G_1
kg/s	kg/s	kg/s	g/s	g/s	g/s	%	%	%	-	-
25.43	24.25	1.173	2.93	0.16	2.771	0.012	7e-04	0.236	0.046	0.946
25.66	23.4	2.253	2.904	0.099	2.806	0.011	4e-04	0.124	0.088	0.966
27.67	24.4	3.267	2.978	0.138	2.84	0.011	6e-04	0.087	0.118	0.954
24.78	21.34	3.447	2.993	0.051	2.942	0.012	2e-04	0.085	0.139	0.983
25.26	20.95	4.307	3.085	0.034	3.051	0.012	2e-04	0.071	0.171	0.989
25.48	20.24	5.234	3.171	0.075	3.097	0.012	4e-04	0.059	0.205	0.976
24.67	19.23	5.441	3.179	0.102	3.076	0.013	5e-04	0.057	0.221	0.968
25.48	19.35	6.124	3.157	0.066	3.091	0.012	3e-04	0.05	0.24	0.979
25.88	19.13	6.742	3.162	0.081	3.081	0.012	4e-04	0.046	0.261	0.974
25.12	12.89	12.23	2.948	0.172	2.776	0.012	0.001	0.023	0.487	0.942

w_3/w_1	x_3/x_1	$\overline{\rho_1}$	$\overline{\rho_2}$	$\overline{\rho_3}$	u_{LS1}	u_{GS1}	u_{LS2}	u_{GS2}	u_{LS3}	u_{GS3}
-	-	kg/m³	kg/m³	kg/m³	m/s	m/s	m/s	m/s	m/s	m/s
0.046	20.46	932.6	994	409.9	0.612	0.043	0.584	0.002	0.149	0.225
0.088	10.99	933.3	995.4	566.6	0.617	0.043	0.563	0.001	0.287	0.296
0.118	8.071	936.7	994.6	653	0.666	0.044	0.587	0.002	0.416	0.3
0.139	7.064	928.4	996.5	652.5	0.596	0.045	0.514	8e-04	0.439	0.311
0.171	5.797	927.5	997	692.8	0.608	0.046	0.504	5e-04	0.548	0.322
0.206	4.751	926	995.7	728.8	0.613	0.048	0.487	0.001	0.666	0.327
0.221	4.386	923.3	994.7	736.7	0.594	0.048	0.463	0.002	0.693	0.325
0.24	4.071	926	995.9	758.2	0.613	0.048	0.466	0.001	0.78	0.327
0.261	3.738	926.8	995.4	775.4	0.623	0.048	0.46	0.001	0.858	0.325
0.487	1.934	933.6	990.2	880.5	0.605	0.042	0.31	0.002	1.557	0.293

2

L_1	L_2	L_3	G_1	G_2	G_3	x_1	x_2	x_3	L_3/L_1	G_3/G_1
kg/s	kg/s	kg/s	g/s	g/s	g/s	%	%	%	-	-
27.34	26.03	1.31	3.81	0.318	3.491	0.014	0.001	0.266	0.048	0.916
28.12	25.56	2.567	3.95	0.169	3.78	0.014	7e-04	0.147	0.091	0.957
28.62	25.15	3.47	3.826	0.15	3.676	0.013	6e-04	0.106	0.121	0.961
29.04	24.61	4.427	3.916	0.115	3.801	0.013	5e-04	0.086	0.152	0.971
29.25	23.89	5.357	4.181	0.076	4.105	0.014	3e-04	0.077	0.183	0.982
28.25	22.07	6.178	3.599	0.124	3.475	0.013	6e-04	0.056	0.219	0.966
27.79	20.85	6.931	3.842	0.101	3.74	0.014	5e-04	0.054	0.249	0.974
28.23	20.53	7.701	4.015	0.075	3.94	0.014	4e-04	0.051	0.273	0.981
27.35	16.05	11.3	3.939	0.098	3.842	0.014	6e-04	0.034	0.413	0.975

w_3/w_1	x_3/x_1	$\overline{\rho_1}$	$\overline{\rho_2}$	$\overline{\rho_3}$	u_{LS1}	u_{GS1}	u_{LS2}	u_{GS2}	u_{LS3}	u_{GS3}
-	-	kg/m^3	kg/m^3	kg/m^3	m/s	m/s	m/s	m/s	m/s	m/s
0.048	19.07	921	990.7	384.6	0.658	0.055	0.626	0.005	0.167	0.284
0.091	10.47	920.2	994	529.4	0.677	0.057	0.615	0.002	0.327	0.399
0.121	7.918	923.4	994.4	608.6	0.689	0.056	0.605	0.002	0.442	0.388
0.153	6.362	922.4	995.2	656	0.699	0.057	0.592	0.002	0.563	0.401
0.183	5.357	918.1	996.1	680.6	0.704	0.062	0.575	0.001	0.682	0.434
0.219	4.413	925.3	994.6	741.1	0.68	0.054	0.531	0.002	0.786	0.367
0.25	3.901	919	995	747.3	0.669	0.058	0.502	0.002	0.882	0.395
0.273	3.596	916.8	995.7	756.8	0.679	0.06	0.494	0.001	0.98	0.416
0.413	2.36	919.3	994.4	830.3	0.658	0.057	0.386	0.001	1.438	0.406

3

L_1	L_2	L_3	G_1	G_2	G_3	x_1	x_2	x_3	L_3/L_1	G_3/G_1
kg/s	kg/s	kg/s	g/s	g/s	g/s	%	%	%	-	-
33.19	30.7	2.497	1.962	0.158	1.804	0.006	5e-04	0.072	0.075	0.92
32.99	29.52	3.47	2.43	0.163	2.267	0.007	6e-04	0.065	0.105	0.933
32.11	27.87	4.243	2.462	0.075	2.387	0.008	3e-04	0.056	0.132	0.97
32.16	27.02	5.142	1.92	0.03	1.89	0.006	1e-04	0.037	0.16	0.984
32.71	26.66	6.051	2.016	0.063	1.952	0.006	2e-04	0.032	0.185	0.969
32.68	25.76	6.925	2.248	0.068	2.18	0.007	3e-04	0.031	0.212	0.97
33.29	25.55	7.748	2.452	0.086	2.366	0.007	3e-04	0.031	0.233	0.965
31.52	22.11	9.402	2.409	0.022	2.387	0.008	1e-04	0.025	0.298	0.991
32.89	18.38	14.5	2.423	0.034	2.389	0.007	2e-04	0.016	0.441	0.986

w_3/w_1	x_3/x_1	$\overline{\rho_1}$	$\overline{\rho_2}$	$\overline{\rho_3}$	u_{LS1}	u_{GS1}	u_{LS2}	u_{GS2}	u_{LS3}	u_{GS3}
-	-	kg/m³	kg/m³	kg/m³	m/s	m/s	m/s	m/s	m/s	m/s
0.075	12.22	963.7	994.9	695.5	0.799	0.029	0.739	0.002	0.318	0.142
0.105	8.864	955.2	994.7	714.2	0.794	0.036	0.71	0.002	0.442	0.181
0.132	7.335	952.9	996.3	740.9	0.773	0.037	0.671	0.001	0.54	0.194
0.16	6.154	962.4	997.3	812.8	0.774	0.029	0.65	5e-04	0.655	0.154
0.185	5.234	961.2	996.5	831.5	0.787	0.03	0.642	1e-03	0.77	0.16
0.212	4.576	956.9	996.4	834	0.787	0.034	0.62	0.001	0.882	0.18
0.233	4.145	954	995.9	837.9	0.801	0.037	0.615	0.001	0.986	0.195
0.298	3.321	953.5	997.4	864	0.759	0.036	0.532	3e-04	1.197	0.193
0.441	2.236	958.2	997	913.2	0.792	0.033	0.442	5e-04	1.846	0.18

4

L_1	L_2	L_3	G_1	G_2	G_3	x_1	x_2	x_3	L_3/L_1	G_3/G_1
kg/s	kg/s	kg/s	g/s	g/s	g/s	%	%	%	-	-
24.85	24.21	0.643	7.241	0.975	6.266	0.029	0.004	0.965	0.026	0.865
25.13	23.67	1.458	7.477	0.614	6.863	0.03	0.003	0.468	0.058	0.918
24.34	22.39	1.948	8.253	0.74	7.512	0.034	0.003	0.384	0.08	0.91
26.22	22.58	3.635	8.952	0.472	8.481	0.034	0.002	0.233	0.139	0.947
26.43	21.92	4.508	8.572	0.294	8.278	0.032	0.001	0.183	0.171	0.966
26.45	21.24	5.217	8.534	0.247	8.287	0.032	0.001	0.159	0.197	0.971
26.49	20.73	5.763	8.361	0.203	8.158	0.032	1e-03	0.141	0.218	0.976
26.92	19.68	7.241	8.438	0.166	8.273	0.031	8e-04	0.114	0.269	0.98
25.03	13.71	11.32	8.506	0.165	8.341	0.034	0.001	0.074	0.452	0.981
w_3/w_1	x_3/x_1	$\overline{\rho_1}$	$\overline{\rho_2}$	$\overline{\rho_3}$	u_{LS1}	u_{GS1}	u_{LS2}	u_{GS2}	u_{LS3}	u_{GS3}
-	-	kg/m^3	kg/m^3	kg/m^3	m/s	m/s	m/s	m/s	m/s	m/s
0.026	33.15	848	974.2	145.5	0.598	0.106	0.583	0.014	0.082	0.509
0.058	15.75	845	982.5	259.1	0.605	0.11	0.57	0.009	0.186	0.725
0.08	11.33	826.8	978.2	298.3	0.586	0.122	0.539	0.011	0.248	0.794
0.139	6.82	825.4	985.4	411.4	0.631	0.132	0.543	0.007	0.463	0.896
0.171	5.654	831.7	989.8	468.4	0.636	0.128	0.528	0.004	0.574	0.875
0.197	4.918	831.9	990.9	503.5	0.637	0.128	0.511	0.004	0.664	0.875
0.218	4.48	834.4	992	531.3	0.638	0.126	0.499	0.003	0.734	0.862
0.269	3.642	834.4	992.8	582.2	0.648	0.128	0.474	0.003	0.922	0.874
0.452	2.168	826.9	990.7	689	0.602	0.125	0.33	0.002	1.441	0.673

5

L_1	L_2	L_3	G_1	G_2	G_3	x_1	x_2	x_3	L_3/L_1	G_3/G_1
kg/s	kg/s	kg/s	g/s	g/s	g/s	%	%	%	-	-
29,64	29,04	0,601	5,323	0,758	4,566	0,018	0,003	0,754	0,02	0,858
31,74	30,39	1,354	5,487	0,489	4,998	0,017	0,002	0,368	0,043	0,911
28,87	26,67	2,204	6,364	0,455	5,909	0,022	0,002	0,267	0,076	0,928
30,04	27,2	2,836	5,877	0,391	5,486	0,02	0,001	0,193	0,094	0,933
30,6	27,01	3,59	5,889	0,238	5,651	0,019	9e-04	0,157	0,117	0,96
29,5	25,57	3,932	5,466	0,181	5,285	0,019	7e-04	0,134	0,133	0,967
30,78	24,51	6,268	5,483	0,226	5,258	0,018	9e-04	0,084	0,204	0,959
30,68	23,85	6,834	5,49	0,22	5,27	0,018	9e-04	0,077	0,223	0,96
31,29	23,12	8,173	5,659	0,266	5,393	0,018	0,001	0,066	0,261	0,953
30,69	22,13	8,553	5,528	0,238	5,29	0,018	0,001	0,062	0,279	0,957
25,2	13,48	11,72	5,542	0,189	5,352	0,022	0,001	0,046	0,465	0,966

w_3/w_1	x_3/x_1	$\overline{\rho_1}$	$\overline{\rho_2}$	$\overline{\rho_3}$	u_{LS1}	u_{GS1}	u_{LS2}	u_{GS2}	u_{LS3}	u_{GS3}
-	-	kg/m^3	kg/m^3	kg/m^3	m/s	m/s	m/s	m/s	m/s	m/s
0,02	42,01	900,2	982,5	179,4	0,713	0,078	0,699	0,011	0,076	0,361
0,043	21,28	903,8	988,4	310,2	0,764	0,08	0,731	0,007	0,172	0,394
0,077	12,13	878,3	987,6	376,1	0,695	0,095	0,642	0,007	0,281	0,478
0,095	9,868	894	989,5	464,7	0,723	0,084	0,655	0,006	0,361	0,579
0,117	8,168	895,6	992,8	516	0,736	0,085	0,65	0,003	0,457	0,597
0,133	7,247	897,8	993,8	551,7	0,71	0,08	0,615	0,003	0,501	0,558
0,204	4,705	900,6	992,4	661,3	0,741	0,08	0,59	0,003	0,798	0,555
0,223	4,307	899,6	992,4	678,5	0,738	0,081	0,574	0,003	0,87	0,557
0,261	3,648	898,3	991	710,5	0,753	0,084	0,556	0,004	1,04	0,57
0,279	3,432	898	991,4	722	0,739	0,083	0,533	0,004	1,089	0,559
0,465	2,076	880,1	989,5	780,9	0,607	0,082	0,324	0,003	1,492	0,432

L_1	L_2	L_3	G_1	G_2	G_3	x_1	x_2	x_3	L_3/L_1	G_3/G_1
kg/s	kg/s	kg/s	g/s	g/s	g/s	%	%	%	-	-
35.75	34.71	1.049	6.23	0.894	5.336	0.017	0.003	0.506	0.029	0.856
34.92	33.72	1.195	5.193	0.84	4.354	0.015	0.002	0.363	0.034	0.838
32.21	29.51	2.703	6.044	0.544	5.5	0.019	0.002	0.203	0.084	0.91
33.87	29.43	4.435	6.275	0.243	6.032	0.019	8e-04	0.136	0.131	0.961
33.34	28.45	4.895	6.207	0.058	6.149	0.019	2e-04	0.125	0.147	0.991
34	27.1	6.907	6.163	0.037	6.127	0.018	1e-04	0.089	0.203	0.994
33	25.82	7.181	6.363	0.15	6.212	0.019	6e-04	0.086	0.218	0.976
33.34	24.17	9.165	6.455	0.123	6.332	0.019	5e-04	0.069	0.275	0.981
34.3	21.48	12.82	6.688	0.126	6.562	0.019	6e-04	0.051	0.374	0.981
w_3/w_1	x_3/x_1	$\overline{\rho_1}$	$\overline{\rho_2}$	$\overline{\rho_3}$	u_{LS1}	u_{GS1}	u_{LS2}	u_{GS2}	u_{LS3}	u_{GS3}
-	-	kg/m^3	kg/m^3	kg/m^3	m/s	m/s	m/s	m/s	m/s	m/s
0.029	29.06	906.8	983.4	254.6	0.861	0.087	0.835	0.012	0.134	0.402
0.034	24.42	918.5	983.7	320.6	0.84	0.073	0.812	0.012	0.152	0.331
0.084	10.82	895.5	986.9	445.9	0.775	0.089	0.71	0.008	0.344	0.439
0.131	7.332	897.8	993.1	549	0.815	0.091	0.708	0.004	0.565	0.476
0.147	6.74	896.4	996.8	565.8	0.802	0.091	0.685	9e-04	0.623	0.491
0.203	4.89	898.9	997.2	648.5	0.818	0.091	0.652	5e-04	0.879	0.49
0.218	4.484	892.6	994.5	652.5	0.794	0.094	0.621	0.002	0.914	0.501
0.275	3.567	891.3	994.9	699.3	0.802	0.096	0.582	0.002	1.167	0.517
0.374	2.624	897.2	994.6	770.8	0.826	0.093	0.517	0.002	1.632	0.481

7

L_1	L_2	L_3	G_1	G_2	G_3	x_1	x_2	x_3	L_3/L_1	G_3/G_1
kg/s	kg/s	kg/s	g/s	g/s	g/s	%	%	%	-	-
41,31	40,12	1,187	4,074	0,498	3,577	0,01	0,001	0,301	0,029	0,878
41,19	38,8	2,39	4,08	0,308	3,772	0,01	8e-04	0,158	0,058	0,924
42,34	37,75	4,59	4,309	0,303	4,005	0,01	8e-04	0,087	0,108	0,93
42,78	36,39	6,389	4,317	0,371	3,946	0,01	0,001	0,062	0,149	0,914
43,21	34,95	8,257	4,399	0,34	4,058	0,01	1e-03	0,049	0,191	0,923
42,72	32,89	9,831	4,534	0,279	4,254	0,011	8e-04	0,043	0,23	0,938
42,99	32,56	10,43	4,311	0,267	4,044	0,01	8e-04	0,039	0,243	0,938
43,72	32,19	11,53	4,484	0,194	4,29	0,01	6e-04	0,037	0,264	0,957
42,74	29,94	12,8	4,367	0,211	4,157	0,01	7e-04	0,032	0,299	0,952
41,84	25,49	16,35	4,166	0,188	3,977	0,01	7e-04	0,024	0,391	0,955

w_3/w_1	x_3/x_1	$\overline{\rho_1}$	$\overline{\rho_2}$	$\overline{\rho_3}$	u_{LS1}	u_{GS1}	u_{LS2}	u_{GS2}	u_{LS3}	u_{GS3}
-	-	kg/m³	kg/m³	kg/m³	m/s	m/s	m/s	m/s	m/s	m/s
0,029	30,47	947,2	991,3	378,8	0,994	0,054	0,966	0,007	0,151	0,254
0,058	15,91	946	993,6	532,5	0,991	0,055	0,934	0,004	0,304	0,273
0,108	8,569	944,3	993,5	671,1	1,019	0,058	0,909	0,004	0,584	0,291
0,149	6,118	944,3	992,3	740,5	1,03	0,059	0,876	0,005	0,813	0,289
0,191	4,826	943	992,5	778,9	1,04	0,061	0,841	0,005	1,051	0,304
0,23	4,076	939,9	993,1	797,2	1,028	0,064	0,792	0,004	1,251	0,326
0,243	3,865	942,5	993,2	813	1,035	0,061	0,784	0,004	1,328	0,312
0,264	3,626	941	994,5	818,2	1,052	0,064	0,775	0,003	1,468	0,335
0,3	3,177	941,2	993,9	837,5	1,029	0,062	0,721	0,003	1,629	0,324
0,391	2,443	946,6	994	881,1	1,007	0,055	0,613	0,002	2,081	0,292

L_1	L_2	L_3	G_1	G_2	G_3	x_1	x_2	x_3	L_3/L_1	G_3/G_1
kg/s	kg/s	kg/s	g/s	g/s	g/s	%	%	%	-	-
45.39	42.5	2.893	8.108	1.484	6.624	0.018	0.003	0.228	0.064	0.817
41.21	37.7	3.513	7.536	0.984	6.552	0.018	0.003	0.186	0.085	0.869
42.26	36.51	5.753	7.862	0.643	7.219	0.019	0.002	0.125	0.136	0.918
41.13	33.89	7.249	7.799	0.606	7.192	0.019	0.002	0.099	0.176	0.922
41.29	32.61	8.675	7.644	0.228	7.416	0.019	7e-04	0.085	0.21	0.97
41.24	31.27	9.972	7.29	0.223	7.066	0.018	7e-04	0.071	0.242	0.969
41.61	30.2	11.41	7.463	0.214	7.249	0.018	7e-04	0.064	0.274	0.971
41.76	29.41	12.35	7.64	0.125	7.516	0.018	4e-04	0.061	0.296	0.984
41.89	25.89	16	8.454	0.171	8.283	0.02	7e-04	0.052	0.382	0.98

w_3/w_1	x_3/x_1	$\overline{\rho_1}$	$\overline{\rho_2}$	$\overline{\rho_3}$	u_{LS1}	u_{GS1}	u_{LS2}	u_{GS2}	u_{LS3}	u_{GS3}
-	-	kg/m³	kg/m³	kg/m³	m/s	m/s	m/s	m/s	m/s	m/s
0.064	12.79	909.2	979.3	443.7	1.092	0.107	1.023	0.02	0.368	0.497
0.085	10.18	905.5	983.6	489.1	0.992	0.102	0.907	0.013	0.447	0.479
0.136	6.738	903.6	988.2	585.7	1.017	0.107	0.879	0.009	0.732	0.527
0.176	5.229	900.4	987.9	637.1	0.99	0.108	0.816	0.008	0.923	0.535
0.21	4.615	902	994	669.2	0.994	0.106	0.785	0.003	1.104	0.557
0.242	4.007	905.1	993.9	707.3	0.993	0.102	0.753	0.003	1.269	0.538
0.274	3.542	903.5	993.9	728.1	1.001	0.105	0.727	0.003	1.452	0.556
0.296	3.324	901.6	995.5	736.3	1.005	0.108	0.708	0.002	1.573	0.578
0.382	2.564	900.4	994.5	781	1.008	0.11	0.623	0.002	2.037	0.598

L_1	L_2	L_3	G_1	G_2	G_3	x_1	x_2	x_3	L_3/L_1	G_3/G_1
kg/s	kg/s	kg/s	g/s	g/s	g/s	%	%	%	-	-
39.88	37.72	2.161	14.15	4.409	9.739	0.035	0.012	0.449	0.054	0.688
41.13	37.39	3.741	12.25	2.418	9.83	0.03	0.006	0.262	0.091	0.803
41.25	36.85	4.404	12.4	1.635	10.77	0.03	0.004	0.244	0.107	0.868
41.01	36.11	4.903	12.52	0.928	11.59	0.031	0.003	0.236	0.12	0.926
40.77	34.6	6.172	12.74	0.965	11.78	0.031	0.003	0.19	0.151	0.924
41.91	34.2	7.708	12.75	0.879	11.87	0.03	0.003	0.154	0.184	0.931
41.31	33.09	8.223	12.96	0.85	12.12	0.031	0.003	0.147	0.199	0.934
41.95	32.89	9.054	13.1	0.571	12.53	0.031	0.002	0.138	0.216	0.956
42.77	31.91	10.87	12.83	0.617	12.21	0.03	0.002	0.112	0.254	0.952
44.33	29.3	15.04	12.84	0.35	12.49	0.029	0.001	0.083	0.339	0.973
41.65	23.9	17.75	12.85	0.512	12.34	0.031	0.002	0.069	0.426	0.96
42.08	20.99	21.09	13.53	0.483	13.05	0.032	0.002	0.062	0.501	0.964

w_3/w_1	x_3/x_1	$\overline{\rho_1}$	$\overline{\rho_2}$	$\overline{\rho_3}$	u_{LS1}	u_{GS1}	u_{LS2}	u_{GS2}	u_{LS3}	u_{GS3}
-	-	kg/m³	kg/m³	kg/m³	m/s	m/s	m/s	m/s	m/s	m/s
0.054	12.65	835.2	937.8	287.9	0.96	0.188	0.908	0.059	0.275	0.696
0.091	8.803	856.7	963.5	407.1	0.99	0.164	0.9	0.032	0.476	0.711
0.107	8.116	853.7	973.7	420.7	0.993	0.169	0.887	0.022	0.561	0.792
0.12	7.728	850.2	983.6	425.8	0.987	0.172	0.869	0.013	0.624	0.862
0.152	6.095	846.5	982.3	477.3	0.981	0.176	0.833	0.013	0.786	0.883
0.184	5.056	849.7	983.5	530.1	1.009	0.177	0.823	0.012	0.981	0.893
0.199	4.689	844.3	983.3	538.4	0.994	0.182	0.796	0.012	1.047	0.924
0.216	4.426	844.6	988	553.3	1.01	0.184	0.792	0.008	1.152	0.959
0.254	3.744	849.7	986.9	603.5	1.029	0.18	0.768	0.009	1.383	0.939
0.339	2.866	863.8	991.6	690.5	1.067	0.166	0.705	0.005	1.914	0.9
0.426	2.252	854.3	986.5	723.8	1.002	0.169	0.575	0.007	2.26	0.901
0.501	1.923	868.4	987.5	775.4	1.013	0.152	0.505	0.005	2.684	0.822

10

L_1	L_2	L_3	G_1	G_2	G_3	x_1	x_2	x_3	L_3/L_1	G_3/G_1
kg/s	kg/s	kg/s	g/s	g/s	g/s	%	%	%	-	-
50.65	48.46	2.192	14.5	4.4	10.1	0.029	0.009	0.459	0.043	0.697
50.1	46.22	3.878	15.15	4.206	10.95	0.03	0.009	0.282	0.077	0.722
49.94	44.91	5.024	14.23	3.129	11.11	0.028	0.007	0.221	0.101	0.78
50.83	44.41	6.42	15.42	3.085	12.34	0.03	0.007	0.192	0.126	0.8
52.35	44.45	7.896	14.44	2.522	11.92	0.028	0.006	0.151	0.151	0.825
51.89	42.59	9.296	15.09	2.148	12.94	0.029	0.005	0.139	0.179	0.858
53	41.38	11.62	14.68	1.983	12.69	0.028	0.005	0.109	0.219	0.865
50.84	38.52	12.33	14.31	2.005	12.31	0.028	0.005	0.1	0.242	0.86
53.04	38.63	14.41	14.87	2.349	12.52	0.028	0.006	0.087	0.272	0.842
50.48	33.22	17.26	14.57	1.866	12.71	0.029	0.006	0.074	0.342	0.872
50.18	26.4	23.78	16.5	2.202	14.3	0.033	0.008	0.06	0.474	0.867

w_3/w_1	x_3/x_1	$\overline{\rho_1}$	$\overline{\rho_2}$	$\overline{\rho_3}$	u_{LS1}	u_{GS1}	u_{LS2}	u_{GS2}	u_{LS3}	u_{GS3}
-	-	kg/m³	kg/m³	kg/m³	m/s	m/s	m/s	m/s	m/s	m/s
0.043	16.03	876.2	955.9	309.2	1.219	0.17	1.166	0.052	0.279	0.639
0.078	9.311	867.9	954.9	416.6	1.206	0.182	1.112	0.05	0.494	0.707
0.101	7.74	872.2	964	471.5	1.202	0.174	1.081	0.038	0.639	0.734
0.127	6.324	865	964.1	506	1.223	0.189	1.069	0.038	0.817	0.816
0.151	5.465	875.2	970	564.8	1.26	0.178	1.07	0.031	1.005	0.793
0.179	4.782	866.8	972.5	579	1.249	0.19	1.025	0.027	1.183	0.885
0.219	3.942	871.6	973.6	635	1.276	0.186	0.996	0.025	1.479	0.877
0.243	3.545	864.6	970.3	645.1	1.224	0.19	0.927	0.027	1.569	0.896
0.272	3.097	864.5	965.6	675.1	1.277	0.198	0.93	0.031	1.835	0.924
0.342	2.549	859	967.5	706.5	1.215	0.197	0.8	0.025	2.197	0.952
0.474	1.828	872.5	962.9	790.2	1.208	0.175	0.635	0.023	3.027	0.863

L_1	L_2	L_3	G_1	G_2	G_3	x_1	x_2	x_3	L_3/L_1	G_3/G_1
kg/s	kg/s	kg/s	g/s	g/s	g/s	%	%	%	-	-
43.4	41.24	2.159	2.562	0.547	2.015	0.006	0.001	0.093	0.05	0.787
45.17	41.31	3.863	2.591	0.437	2.154	0.006	0.001	0.056	0.086	0.831
44.75	39.94	4.812	2.709	0.417	2.292	0.006	0.001	0.048	0.108	0.846
44.06	37.94	6.112	2.423	0.179	2.244	0.005	5e-04	0.037	0.139	0.926
44.44	36.93	7.504	2.554	0.193	2.361	0.006	5e-04	0.031	0.169	0.924
44.33	35.49	8.848	2.539	0.221	2.319	0.006	6e-04	0.026	0.2	0.913
44.59	34.92	9.676	2.616	0.208	2.408	0.006	6e-04	0.025	0.217	0.92
46.32	35.43	10.89	2.315	0.186	2.13	0.005	5e-04	0.02	0.235	0.92
46.08	33.62	12.46	2.378	0.14	2.238	0.005	4e-04	0.018	0.27	0.941
45.68	31.35	14.32	2.438	0.067	2.37	0.005	2e-04	0.017	0.314	0.972
46.48	27.4	19.08	2.885	0.084	2.8	0.006	3e-04	0.015	0.41	0.971

w_3/w_1	x_3/x_1	$\overline{\rho_1}$	$\overline{\rho_2}$	$\overline{\rho_3}$	u_{LS1}	u_{GS1}	u_{LS2}	u_{GS2}	u_{LS3}	u_{GS3}
-	-	kg/m^3	kg/m^3	kg/m^3	m/s	m/s	m/s	m/s	m/s	m/s
0.05	15.8	967.5	991	666.5	1.044	0.033	0.992	0.007	0.275	0.166
0.086	9.717	968.4	992.4	769.3	1.087	0.033	0.994	0.006	0.492	0.177
0.108	7.866	966.2	992.4	792.9	1.077	0.036	0.961	0.005	0.612	0.192
0.139	6.674	968.4	995.4	829	1.06	0.033	0.913	0.002	0.778	0.193
0.169	5.472	966.8	995.1	848.2	1.069	0.035	0.889	0.003	0.955	0.206
0.2	4.574	966.4	994.5	868.2	1.067	0.035	0.854	0.003	1.126	0.206
0.217	4.242	965.4	994.6	872.8	1.073	0.036	0.84	0.003	1.232	0.217
0.235	3.912	970.2	995	897.5	1.115	0.032	0.853	0.003	1.386	0.191
0.27	3.48	968.8	995.6	903.4	1.109	0.034	0.809	0.002	1.586	0.206
0.314	3.101	968.8	996.8	912.6	1.099	0.033	0.755	9e-04	1.823	0.212
0.411	2.365	967.2	996.4	928.2	1.119	0.036	0.659	0.001	2.428	0.229

L_1	L_2	L_3	G_1	G_2	G_3	x_1	x_2	x_3	L_3/L_1	G_3/G_1
kg/s	kg/s	kg/s	g/s	g/s	g/s	%	%	%	-	-
50.55	48.11	2.442	5.035	1.166	3.869	0.01	0.002	0.158	0.048	0.769
51.66	47.2	4.463	4.84	0.982	3.858	0.009	0.002	0.086	0.086	0.797
50.62	44.32	6.301	4.989	0.946	4.043	0.01	0.002	0.064	0.124	0.81
49.77	41.92	7.841	5.018	0.811	4.207	0.01	0.002	0.054	0.158	0.838
51.28	42.33	8.952	4.894	0.55	4.344	0.01	0.001	0.049	0.175	0.888
49.46	39.57	9.891	4.593	0.436	4.157	0.009	0.001	0.042	0.2	0.905
51.39	39.12	12.27	5.054	0.542	4.512	0.01	0.001	0.037	0.239	0.893
49.93	36.06	13.87	4.402	0.378	4.024	0.009	0.001	0.029	0.278	0.914
50.32	34.54	15.78	5.219	0.444	4.774	0.01	0.001	0.03	0.314	0.915
48.81	28.84	19.97	5.597	0.398	5.199	0.011	0.001	0.026	0.409	0.929
47.73	23.27	24.47	4.999	0.387	4.612	0.01	0.002	0.019	0.513	0.923
w_3/w_1	x_3/x_1	$\overline{\rho_1}$	$\overline{\rho_2}$	$\overline{\rho_3}$	u_{LS1}	u_{GS1}	u_{LS2}	u_{GS2}	u_{LS3}	u_{GS3}
-	-	kg/m^3	kg/m^3	kg/m^3	m/s	m/s	m/s	m/s	m/s	m/s
0.048	15.88	951.5	986.3	562	1.217	0.06	1.158	0.014	0.311	0.247
0.086	9.219	953.7	987.8	698.6	1.243	0.058	1.136	0.012	0.568	0.25
0.125	6.508	949.9	987.2	750.5	1.218	0.062	1.067	0.012	0.802	0.272
0.158	5.319	947.6	987.9	778.1	1.198	0.064	1.009	0.01	0.998	0.291
0.175	5.083	950.3	991.2	795.2	1.234	0.062	1.019	0.007	1.139	0.3
0.2	4.524	949.9	992	811.9	1.19	0.061	0.952	0.006	1.259	0.299
0.239	3.739	947.6	990.6	832.4	1.237	0.066	0.942	0.007	1.561	0.323
0.278	3.29	950.3	992.1	856.5	1.202	0.061	0.868	0.005	1.765	0.306
0.314	2.917	944.8	991.1	857.2	1.211	0.068	0.831	0.006	2.009	0.348
0.409	2.27	944.6	991.3	884.6	1.175	0.067	0.694	0.005	2.542	0.346
0.513	1.8	953.9	990.7	921.3	1.149	0.053	0.56	0.004	3.114	0.281

L_1	L_2	L_3	G_1	G_2	G_3	x_1	x_2	x_3	L_3/L_1	G_3/G_1
kg/s	kg/s	kg/s	g/s	g/s	g/s	%	%	%	-	-
50.61	48.5	2.108	10.24	2.417	7.819	0.02	0.005	0.369	0.042	0.764
50.57	45.58	4.996	10.68	1.936	8.743	0.021	0.004	0.175	0.099	0.819
51.27	44.5	6.775	10.46	1.898	8.562	0.02	0.004	0.126	0.132	0.819
50.64	42.17	8.47	10.07	1.859	8.211	0.02	0.004	0.097	0.167	0.815
50.3	39.49	10.8	8.653	1.119	7.533	0.017	0.003	0.07	0.215	0.871
49.74	38.18	11.57	8.389	1.102	7.287	0.017	0.003	0.063	0.233	0.869
49.58	36.39	13.19	8.325	0.893	7.432	0.017	0.002	0.056	0.266	0.893
51.17	37.22	13.95	10.06	1.19	8.872	0.02	0.003	0.064	0.273	0.882
50.05	34.55	15.5	9.65	1.229	8.421	0.019	0.004	0.054	0.31	0.873
50.56	32.72	17.84	9.888	1.053	8.835	0.02	0.003	0.049	0.353	0.894
50.78	27.24	23.54	10.25	1.11	9.143	0.02	0.004	0.039	0.464	0.892
w_3/w_1	x_3/x_1	$\overline{\rho_1}$	$\overline{\rho_2}$	$\overline{\rho_3}$	u_{LS1}	u_{GS1}	u_{LS2}	u_{GS2}	u_{LS3}	u_{GS3}
-	-	kg/m^3	kg/m^3	kg/m^3	m/s	m/s	m/s	m/s	m/s	m/s
0.042	18.27	908.5	974.3	356.4	1.218	0.121	1.167	0.028	0.268	0.496
0.099	8.276	902	977.1	530.6	1.217	0.13	1.097	0.024	0.636	0.575
0.132	6.188	904.1	976.8	607.5	1.234	0.129	1.071	0.023	0.862	0.57
0.167	4.872	903.9	975.5	662	1.219	0.127	1.015	0.024	1.078	0.564
0.215	4.051	912.6	982.8	723.6	1.211	0.114	0.95	0.015	1.375	0.541
0.233	3.734	912.9	982.3	740.4	1.197	0.112	0.919	0.015	1.472	0.533
0.266	3.353	911.4	984.3	756.9	1.193	0.114	0.876	0.012	1.68	0.561
0.273	3.232	899.3	980.5	736.8	1.232	0.136	0.896	0.016	1.776	0.662
0.31	2.817	903.5	979.1	770.9	1.205	0.126	0.832	0.016	1.973	0.613
0.353	2.531	907.2	981.8	796.4	1.217	0.122	0.787	0.013	2.271	0.612
0.464	1.923	916	980.3	851.3	1.222	0.11	0.656	0.012	2.996	0.559

L_1	L_2	L_3	G_1	G_2	G_3	x_1	x_2	x_3	L_3/L_1	G_3/G_1
kg/s	kg/s	kg/s	g/s	g/s	g/s	%	%	%	-	-
60.83	59.77	1.054	10.74	5.476	5.262	0.018	0.009	0.497	0.017	0.49
60.11	57.31	2.797	10.24	3.887	6.357	0.017	0.007	0.227	0.047	0.621
60.42	54.97	5.444	10.25	3.188	7.062	0.017	0.006	0.13	0.09	0.689
59.69	52.17	7.516	11.15	3.297	7.853	0.019	0.006	0.104	0.126	0.704
60.02	50.04	9.976	10.7	2.949	7.751	0.018	0.006	0.078	0.166	0.724
60.47	47.77	12.7	10.41	2.409	8.001	0.017	0.005	0.063	0.21	0.769
59.93	45.28	14.65	11.18	2.672	8.512	0.019	0.006	0.058	0.244	0.761
60.14	41.14	19	10.64	2.075	8.561	0.018	0.005	0.045	0.316	0.805
61.24	38.74	22.51	10.95	2.15	8.798	0.018	0.006	0.039	0.367	0.804
61.77	35.74	26.02	10.49	1.225	9.265	0.017	0.003	0.036	0.421	0.883

w_3/w_1	x_3/x_1	$\overline{\rho_1}$	$\overline{\rho_2}$	$\overline{\rho_3}$	u_{LS1}	u_{GS1}	u_{LS2}	u_{GS2}	u_{LS3}	u_{GS3}
-	-	kg/m³	kg/m³	kg/m³	m/s	m/s	m/s	m/s	m/s	m/s
0.017	28.15	929.7	961.4	325.5	1.464	0.108	1.439	0.055	0.134	0.284
0.047	13.31	929.5	969.6	504	1.447	0.107	1.379	0.041	0.356	0.357
0.09	7.638	927.4	972.7	631.2	1.454	0.111	1.323	0.035	0.693	0.413
0.126	5.589	918.7	969.7	673.4	1.437	0.124	1.256	0.037	0.957	0.474
0.166	4.356	920.4	970.9	729.9	1.445	0.122	1.204	0.034	1.27	0.482
0.21	3.657	920.4	973.9	762.9	1.455	0.123	1.15	0.029	1.617	0.52
0.245	3.112	912.7	969.3	773.1	1.442	0.135	1.09	0.032	1.865	0.57
0.316	2.547	914.4	972.6	809.5	1.448	0.133	0.99	0.026	2.419	0.599
0.368	2.186	923.9	973.7	849.1	1.474	0.119	0.932	0.023	2.865	0.545
0.421	2.096	934.2	984.4	872.9	1.487	0.102	0.86	0.012	3.313	0.521

APPENDIX III. TABLES CONTAINING THE PRESSURE DROP DATA

The numbers given at the top left hand corner of the tables correspond to the numbers in the flow map (figure 4.6).

In the tables in this appendix, some indexes are used, that do not occur in the thesis. These are:

index	meaning
HYD	hydrostatic
TOT	total
R	'reduced', i.e. predicted divided by measured (pressure drop)
RK	the same,yet involving the correction factor K

The symbol $d\Delta p_j$ denoted the inaccuracy in the pressure drop of pressure transducer j. These values are used in determining the churn-slug-transition in the branch.

1	2		4			
	Δp_l	$d\Delta p_l$	Δp_l	$d\Delta p_l$	Δp_l	$d\Delta p_l$
	bar	bar	bar	bar	bar	bar
	0.359	0.018	0.378	0.021	0.362	0.016
	0.350	0.012	0.373	0.015	0.359	
	0.359	0.021	0.368	0.009	0.354	
	0.332	0.007	0.361	0.007	0.35	
	0.329	0.005	0.358	0.005	0.341	0.011
	0.324	0.004	0.341	0.004	0.335	0.006
	0.317	0.003	0.33	0.003	0.33	0.006
	0.319	0.003	0.327	0.003	0.321	

3

Δp_1	Δp_2	Δp_3	Δp_4	Δp_5	Δp_6	Δp_7	Δp_8	$d\Delta p_7$	w_3/w_1	$\Delta p_{13.TOT}$	$\Delta p_{13.HYD}$	$\Delta p_{13.REV}$	Δp_{12}
bar	bar	bar	bar	bar	bar	bar	bar	bar	-	Pa	Pa	Pa	Pa
0.373	0.373	0.379	0.375	0.338	0.339	0.319	0.624	0.011	0.075	5388	4145	-162	187
0.359	0.359	0.369	0.36	0.322	0.324	0.299	0.608	0.009	0.105	6002	4253	-105	114
0.34	0.341	0.35	0.341	0.302	0.304	0.278	0.589	0.006	0.132	6161	4415	-40.9	89
0.334	0.335	0.344	0.334	0.295	0.296	0.269	0.584	0.005	0.16	6440	4858	6.109	72
0.331	0.333	0.342	0.332	0.291	0.292	0.265	0.581	0.004	0.185	6601	4973	84.24	66
0.324	0.325	0.334	0.325	0.282	0.282	0.255	0.573	0.004	0.213	6843	4991	195.1	98
0.321	0.322	0.328	0.323	0.278	0.28	0.258	0.571	0.005	0.233	6298	5015	293.2	257
0.353	0.354	0.361	0.356	0.306	0.308	0.285	0.604	0.005	0.298	6839	5176	565.1	341
0.467	0.468	0.476	0.471	0.402	0.404	0.382	0.718	0.007	0.441	8468	5481	1570	460
homogeneous model				Chisholm model				Reimann and Seeger model				inlet-to-run	
φ_{hm}	K_{13}	$\Delta p_{13.R}$	$\Delta p_{13.RK}$	φ_{cm}	K_{13}	$\Delta p_{13.R}$	$\Delta p_{13.RK}$	φ_{rsm}	K_{13}	$\Delta p_{13.R}$	$\Delta p_{13.RK}$	K_{12}	$\Delta p_{12.R}$
-	-	-	-	-	-	-	-	-	-	-	-	-	-
1.036	1.1	0.184	0.291	7.221	0.213	0.293	0.23	0.738	0.972	0.067	0.038	0.747	0.227
1.045	1.25	0.198	0.285	8.827	0.209	0.304	0.25	0.771	0.95	0.085	0.063	0.747	0.5
1.047	1.32	0.237	0.325	9.259	0.206	0.336	0.282	0.804	0.932	0.118	0.096	0.75	0.739
1.037	1.4	0.3	0.401	7.469	0.204	0.314	0.268	0.868	0.915	0.166	0.142	0.75	1.035
1.038	1.45	0.361	0.467	7.687	0.202	0.37	0.322	0.89	0.902	0.217	0.192	0.748	1.314
1.043	1.55	0.4	0.5	8.505	0.199	0.414	0.368	0.902	0.889	0.251	0.229	0.748	1
1.046	1.6	0.688	0.844	9.052	0.198	0.72	0.647	0.911	0.88	0.449	0.416	0.746	0.426
1.047	2	0.737	0.872	9.154	0.195	0.678	0.627	0.942	0.86	0.493	0.47	0.752	0.352
1.042	4.4	1.048	1.226	8.252	0.193	0.707	0.68	0.987	0.852	0.621	0.607	0.748	0.372

Δp_1	Δp_2	Δp_3	Δp_4	Δp_5	Δp_6	Δp_7	Δp_8	$d\Delta p_7$	w_3/w_1	$\Delta p_{13.TOT}$	$\Delta p_{13.HYD}$	$\Delta p_{13.REV}$	Δp_{12}
bar	bar	bar	bar	bar	bar	bar	bar	bar	-	Pa	Pa	Pa	Pa
0.367	0.367	0.374	0.368	0.337	0.34	0.323	0.612	0.060	0.02	4368	1054	-37.8	102
0.371	0.372	0.379	0.373	0.339	0.342	0.324	0.617	0.024	0.043	4721	1826	-58.7	113
0.337	0.338	0.345	0.338	0.305	0.307	0.289	0.579	0.022	0.077	4839	2217	-7.23	103
0.357	0.358	0.367	0.359	0.308	0.309	0.284	0.599	0.006	0.465	7310	4653	1263	240

homogeneous model				Chisholm model				Reimann and Seeger model				inlet-to-run	
φ_{hm}	K_{13}	$\Delta p_{13.R}$	$\Delta p_{13.RK}$	φ_{cm}	K_{13}	$\Delta p_{13.R}$	$\Delta p_{13.RK}$	φ_{rsm}	K_{13}	$\Delta p_{13.R}$	$\Delta p_{13.RK}$	K_{12}	$\Delta p_{12.R}$
-	-	-	-	-	-	-	-	-	-	-	-	-	-
1.109	1	0.093	0.129	19.88	0.22	0.402	0.34	0.215	1.018	0.009	0.006	0.759	0.254
1.104	1	0.116	0.162	19.12	0.217	0.491	0.414	0.37	0.998	0.025	0.018	0.752	0.348
1.136	1.1	0.146	0.197	24.65	0.213	0.622	0.528	0.475	0.971	0.052	0.044	0.762	0.491
1.134	4.9	0.971	1.14	24.24	0.194	0.894	0.832	0.994	0.855	0.551	0.54	0.777	0.505

6

Δp_1	Δp_2	Δp_3	Δp_4	Δp_5	Δp_6	Δp_7	Δp_8	$d\Delta p_7$	w_3/w_1	$\Delta p_{13.TOT}$	$\Delta p_{13.HYD}$	$\Delta p_{13.REV}$	Δp_{12}
bar	bar	bar	bar	bar	bar	bar	bar	bar	-	Pa	Pa	Pa	Pa
0.433	0.434	0.44	0.435	0.403	0.406	0.389	0.677	0.025	0.029	4426	1682	-93.2	170
0.421	0.422	0.428	0.422	0.399	0.393	0.374	0.666	0.024	0.034	4685	1717	-78.1	147
0.356	0.357	0.363	0.358	0.324	0.327	0.31	0.6	0.018	0.084	4574	2534	-15.6	247
0.373	0.375	0.381	0.377	0.339	0.341	0.32	0.616	0.012	0.131	5304	3394	52.47	371
0.358	0.36	0.366	0.361	0.323	0.325	0.303	0.601	0.009	0.147	5458	3477	107.1	344
0.359	0.362	0.368	0.363	0.321	0.323	0.3	0.602	0.006	0.203	5936	4051	299.1	344
0.35	0.352	0.358	0.353	0.311	0.313	0.291	0.593	0.007	0.218	5928	4099	347.5	321
0.336	0.339	0.345	0.339	0.293	0.295	0.272	0.578	0.006	0.275	6448	4383	644.6	309
0.434	0.436	0.445	0.438	0.376	0.378	0.353	0.675	0.007	0.374	8128	4587	1435	348

homogeneous model				Chisholm model				Reimann and Seeger model				inlet-to-run	
φ_{hm}	K_{13}	$\Delta p_{13.R}$	$\Delta p_{13.RK}$	φ_{cm}	K_{13}	$\Delta p_{13.R}$	$\Delta p_{13.RK}$	φ_{rsm}	K_{13}	$\Delta p_{13.R}$	$\Delta p_{13.RK}$	K_{12}	$\Delta p_{12.R}$
-	-	-	-	-	-	-	-	-	-	-	-	-	-
1.101	1	0.146	0.208	18.48	0.525	1.556	1.318	0.338	1.01	0.022	0.014	0.739	0.214
1.087	1	0.127	0.179	16.06	0.518	1.145	0.97	0.337	1.006	0.021	0.014	0.741	0.269
1.114	1.15	0.227	0.307	20.88	0.481	1.832	1.556	0.523	0.965	0.085	0.071	0.75	0.25
1.112	1.23	0.322	0.422	20.39	0.49	2.181	1.858	0.697	0.933	0.167	0.146	0.745	0.23
1.113	1.39	0.367	0.473	20.7	0.482	2.067	1.765	0.716	0.923	0.187	0.167	0.746	0.264
1.11	1.5	0.524	0.648	20.16	0.482	2.294	1.973	0.829	0.893	0.321	0.297	0.744	0.336
1.118	1.55	0.565	0.692	21.51	0.477	2.409	2.076	0.851	0.887	0.353	0.329	0.747	0.361
1.12	1.8	0.707	0.841	21.81	0.47	2.319	2.018	0.913	0.866	0.467	0.444	0.746	0.451
1.112	3.3	0.844	0.993	20.52	0.526	1.694	1.501	0.943	0.849	0.501	0.487	0.743	0.525

7

Δp_1	Δp_2	Δp_3	Δp_4	Δp_5	Δp_6	Δp_7	Δp_8	$d\Delta p_7$	w_3/w_1	$\Delta p_{13.TOT}$	$\Delta p_{13.HYD}$	$\Delta p_{13.REV}$	Δp_{12}
bar	bar	bar	bar	bar	bar	bar	bar	bar	-	Pa	Pa	Pa	Pa
0.52	0.52	0.527	0.522	0.488	0.49	0.473	0.769	0.025	0.029	4748	2241	-174	184
0.49	0.491	0.498	0.494	0.457	0.46	0.442	0.74	0.019	0.058	4875	3163	-199	325
0.48	0.481	0.483	0.482	0.456	0.448	0.427	0.727	0.013	0.108	5290	4000	-128	200
0.467	0.469	0.471	0.47	0.44	0.434	0.412	0.714	0.008	0.149	5570	4422	16.6	220
0.444	0.446	0.448	0.447	0.412	0.406	0.384	0.691	0.005	0.191	6020	4655	248.5	220
0.42	0.419	0.421	0.419	0.379	0.375	0.352	0.663	0.005	0.23	6720	4762	522.1	-40
0.408	0.41	0.412	0.41	0.368	0.364	0.341	0.654	0.005	0.243	6690	4860	611.2	210
0.399	0.401	0.403	0.401	0.354	0.351	0.328	0.645	0.005	0.264	7080	4889	826.1	230
0.401	0.403	0.405	0.403	0.355	0.355	0.329		0.005	0.3	7160	5009	1106	200
0.515	0.519	0.528	0.52	0.44	0.446	0.421	0.762	0.006	0.391	9374	5275	1988	488

homogeneous model				Chisholm model				Reimann and Seeger model				inlet-to-run	
φ_{hm}	K_{13}	$\Delta p_{13.R}$	$\Delta p_{13.RK}$	φ_{cm}	K_{13}	$\Delta p_{13.R}$	$\Delta p_{13.RK}$	φ_{rsm}	K_{13}	$\Delta p_{13.R}$	$\Delta p_{13.RK}$	K_{12}	$\Delta p_{12.R}$
-	-	-	-	-	-	-	-	-	-	-	-	-	-
1.054	1	0.162	0.24	10.36	0.219	0.428	0.353	0.413	1.01	0.022	0.009	0.724	0.203
1.055	1	0.221	0.336	10.58	0.215	0.612	0.502	0.585	0.986	0.068	0.04	0.724	0.18
1.057	1.15	0.449	0.635	10.92	0.209	0.928	0.774	0.742	0.948	0.218	0.17	0.721	0.485
1.057	1.36	0.758	1.01	10.92	0.205	1.17	0.996	0.82	0.921	0.405	0.347	0.72	0.572
1.058	1.47	0.874	1.109	11.16	0.201	1.18	1.03	0.866	0.899	0.528	0.476	0.719	0.709
1.062	1.59	0.782	0.957	11.78	0.198	0.979	0.872	0.892	0.881	0.506	0.47	0.72	4.446
1.059	1.61	0.894	1.085	11.27	0.197	1.065	0.956	0.905	0.877	0.595	0.556	0.719	0.887
1.061	1.73	0.9	1.078	11.57	0.196	1.024	0.927	0.913	0.869	0.603	0.569	0.718	0.895
1.06	2	1.102	1.302	11.52	0.195	1.136	1.043	0.935	0.86	0.737	0.704	0.72	1.083
1.054	3.33	0.969	1.133	10.48	0.193	0.763	0.721	0.974	0.849	0.599	0.582	0.722	0.513

8

Δp_1	Δp_2	Δp_3	Δp_4	Δp_5	Δp_6	Δp_7	Δp_8	$d\Delta p_7$	w_3/w_1	$\Delta p_{13.TOT}$	$\Delta p_{13.HYD}$	$\Delta p_{13.REV}$	Δp_{12}
bar	bar	bar	bar	bar	bar	bar	bar	bar	-	Pa	Pa	Pa	Pa
0.516	0.517	0.525	0.52	0.485	0.409	0.471	0.76	0.027	0.064	4544	2636	-159	394
0.479	0.48	0.488	0.483	0.446	0.449	0.431	0.723	0.023	0.085	4804	2901	-79.6	359
0.472	0.474	0.479	0.476	0.448	0.442	0.42	0.713	0.014	0.136	5270	3480	101	420
0.446	0.448	0.453	0.45	0.419	0.414	0.39	0.686	0.008	0.176	5620	3788	300.9	390
0.438	0.44	0.443	0.443	0.407	0.401	0.382	0.68	0.006	0.21	5560	3985	525.1	520
0.424	0.427	0.431	0.429	0.389	0.384	0.363	0.666	0.007	0.242	6170	4211	737.6	450
0.417	0.42	0.422	0.422	0.378	0.374	0.352	0.66	0.006	0.274	6480	4337	1029	460
0.414	0.417	0.422	0.419	0.373	0.37	0.348	0.656	0.006	0.296	6690	4380	1258	450
0.539	0.543	0.553	0.545	0.462	0.468	0.444	0.78	0.008	0.382	9541	4645	2218	539
homogeneous model				Chisholm model				Reimann and Seeger model				inlet-to-run	
φ_{hm}	K_{13}	$\Delta p_{13.R}$	$\Delta p_{13.RK}$	φ_{cm}	K_{13}	$\Delta p_{13.R}$	$\Delta p_{13.RK}$	φ_{rsm}	K_{13}	$\Delta p_{13.R}$	$\Delta p_{13.RK}$	K_{12}	$\Delta p_{12.R}$
-	-	-	-	-	-	-	-	-	-	-	-	-	-
1.097	1.05	0.352	0.5	17.93	0.214	1.366	1.149	0.527	0.981	0.112	0.083	0.714	0.221
1.102	1.15	0.357	0.493	18.76	0.211	1.207	1.02	0.585	0.964	0.136	0.109	0.724	0.252
1.104	1.35	0.583	0.763	19.15	0.206	1.45	1.241	0.705	0.929	0.288	0.253	0.721	0.313
1.108	1.42	0.683	0.859	19.83	0.202	1.485	1.287	0.773	0.906	0.395	0.36	0.724	0.386
1.106	1.51	0.976	1.194	19.5	0.2	1.83	1.606	0.81	0.89	0.611	0.569	0.724	0.331
1.103	1.61	0.921	1.106	18.84	0.198	1.517	1.346	0.85	0.877	0.605	0.571	0.724	0.417
1.105	1.78	1.043	1.234	19.19	0.196	1.555	1.394	0.879	0.866	0.698	0.665	0.723	0.455
1.107	1.97	0.9	1.021	19.58	0.195	1.569	1.415	0.891	0.861	0.75	0.719	0.722	0.496
1.108	3.15	0.899	1.051	19.82	0.193	0.942	0.868	0.948	0.849	0.556	0.54	0.722	0.495

Δp_1	Δp_2	Δp_3	Δp_4	Δp_5	Δp_6	Δp_7	Δp_8	$d\Delta p_7$	w_3/w_1	$\Delta p_{13.TOT}$	$\Delta p_{13.HYD}$	$\Delta p_{13.REV}$	Δp_{12}
bar	bar	bar	bar	bar	bar	bar	bar	bar	-	Pa	Pa	Pa	Pa
0.504	0.506	0.513	0.508	0.478	0.482	0.467	0.739	0.027	0.054	3745	1706	-51.7	384
0.493	0.494	0.5	0.497	0.461	0.466	0.452	0.729	0.028	0.091	4070	2416	17.66	430
0.47	0.472	0.478	0.475	0.437	0.442	0.426	0.707	0.026	0.107	4380	2494	102.8	460
0.451	0.454	0.459	0.456	0.42	0.424	0.407	0.687	0.017	0.12	4380	2494	102.8	460
0.443	0.446	0.451	0.448	0.41	0.412	0.394	0.679	0.011	0.152	4430	2523	186.6	470
0.441	0.444	0.449	0.445	0.404	0.406	0.388	0.676	0.007	0.184	5300	3142	561.3	450
0.425	0.428	0.433	0.429	0.386	0.388	0.369	0.66	0.008	0.199	5550	3188	674.5	450
0.422	0.425	0.43	0.427	0.381	0.383	0.364	0.657	0.008	0.216	5840	3276	840.4	450
0.42	0.424	0.428	0.425	0.374	0.376	0.357	0.655	0.007	0.254	6330	3575	1185	460
0.541	0.545	0.552	0.547	0.467	0.473	0.451	0.778	0.009	0.339	8940	4088	2195	640
0.515	0.519	0.526	0.521	0.446	0.452	0.433	0.751	0.01	0.426	8270	4299	3105	560
0.781	0.784	0.793	0.788	0.667	0.677	0.664	1.019	0.011	0.501	11670	4606	4213	760

homogeneous model				Chisholm model				Reimann and Seeger model				inlet-to-run	
φ_{hm}	K_{13}	$\Delta p_{13.R}$	$\Delta p_{13.RK}$	φ_{ch}	K_{13}	$\Delta p_{13.R}$	$\Delta p_{13.RK}$	φ_{rsm}	K_{13}	$\Delta p_{13.R}$	$\Delta p_{13.RK}$	K_{12}	$\Delta p_{12.R}$
-	-	-	-	-	-	-	-	-	-	-	-	-	-
1.195	1	0.361	0.493	34.63	0.215	2.387	2.025	0.405	0.989	0.104	0.085	0.727	0.213
1.165	1.18	0.565	0.753	29.52	0.211	2.518	2.142	0.544	0.96	0.221	0.19	0.724	0.256
1.169	1.25	0.578	0.756	30.24	0.209	2.317	1.978	0.566	0.949	0.247	0.218	0.724	0.273
1.169	1.3	0.597	0.781	30.24	0.209	2.317	1.978	0.566	0.949	0.247	0.218	0.724	0.273
1.174	1.39	0.672	0.867	31.07	0.208	2.374	2.033	0.577	0.94	0.289	0.261	0.724	0.292
1.175	1.43	0.808	0.994	31.18	0.202	2.31	2.002	0.72	0.902	0.472	0.44	0.722	0.408
1.182	1.5	0.805	0.982	32.47	0.2	2.193	1.907	0.74	0.895	0.48	0.451	0.724	0.423
1.182	1.55	0.837	1.01	32.38	0.199	2.122	1.853	0.76	0.887	0.515	0.487	0.722	0.46
1.175	1.65	0.946	1.121	31.2	0.197	2.063	1.818	0.819	0.873	0.62	0.592	0.72	0.509
1.155	2.5	0.906	1.06	27.89	0.193	1.299	1.172	0.906	0.853	0.574	0.555	0.716	0.457
1.168	3.95	1.581	1.852	30.09	0.193	1.787	1.636	0.974	0.85	0.925	0.904	0.723	0.543
1.149	5.5	1.204	1.411	26.79	0.195	1.098	1.023	1.01	0.863	0.68	0.668	0.722	0.438

10

Δp_1	Δp_2	Δp_3	Δp_4	Δp_5	Δp_6	Δp_7	Δp_8	$d\Delta p_7$	w_3/w_1	$\Delta p_{13.TOT}$	$\Delta p_{13.HYD}$	$\Delta p_{13.REV}$	Δp_{12}
bar	bar	bar	bar	bar	bar	bar	bar	bar	-	Pa	Pa	Pa	Pa
0.702	0.703	0.711	0.706	0.67	0.676	0.663	0.94	0.035	0.043	3836	1836	-165	445
0.667	0.669	0.677	0.672	0.636	0.641	0.628	0.904	0.032	0.078	3882	2479	-98.2	488
0.633	0.634	0.644	0.638	0.598	0.604	0.588	0.872	0.032	0.101	4427	2803	1.33	587
0.631	0.638	0.641	0.636	0.596	0.602	0.586	0.868	0.019	0.127	4504	3011	173.4	576
0.625	0.627	0.636	0.631	0.587	0.592	0.575	0.863	0.011	0.151	4940	3362	332.9	647
0.588	0.591	0.6	0.595	0.545	0.55	0.532	0.825	0.009	0.179	5570	3441	640.8	682
0.578	0.582	0.59	0.585	0.529	0.535	0.517	0.815	0.009	0.219	6042	3776	1083	732
0.508	0.513	0.521	0.513	0.452	0.456	0.436	0.742	0.01	0.243	7226	3824	1314	555
0.5	0.505	0.513	0.508	0.431	0.439	0.422	0.735	0.009	0.272	7816	4002	1823	763
0.475	0.479	0.487	0.481	0.41	0.416	0.398	0.709	0.01	0.342	7707	4195	2785	650
0.889	0.893	0.903	0.898	0.751	0.763	0.757	1.126	0.012	0.474	13176	4694	5160	951

homogeneous model				Chisholm model				Reimann and Seeger model				inlet-to-run	
φ_{hm}	K_{13}	$\Delta p_{13.R}$	$\Delta p_{13.RK}$	φ_{cm}	K_{13}	$\Delta p_{13.R}$	$\Delta p_{13.RK}$	φ_{rsm}	K_{13}	$\Delta p_{13.R}$	$\Delta p_{13.RK}$	K_{12}	$\Delta p_{12.R}$
-	-	-	-	-	-	-	-	-	-	-	-	-	-
1.139	1	0.468	0.655	25.06	0.217	2.543	2.149	0.396	0.998	0.108	0.079	0.703	0.216
1.15	1.1	0.799	1.094	26.92	0.212	3.859	3.269	0.544	0.97	0.293	0.238	0.704	0.274
1.144	1.2	0.803	1.075	25.97	0.21	3.181	2.704	0.61	0.953	0.34	0.289	0.704	0.267
1.154	1.3	1.119	1.46	27.59	0.207	3.934	3.361	0.666	0.936	0.532	0.47	0.702	0.333
1.14	1.4	1.258	1.613	25.3	0.204	3.602	3.094	0.726	0.92	0.649	0.583	0.699	0.343
1.151	1.45	1.113	1.39	27.18	0.202	2.973	2.572	0.757	0.905	0.634	0.584	0.7	0.369
1.145	1.55	1.316	1.601	26.11	0.199	2.93	2.562	0.822	0.886	0.822	0.77	0.698	0.405
1.154	1.62	0.936	1.123	27.71	0.197	1.995	1.754	0.846	0.877	0.604	0.572	0.702	0.536
1.154	1.78	1.064	1.264	27.74	0.196	2.029	1.796	0.886	0.867	0.697	0.664	0.698	0.453
1.162	2.6	1.652	1.944	29	0.193	2.388	2.149	0.94	0.852	1.021	0.987	0.703	0.572
1.144	5.2	1.279	1.507	25.85	0.194	1.174	1.089	1.02	0.857	0.707	0.692	0.704	0.464

Δp_1	Δp_2	Δp_3	Δp_4	Δp_5	Δp_6	Δp_7	Δp_8	$d\Delta p_7$	w_3/w_1	$\Delta p_{13,TOT}$	$\Delta p_{13,HYD}$	$\Delta p_{13,REV}$	Δp_{12}
bar	bar	bar	bar	bar	bar	bar	bar	bar	-	Pa	Pa	Pa	Pa
0,55	0,55	0,559	0,552	0,517	0,519	0,499	0,801	0,019	0,05	5125	3976	-327	167
0,55	0,55	0,559	0,552	0,515	0,517	0,496	0,801	0,013	0,086	5380	4603	-322	192
0,522	0,522	0,531	0,524	0,487	0,487	0,466	0,772	0,009	0,108	5531	4747	-250	207
0,488	0,489	0,497	0,49	0,45	0,451	0,43	0,738	0,007	0,139	5811	4967	-125	222
0,473	0,475	0,485	0,478	0,432	0,433	0,406	0,721	0,005	0,169	6690	5081	27,58	503
0,449	0,451	0,459	0,454	0,405	0,408	0,385	0,697	0,004	0,2	6471	5206	210,4	439
0,435	0,437	0,445	0,439	0,387	0,39	0,367	0,684	0,004	0,217	6807	5233	340	427
0,444	0,446	0,454	0,448	0,392	0,395	0,372	0,693	0,004	0,235	7187	5386	488,8	437
0,416	0,419	0,427	0,42	0,359	0,361	0,337	0,664	0,004	0,27	7894	5419	814,3	463
0,462	0,465	0,473	0,467	0,398	0,401	0,378	0,711	0,005	0,314	8373	5477	1249	492
0,613	0,617	0,625	0,62	0,525	0,529	0,509	0,863	0,006	0,411	10422	5573	2580	661

homogeneous model				Chisholm model				Reimann and Seeger model				inlet-to-run	
φ_{hm}	K_{13}	$\Delta p_{13,R}$	$\Delta p_{13,RK}$	φ_{cm}	K_{13}	$\Delta p_{13,R}$	$\Delta p_{13,RK}$	φ_{rsm}	K_{13}	$\Delta p_{13,R}$	$\Delta p_{13,RK}$	K_{12}	$\Delta p_{12,R}$
-	-	-	-	-	-	-	-	-	-	-	-	-	-
1,031	1	0,238	0,415	6,502	0,216	0,426	0,32	0,703	0,992	0,069	0,016	0,718	0,287
1,031	1,15	0,545	0,872	6,347	0,211	0,672	0,509	0,812	0,964	0,219	0,124	0,714	0,418
1,033	1,25	0,702	1,05	6,746	0,209	0,796	0,629	0,841	0,948	0,312	0,217	0,715	0,466
1,031	1,35	0,838	1,173	6,341	0,206	0,776	0,638	0,876	0,928	0,428	0,342	0,717	0,522
1,032	1,4	0,566	0,752	6,64	0,203	0,528	0,452	0,899	0,91	0,328	0,281	0,716	0,277
1,033	1,5	0,912	1,165	6,711	0,2	0,813	0,716	0,922	0,895	0,563	0,504	0,716	0,363
1,034	1,55	0,844	1,058	6,907	0,199	0,755	0,674	0,929	0,887	0,539	0,491	0,716	0,405
1,029	1,6	0,874	1,078	6,004	0,198	0,706	0,641	0,947	0,879	0,576	0,53	0,712	0,448
1,03	1,75	0,805	0,967	6,267	0,196	0,654	0,605	0,955	0,867	0,548	0,515	0,712	0,471
1,03	2,15	0,923	1,09	6,274	0,194	0,702	0,661	0,965	0,857	0,615	0,587	0,713	0,49
1,032	3,7	1,058	1,236	6,557	0,193	0,706	0,68	0,985	0,849	0,647	0,63	0,711	0,461

Δp_1	Δp_2	Δp_3	Δp_4	Δp_5	Δp_6	Δp_7	Δp_8	$d\Delta p_7$	w_3/w_1	$\Delta p_{13.TOT}$	$\Delta p_{13.HYD}$	$\Delta p_{13.REV}$	Δp_{12}
bar	bar	bar	bar	bar	bar	bar	bar	bar	-	Pa	Pa	Pa	Pa
0.685	0.685	0.695	0.688	0.652	0.655	0.637	0.933	0.021	0.048	4778	3348	-366	251
0.666	0.667	0.676	0.669	0.631	0.635	0.615	0.914	0.018	0.086	5111	4175	-354	324
0.607	0.609	0.618	0.611	0.57	0.574	0.553	0.855	0.012	0.125	5411	4489	-179	383
0.568	0.57	0.579	0.572	0.528	0.532	0.511	0.815	0.007	0.158	5725	4655	30.79	400
0.572	0.574	0.584	0.577	0.528	0.533	0.512	0.819	0.005	0.175	6014	4759	159.8	457
0.515	0.518	0.525	0.518	0.469	0.471	0.449	0.763	0.004	0.198	6583	4849	341.7	336
0.528	0.531	0.541	0.534	0.476	0.482	0.461	0.775	0.004	0.239	6703	4984	775.1	517
0.452	0.457	0.464	0.456	0.389	0.399	0.371	0.699	0.005	0.278	8119	5124	1159	435
0.523	0.527	0.533	0.529	0.447	0.457	0.438	0.77	0.006	0.314	8446	5129	1680	628
0.677	0.682	0.689	0.685	0.573	0.586	0.572	0.925	0.007	0.409	10558	5296	3009	786
0.871	0.875	0.883	0.879	0.734	0.752	0.739	1.12	0.008	0.513	13169	5526	4640	885

homogeneous model				Chisholm model				Reimann and Seeger model				inlet-to-run	
φ_{hm}	K_{13}	$\Delta p_{13.R}$	$\Delta p_{13.RK}$	φ_{cm}	K_{13}	$\Delta p_{13.R}$	$\Delta p_{13.RK}$	φ_{rm}	K_{13}	$\Delta p_{13.R}$	$\Delta p_{13.RK}$	K_{12}	$\Delta p_{12.R}$
-	-	-	-	-	-	-	-	-	-	-	-	-	-
1.049	1	0.342	0.546	9.533	0.216	0.918	0.742	0.612	0.994	0.091	0.039	0.703	0.275
1.046	1.15	0.712	1.083	9.111	0.211	1.367	1.105	0.759	0.963	0.285	0.185	0.701	0.341
1.051	1.3	1.022	1.436	9.843	0.207	1.621	1.349	0.823	0.937	0.493	0.39	0.703	0.376
1.053	1.38	1.112	1.48	10.27	0.204	1.59	1.355	0.858	0.917	0.615	0.527	0.704	0.426
1.05	1.41	1.12	1.458	9.756	0.202	1.451	1.253	0.872	0.907	0.658	0.578	0.701	0.427
1.051	1.5	0.91	1.152	9.843	0.2	1.089	0.955	0.889	0.895	0.557	0.503	0.705	0.603
1.053	1.6	1.285	1.568	10.28	0.198	1.456	1.306	0.918	0.878	0.85	0.79	0.701	0.488
1.05	1.8	0.891	1.062	9.762	0.196	0.896	0.82	0.939	0.865	0.603	0.571	0.704	0.615
1.056	2.15	1.068	1.259	10.82	0.194	1.026	0.948	0.951	0.857	0.708	0.678	0.703	0.479
1.057	3.7	1.145	1.34	10.85	0.193	0.879	0.833	0.982	0.849	0.694	0.676	0.706	0.438
1.046	5.5	1.152	1.338	9.071	0.195	0.775	0.75	1.005	0.866	0.69	0.677	0.709	0.427

13

Δp_1	Δp_2	Δp_3	Δp_4	Δp_5	Δp_6	Δp_7	Δp_8	$d\Delta p_7$	w_3/w_1	$\Delta p_{13.TOT}$	$\Delta p_{13.HYD}$	$\Delta p_{13.REV}$	Δp_{12}
bar	bar	bar	bar	bar	bar	bar	bar	bar	-	Pa	Pa	Pa	Pa
0.696	0.697	0.705	0.7	0.664	0.669	0.655	0.938	0.032	0.042	4098	2116	-212	393
0.639	0.641	0.649	0.644	0.606	0.609	0.593	0.881	0.024	0.099	4605	3158	-88.6	459
0.623	0.625	0.633	0.627	0.587	0.59	0.571	0.864	0.016	0.132	5155	3618	63.74	467
0.578	0.581	0.589	0.583	0.539	0.542	0.521	0.819	0.007	0.167	5627	3945	297.1	530
0.519	0.523	0.531	0.524	0.47	0.474	0.453	0.76	0.006	0.215	6590	4312	698.1	525
0.496	0.5	0.508	0.501	0.445	0.449	0.427	0.737	0.007	0.233	6926	4412	857.3	503
0.461	0.465	0.473	0.466	0.401	0.407	0.385	0.702	0.007	0.266	7671	4506	1253	508
0.481	0.486	0.494	0.488	0.415	0.423	0.401	0.721	0.007	0.273	8026	4379	1498	609
0.528	0.528	0.537	0.531	0.451	0.46	0.44	0.764	0.007	0.31	8736	4590	1889	341
0.616	0.62	0.629	0.623	0.524	0.535	0.52	0.857	0.008	0.353	9566	4744	2580	768
0.863	0.867	0.878	0.872	0.726	0.741	0.735	1.105	0.009	0.464	12782	5081	4592	965

homogeneous model				Chisholm model				Reimann and Seeger model				inlet-to-run	
φ_{hm}	K_{13}	$\Delta p_{13.R}$	$\Delta p_{13.RK}$	φ_{cm}	K_{13}	$\Delta p_{13.R}$	$\Delta p_{13.RK}$	φ_{rsm}	K_{13}	$\Delta p_{13.R}$	$\Delta p_{13.RK}$	K_{12}	$\Delta p_{12.R}$
-	-	-	-	-	-	-	-	-	-	-	-	-	-
1.099	1	0.391	0.56	18.12	0.217	1.674	1.407	0.424	0.999	0.085	0.056	0.703	0.21
1.106	1.2	0.773	1.057	19.48	0.21	2.509	2.123	0.642	0.954	0.324	0.266	0.703	0.315
1.104	1.33	0.93	1.232	19.05	0.206	2.42	2.063	0.732	0.932	0.454	0.393	0.701	0.384
1.104	1.4	1.011	1.295	19.09	0.203	2.269	1.955	0.799	0.911	0.569	0.511	0.703	0.39
1.094	1.5	0.939	1.154	17.28	0.199	1.634	1.435	0.856	0.888	0.6	0.556	0.703	0.46
1.093	1.6	0.938	1.141	17.2	0.198	1.504	1.33	0.876	0.88	0.604	0.565	0.704	0.498
1.095	1.73	0.908	1.082	17.52	0.196	1.325	1.186	0.897	0.869	0.607	0.575	0.705	0.544
1.11	1.8	0.924	1.098	20.06	0.196	1.419	1.268	0.896	0.867	0.61	0.58	0.702	0.5
1.104	2.1	0.952	1.121	19.12	0.194	1.251	1.132	0.93	0.858	0.626	0.601	0.704	0.929
1.1	2.73	1.094	1.284	18.38	0.193	1.196	1.097	0.953	0.851	0.686	0.663	0.703	0.458
1.09	4.87	1.209	1.417	16.56	0.194	0.966	0.911	1.002	0.855	0.695	0.68	0.702	0.434

Δp_1	Δp_2	Δp_3	Δp_4	Δp_5	Δp_6	Δp_7	Δp_8	$d\Delta p_7$	w_3/w_1	$\Delta p_{13.TOT}$	$\Delta p_{13.HYD}$	$\Delta p_{13.REV}$	Δp_{12}
bar	bar	bar	bar	bar	bar	bar	bar	bar	-	Pa	Pa	Pa	Pa
0.986	0.986	0.997	0.99	0.956	0.96	0.945	1.229	0.019	0.017	4110	1936	-370	356
0.912	0.913	0.923	0.916	0.88	0.884	0.869	1.154	0.024	0.046	4308	3007	-495	396
0.842	0.844	0.854	0.847	0.807	0.812	0.795	1.084	0.021	0.09	4740	3772	-383	488
0.789	0.792	0.802	0.795	0.751	0.756	0.738	1.029	0.013	0.126	5095	4024	-127	539
0.747	0.75	0.76	0.753	0.7	0.706	0.689	0.988	0.007	0.166	5808	4363	227.2	584
0.688	0.693	0.702	0.695	0.627	0.636	0.62	0.928	0.007	0.21	6824	4557	790.8	653
0.65	0.655	0.664	0.657	0.577	0.587	0.571	0.888	0.009	0.245	7830	4612	1326	698
0.598	0.604	0.614	0.606	0.509	0.519	0.505	0.836	0.007	0.316	9272	4827	2663	817
0.841	0.847	0.858	0.851	0.705	0.718	0.719	1.088	0.007	0.368	12123	5069	3826	1023
1.053	1.06	1.071	1.064	0.879	0.892	0.904	1.295	0.006	0.421	14868	5215	5266	1183
homogeneous model				Chisholm model				Reimann and Seeger model				inlet-to-run	
φ_{hm}	K_{13}	$\Delta p_{13.R}$	$\Delta p_{13.RK}$	φ_{cm}	K_{13}	$\Delta p_{13.R}$	$\Delta p_{13.RK}$	φ_{cm}	K_{13}	$\Delta p_{13.R}$	$\Delta p_{13.RK}$	K_{12}	$\Delta p_{12.R}$
-	-	-	-	-	-	-	-	-	-	-	-	-	-
1.073	1	0.441	0.649	13.77	0.22	1.558	1.299	0.371	1.021	0.045	0.013	0.684	0.147
1.072	1	0.647	0.997	13.6	0.216	2.441	2.018	0.574	0.996	0.168	0.086	0.684	0.254
1.076	1.2	1.241	1.797	14.24	0.211	3.409	2.838	0.725	0.961	0.487	0.355	0.685	0.338
1.086	1.3	1.491	2.038	16	0.207	3.654	3.088	0.789	0.936	0.722	0.596	0.686	0.395
1.084	1.4	1.449	1.889	15.66	0.203	2.865	2.459	0.852	0.912	0.818	0.719	0.686	0.454
1.084	1.52	1.256	1.565	15.66	0.2	2.07	1.812	0.89	0.89	0.785	0.719	0.685	0.496
1.093	1.6	1.09	1.321	17.25	0.197	1.731	1.533	0.916	0.876	0.723	0.676	0.686	0.518
1.091	2.16	1.263	1.488	16.9	0.194	1.523	1.384	0.955	0.856	0.829	0.795	0.686	0.539
1.08	2.9	1.107	1.298	14.95	0.193	1.062	0.984	0.982	0.85	0.693	0.67	0.684	0.488
1.068	3.95	1.098	1.286	12.89	0.193	0.871	0.822	0.989	0.85	0.656	0.639	0.683	0.466